TECHNISCHE UNIVERSITÄT WIEN
Vienna University of Technology

INSTITUT FÜR MECHANIK UND MECHATRONIK
Mechanics & Mechatronics

Master Thesis

Implementation and Validation of a Multi Layer Model Predictive Controller for Energy Supply Systems

A thesis submitted by
Michael Sack
Matr.Nr.:01125986

Submitted in partial fulfilment of the requirements for the degree of
Master of Science

TU Wien

Faculty of Mechanical and Industrial Engineerings

Privatdoz. Dipl.-Ing. Dr.techn. Alexander Schirrer

Institute of Mechanics and Mechatronics
Division for Control and Process Automation

Vienna, August 1, 2021

I confirm, that going to press of this thesis needs the confirmation of the examination committee.

Affidavit

I declare in lieu of oath, that I wrote this thesis and performed the associated research myself, using only literature cited in this volume. If text passages from sources are used literally, they are marked as such. I confirm that this work is original and has not been submitted elsewhere for any examination, nor is it currently under consideration for a thesis elsewhere. I acknowledge that the submitted work will be checked electronically-technically using suitable and state-of-the-art means (plagiarism detection software). On the one hand, this ensures that the submitted work was prepared according to the high-quality standards within the applicable rules to ensure good scientific practice "Code of Conduct" at the TU Wien. On the other hand, a comparison with other student theses avoids violations of my personal copyright.

City and Date, Signature

Acknowledgements:

First of all, I would like to thank my professors Alexander Schirrer and Martin Kozek, whose expertise was invaluable.

My special thanks go to my thesis adviser Florian Fuhrmann, for his guidance, help, and constant support throughout this thesis.

I would like to thank my colleagues at the TU Vienna, without whom I would never have made it this far.

I would also like to thank my wonderful wife and our three children for their unwavering support.

I also want to thank you, Christian, for your powerful computer and your IT support.

And thank you David.

Contents

Abstract: In this thesis, a newly developed multi-layer model predictive control concept, the Energy Demand Control System (EDCS), is implemented and validated on a simulation model. The simulation model is developed, verified, and validated with industrial measurement data. The model consists of three main components: a heat supply controlled by a hysteresis controller, sensible heat storage, and heat demand. The EDCS replaces the hysteresis controller and calculates the optimal trajectories for the heat pump operation. The trajectory is calculated by solving a linear mixed-integer optimization problem considering the heat demand prediction, the power price prediction, model constraints, and objectives. The EDCS enables a reduction of energy costs by utilizing the flexible power price market while ensuring process quality with optimal heat supply. In this thesis, the online heat demand predictor of the EDCS is developed further with focus on robustness against unpredicted time shifts in the heat demand. A simulation study is conducted to examine the effect of unpredicted heat demand starts and the robustness of the EDCS on the process quality. This thesis shows that the EDCS is applicable for the examined process and reached a software status, which ensures an error-free and comprehensible execution. The study results illustrate that the EDCS can reduce insufficient heat supply while reducing the cost of power consumption. A Pareto front is presented visualizing the trade-off between process safety and consumed power cost.

Kurzfassung: In dieser Arbeit wird das neu entwickelte mehrschichtige modellprädiktive Regelkonzept Energy Demand Control System (EDCS), implementiert und an einem Simulationsmodell validiert. Das Simulationsmodell wird mit industriellen Messdaten erstellt, verifiziert und validiert. Es besteht aus folgenden Komponenten: eine Hystere geregelte Wärmeversorgung, ein thermischer Wärmespeicher und eine Wärmesenke. Das EDCS ersetzt den Hystereseregler und berechnet die optimale Prädiktion des Eingangssignals für die Wärmepumpe. Die Prädiktion wird durch Lösen eines linearen gemischtganzzahligen Optimierungsproblems berechnet. Dabei werden die Prädiktion des Wärmebedarfs, die Prädiktion des Strompreises sowie linearisierte Modelle und Kostenfunktionen benutzt. Das EDCS reduziert die Energiekosten durch Nutzung des flexiblen Strompreismarktes. Weiters wird die Prozessqualität durch eine optimale Wärmeversorgung auf Basis der Wärmeprädiktion sichergestellt. In dieser Arbeit wird eine Echtzeit Methode zur Verbesserung der Prädiktion des Wärmebedarfs entwickelt und im EDCS implementiert. Damit soll die Robustheit der Wärmeversorgung gegenüber unvorhergesehenen Startzeitverschiebungen im Wärmebedarf erhöht werden. Es wird eine Simulationsstudie durchgeführt, um die Auswirkung von unvorhergesehenen Wärmelasten auf die Prozessqualität und die Robustheit des EDCS gegenüber ungenau prädizierten Wärmelasten zu untersuchen. Diese Arbeit zeigt ein Simulationsmodell welches mit den Messdaten der untersuchten Anlage validiert wurde. Die durchgeführten Simulationen zeigen, dass das EDCS in der untersuchten Anlage anwendbar ist. Weiters zeigen die Ergebnisse, dass das EDCS einen Softwarestatus erreicht hat, der eine fehlerfreie und reproduzierbare Ausführung gewährleistet. Die Ergebnisse der Studie zeigen, dass das EDCS Fälle von unzureichender Wärmeversorgung reduziert und gleichzeitig die Kosten für den Stromverbrauch senkt. Der Zusammenhang zwischen Prozesssicherheit und Kosten wird mittels Pareto-Front dargestellt.

Acronyms

AIAA	American Institute of Aeronautics and Astronautics
ASME	American Society of Mechanical Engineers
BC	batch consumer
DoD	Department of Defence
DSM	demand-side management
EDCS	Energy Demand Control System
EDCSproof	Energy Demand Control System - PROcess Optimization For industrial low temperature systems
FMU	functional mockup unit
HP	heat pump
HT	heat treatment
HTF	heat transfer fluid
IEEE	Institute of Electrical and Electronics Engineers
ISO	International Organization for Standardization
LHS	latent heat storage
LP	linear programming
LQR	linear quadratic regulator
LS	least square
MILP	mixed-integer linear programming
MIMO	multiple input multiple output
MPC	model predictive control
NRMSE	normalized root mean squared error
OP	Operation Planner
OR	Operational Research
PDE	partial differential equation
PID	proportional-integral-derivative
QP	quadratic programming
SHS	sensible heat storage
SISO	single input single output
SOC	state of charge
SQA	software quality assurance
TES	thermal energy storage
V&V	verification and validation

Symbols

Greek letters

Parameter	Unit	Description
α	–	significance level
α_{w}	$W/m^2 \cdot K$	heat transfer coefficient wall
ε	–	error between reference and estimation data
μ	–	mean value
θ	–	variable parameter for the least square fit
ρ	kg/m^3	density
ρ_{w80}	kg/m^3	density water at 80°C
σ	–	standard deviation
τ	min	time constant
Θ	–	multiplication factor

Roman letters

Parameter	Unit	Description
$\mathbf{A}$	–	state model matrix
A_{h}	m^2	horizontal area of the SHS
A_{l}	m^2	lateral area of the SHS
$A_{\mathrm{l}\Delta}$	m^2	lateral area of one layer of the SHS
$\mathbf{B}$	–	input model matrix
$\mathbf{C}$	–	output model matrix
C_{MWH}	MWh	charge power in the optimized model
cp	$J/kg \cdot K$	specific heat capacity, constant pressure
cp_{w80}	$J/kg \cdot K$	specific heat capacity, water, constant pressure, 80°C
D_{MWH}	MWh	discharge power in the optimized model
f	–	function
G	%	valve position
H	J	SHS absolute enthalpy
h	W	enthalpy stream
h_{Δ}	m	height of one layer of the SHS
J	–	cost function

Parameter	Unit	Description
k	$W/m \cdot K$	thermal conductivity
M	–	number of heat demand treatments
$\dot{m}$	kg/s	mass flow
N	–	number of constant volume layers
n	–	number of measured values
N_p	–	prediction horizon
n_HT	–	number of heat treatments
O	–	objective function for the controller
P_HP	MWh	power consumption of the heatpump
p	$€/MWh$	price per MWh
$\dot{Q}$	W	heat flow
$\mathbf{R}$	–	weighting matrix
r	–	weighting value
S^2	–	sample variance
T	°C	temperature
t	min	time
$t_{\mathrm{SOC}_\mathrm{undercut}}$	min	time the SOC is below the SOC_{min}
t_max	min	time duration of the prediction
t_s	$seconds$	discretization time
t_safety	min	EDCS parameter for the extension of the SOC_{min}
t_step	min	time step of the controller output values
U	%	power control input
$\mathbf{u}$	–	input vector
$\Delta\mathbf{U}$	–	control move vector
V	m^3	volume of the SHS
V_Δ	m^3	volume of one layer of the SHS
W	–	number of experiments
X	–	statistically independent, identically distributed variable
$\mathbf{x}$	–	state vector
x_in	–	input values for a function
$\bar{X}$	–	sample mean
$\mathbf{Y}$	–	output prediction
y	–	function output value
$\mathbf{y}$	–	output vector
$\bar{y}$	–	mean of values
y_out	–	output values of a function
y_ref	–	output reference values
$\mathbf{Y}_\mathrm{traj}$	–	output trajectory

1 Introduction

Climate change and its consequences lead to the decarbonization of the energy sector. Renewable energy sources replace fossil energies, and the fluctuation of the power supply rises due to volatile electricity generation. The fluctuation of power supply is a challenge for the power grid balance. Therefore a variable power price penalizes the energy consumption when the energy supply is low and vice versa. The customers can utilize variable power prices with demand-side management (DSM). DSM are methods at the demand-side of an energy system that influences energy use (Palensky *et al.,* 2011). One DSM activity consumers can utilize, is the movement of energy demand into times, where the energy supply of renewable energy sources is high, and electricity price is low. Due to production safety, few industries use DSM (McKane *et al.,* 2008). The control technique model predictive control (MPC) can achieve both: safe production and efficient DSM by keeping the operating point of the plant within its boundary conditions.

The performance of an MPC depends on the model prediction accuracy and the prediction data. Prediction data uncertainty has a negative effect on the control performance of MPC. In partially automated manufacturing plants, prediction can be inaccurate because of manually started processes. The predicted process start time differs from the real start time, which influences the energy demand schedule. This can lead to an insufficient energy supply, and production reliability constraints can be violated due to falling below a minimum temperature. Thereby, the process and product quality is negatively affected. Startup timing inaccuracies are hard to predict and are an intensified problem for batch pulsed energy loads. Therefore the Energy Demand Control System (EDCS) is introduced. It provides a cost-efficient DSM and ensures product safety, despite the unpredicted manual actions.

The EDCS is an online, predictive and holistic, and reconfigurable control system (Windholz, 2018-2021) and is the newly developed control system of the project 'Energy Demand Control System - PROcess Optimization For industrial low temperature systems (EDCSproof)'. It is a two-layer MPC hierarchical system that controls the energy supply of a plant. The goal of the EDCS is to ensure the optimal energy supply in terms of energy demand and energy cost and keep the operating point within the process limits. Its implementation enables the utilization of the flexible power price market and allows consumers to integrate renewable energies such as photovoltaic efficiently. The EDCS shall be implemented in several industrial plants. Therefore it is necessary to test and validate it to ensure its functionality on the physical system.

In this thesis, measured data of an existing production facility process is used to develop a simulation model and validate the EDCS. The investigated process is characterized by heat

treatment (HT)'s with pulsed heat loads, which are started manually by the employees. The heat amount per HT is known, and an accurate prediction for the HT profile exists. The planned start time is known but differs from the real start time of the HT. This thesis provides a validated simulation model of the plant under study. Further, the EDCS is implemented in the simulation, tested, and extended with additional functionality that can correct the prediction of the HT's in case of prediction errors in real-time. Finally, a simulation study is conducted to evaluate the impact of inaccurately predicted HT start times on the process quality and to assess the ability of the EDCS to ensure process quality.

This thesis is organized as follows. The plant, the control system EDCS, and the research questions are introduced in Chapter 2. In Chapter 3 a literature review of the topics verification and validation (V&V), model predictive control and multi-layer model predictive control, and sensible heat storage (SHS) is given. Chapter 4 is concerned with the methodology of this thesis. In Chapter 5, first the verification and validation results are presented. The simulation results with the EDCS are shown and the simulation study's output are evaluated, and discussed. In Chapter 6, a brief resume and outlook of this thesis are given.

2 Problem Setup

The Energy Demand Control System (EDCS) is a two-layer model predictive control (MPC) and is the newly developed control system of the project Energy Demand Control System - PROcess Optimization For industrial low temperature systems (EDCSproof). In this thesis, the EDCS and its robustness and performance are validated with an industrial plant's measured data. The plant under study is a facility subsystem. Production measurement data is utilized to develop a valid simulation model and implement the EDCS in the simulation to control the heat supply. Additional functionality that improves the prediction accuracy in real-time is developed and added to the EDCS. Simulation studies are executed to verify and validate the robustness, stability, correctness of the functionality, and applicability of the EDCS.

This chapter gives an introduction to the problem setup. Section 2.1 describes the plant and the process. In Section 2.2, the EDCS and its main functionality are introduced. The model requirements for the simulation model are stated, and necessary steps for implementing the EDCS in the simulation are defined. Section 2.3 presents the research questions.

2.1 Plant

The examined plant is a production facility with batch-like heat consumers. Heat is used to warm up a product in tanks called batch consumer (BC). The products are inside the tank, which is flooded with water. During the warm-up process, the product must be subjected to a specific temperature trajectory to achieve the necessary quality requirements. Four BC's are installed and the process can be conducted parallel on different BC's. The water in the BC is heated up with heat exchangers. The installed heat exchangers in the plant are two fluids counter flow plate heat exchangers with indirect heat exchange. Those plates separate the fluids and there is no contact between them. The BC heat exchangers are connected to a sensible heat storage (SHS) tank.

The SHS is a cylindric tank filled with water. The temperature in the SHS is between 60°C and 90°C. On the top and bottom of the SHS, there are two ports located which can be used as inlets or outlets. In the SHS, there is no further extension and no stratification device installed. The SHS can be charged and discharged separately. The enthalpy level in the SHS is called the state of charge (SOC). The SHS stores the heat for the BC's and is connected to a heat pump (HP). The HP heats the water while pumping it from the bottom to the top of the SHS. The connected heat demand components exchange heat at the BC's while pumping water from the top to the bottom of the SHS.

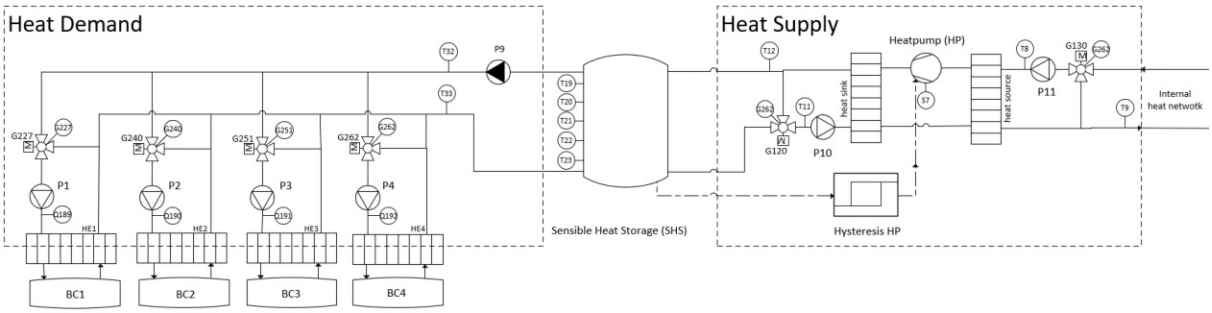

Figure 2.1: The scheme of the plant under study with its components and its connection. Measurement device labels are depicted in circles.

The HP consists of a compressor, an expansion valve, and two heat exchangers called heat sink and heat source. The condenser is at the heat sink side and the evaporator is at the heat source side. The heat sink of the HP is connected to the SHS and the heat source of the HP is connected to the internal heat network of the plant. The HP is controlled by a hysteresis controller. It utilizes the temperature in the SHS in the desired range. The hysteresis controller starts and stops the HP without any dynamic operation. The heat demand of the BC is above the maximum heat supply of the HP. Therefore, the SHS is used as a buffer storage for peak heat demand of the BC.

Figure 2.1 shows the energy supply plant schematically. It is categorized into the heat demand and the heat supply, separated by the SHS. Pumps and valves are used for the heat supply of the heat exchangers. Filled triangles indicate variable mass flow pumps and empty triangles indicate constant mass flow pumps. Further, descriptions of hydraulic components are given in Chapter VI. Each valve is proportional-integral-derivative (PID) controlled. The following interactions of the system with the environment are considered:

- The loss of heat in the SHS and the pipes
- The heat exchange at the BC
- The heat exchange at the internal heat network with the HP

Measurement data of the plant from the 4th of October 2019 to 31st of October 2019 is used for the modelling and validation process. In this range of time, no recognisable adjustment of the system configuration could be detected in the data. Further, the resolution of the measured data in the SHS is more accurate than before the 1st of October 2019. The data was recorded during the usual production time. No validation experiments were executed. The following measurements were recorded: temperature, valve position, heat flow, power, and rotation speed. The sampling time of the recorded data is one minute. The measurement device accuracy is unknown and there is no information about measurement errors. This fact and the assumption that the data is biased reduce the trustworthiness of the data. Due to confidential reasons, exact temperatures and energy levels in the SHS and the heat demand of the production processes are not depicted. Figure 2.1 shows the measurement devices. The measuring devices record the following measured values:

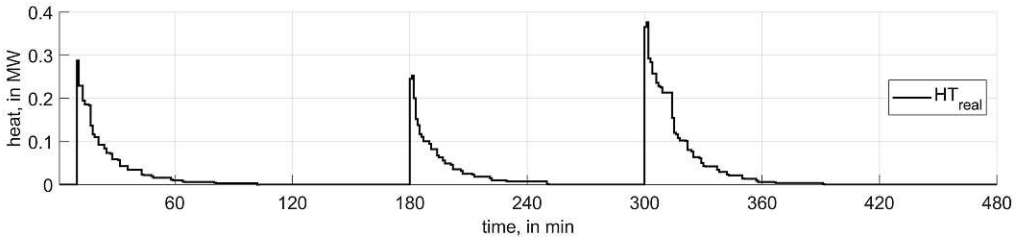

Figure 2.2: Three measured heat treatment examples.

- Q_i: measured heat, in W
- T_i: measured temperature, in °C
- G_i: measured valve position, in %
- S_i: measured rotation speed, in rpm

Where i is an enumeration for the identification of the measurement devices.

Pulsed heat loads characterise the measured heat consumption at the heat exchangers. At the beginning of each warm-up process, the heat consumption increases sharply and decreases exponentially during the running process. One warm-up process is called heat treatment (HT). The different product types and the different loadings of the BC's result in different integral heat consumptions. Figure 2.2 shows the measured heat flow at the heat exchangers for three different HT's.

During a HT, the SOC in the SHS must not be less than a minimum required SOC. The minimum SOC guarantees a sufficient heat supply for the HT and is dependent on the end-temperature of the warmup process. Each HT demands a particular minimum SOC for the product-specific temperature trajectory. This is especially challenging because the manual start of the HT causes prediction errors. Therefore, the hysteresis controller keeps the SOC constantly at a high level to avoid bottlenecks in the heat supply and thereby causes high heat losses. Still, the current hysteresis control cannot avoid that the heat supply of the SHS is insufficient and the temperature trajectory of the product cannot be applied. This leads to reduced product quality. Therefore, an insufficient SOC in the SHS must be prevented at all times.

The examined costs of the process consist of the price per MWh times the power consumption of the HP, and the cost per product with inadequate quality. Heat loss and thus additional costs are induced by the constant high energy level in the SHS and the operating time of the HP in periods without any heat demand.

2.2 EDCS

The EDCS is an online, predictive and holistic, and reconfigurable control system (Windholz, 2018-2021). It is the newly developed control concept of the project EDCSproof and is not implemented in a real industrial plant yet. The EDCS is a two-layer hierarchical MPC system that controls a plant's energy supply regarding the constraints, objectives, costs, and prediction.

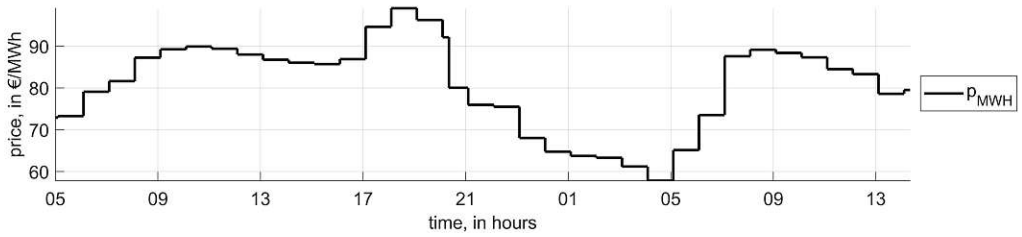

Figure 2.3: Example development for the price per MWh of a flexible power price market over 32 hours.

The first layer optimizes a plant-wide long term problem and calculates trajectories. The second layer optimizes component specific short term problems by following the trajectory of the first layer and calculating the input of the heat supply. The EDCS can be used to control several heat supply components in a plant. It uses simplified analytical models to predict future states keeping the operating point inside the boundaries. The EDCS minimizes a cost function by optimizing the input of the plant. The performance of the EDCS depends on the accuracy of the prediction data and the accuracy of the predicted states calculated with the analytical model. The aim of the EDCS is to control the energy supply for different industrial applications and shall integrate renewable energy by four areas (Windholz, 2018-2021):

- "Use of (thermal) energy storages" (Windholz, 2018-2021)
- "Flexible consumers for electricity networks" (Windholz, 2018-2021)
- "Efficiency through optimum control of the entire system" (Windholz, 2018-2021)
- "[Use] waste heat by using high temperature heat pumps (<150°C)" (Windholz, 2018-2021)

The EDCS can be configured to achieve a desired control aim like low costs, low energy consumption, and process safety. The EDCS can ensure process safety in the examined plant by an optimal supply of heat based on the heat demand prediction. The production plan can be used for the heat demand prediction. The integral heat amount per planned HT is known and can be used to predict the HT profile accurately. The start time of the HT's are known a priori but differ from the real start time caused by manual interactions of the employees. In addition, the EDCS can reduce costs by utilizing the flexible power price market and shifting the SHS charging into periods when power price is low and renewable energy supply is high. The price per MWh of a variable power price of October 2019 is shown in Figure 2.3 and varies between 57€ and 105€. The HP operating time in periods without heat demand can be minimized and heat loss caused by a high energy level induced by a hysteresis controller can be reduced to its minimum.

The implementation of the EDCS in a real plant needs a simplified analytical model of the controlled process. Further, the prediction of the power price and heat demand must be available a priori. Additional functionality is required to improve process safety for disturbed HT

predictions. Before the implementation at the plant, the EDCS must be validated on a simulation model. Therefore a valid simulation model of the plant is necessary. Simulation studies are needed to validate the robustness and performance of the EDCS.

2.3 Research Questions

The EDCS shall be implemented in the examined plant described in Section 2.1. Its implementation leads to access to the flexible power price market. Therefore, it is intended to control the energy supply in terms of electricity price prediction and heat demand prediction. The EDCS shall ensure process quality while reducing costs. Before the EDCS can be implemented in the real plant, tests and a simulation study must be conducted on a simulation model to validate it.

In this thesis, a valid simulation model is developed based on measured data of the studied process. The simulation model is used to validate the EDCS and must meet the following criteria:

- A simulation duration of 24 hours must be executed in less than 1 minute. The simulation is executed without the EDCS.
- The error between the simulation and the measured data is not allowed to exceed 10% except for short periods and the error must not exhibit any trend.
- The simulation must be stable and must not interrupt during the whole simulation time.
- The main dynamics of the system, like charging and discharging the SHS, heat loss through the wall of the SHS, the heat supply via the HP, and the heat transfer through the heat exchangers, must be mapped by the simulation.
- The main scenarios: 'the SOC is below the lower limit', 'more heat demand than heat supply' and 'run the system after a pause of up to seven days with no heat demand' must be mapped by the simulation correctly.
- The simulation must be developed and deployable in Matlab/Simulink (MATLAB, 2019).
- The simulation must be applicable for the EDCS Framework and usable with its controllers.
- The inputs and outputs of the simulation must be usable by the EDCS.
- The simulation states and outputs must be readable by the EDCS.

The EDCS is implemented in the simulation model, tested, and enhanced with additional functionality that can correct the prediction of the HT's online. Prediction data is prepared and a simulation study is conducted. The simulation study evaluates the impact of inaccurately predicted HT start times on the process quality and evaluates the robustness of the EDCS against prediction errors.

This thesis answers the following research questions:

1. Is it possible to use the measured data to develop a valid simulation model of the plant for testing the EDCS?
2. Can the EDCS be used to control the investigated energy supply system?
3. How robust is the EDCS against unpredicted interactions of human operators?
4. Which influence has the EDCS on the cost and quality of the process?

3 Literature Review

In the following chapter a literature review is presented about verification and validation (V&V), model predictive control (MPC), multi-layer model predictive control, and sensible heat storage (SHS). First V&V definitions are stated and V&V is explained. Then the distinct procedures verification and validation are explained separately. the purpose of V&V is summarized and processes are shown. At last V&V techniques are categorized.

Second a literature review about MPC and multi-layer model predictive control is provided. The motivation of the development of MPC is summarized and the basic definitions are stated. The concept behind MPC is reviewed and the need for hierarchical control structures are summarized. Several multi-layer control structures are presented.

In the last part a review of the thermal energy storage (TES) system SHS is given.

3.1 Verification and Validation

The history of V&V of simulation models dates back to the 1940s. Research in the field of V&V was initially carried out in the Operational Research (OR) community. The investigations concentrated on discrete-event simulations like world economic models that stand in contrast to the physics and engineering community. The engineering community is dominated by physical processes simulated with partial differential equation (PDE) (W. Oberkampf *et al.,* 2000). This thesis concentrates on V&V philosophies, methods, and goals in the context of physical simulation models, with PDE's, created and used on computer systems. The philosophical aspects and the history of V&V are not mentioned. The following literature gives more insight into the research field V&V in a broader sense: Kleindorfer *et al.* (1998) presented a philosophical view on the history of the V&V, and Sargent *et al.* (2017) summarized the research activities of V&V from 1940 up to 2017, especially in the context of OR. W. L. Oberkampf *et al.* (2012) presented the history of V&V from an engineering perspective.

In literature and scientific communities, no coherent terminology for V&V exists (Sargent *et al.,* 2017), and the interpretation of V&V, its methods and goals are context dependant. Therefore relevant definitions are introduced first.

A first clear definition of verification was formulated by Fishman *et al.* (1968): *"Verification determines whether a model with a particular mathematical structure and data base actually behaves as an experimenter assumes it does"* (Fishman *et al.,* 1968). Furthermore, a definition for validation, commonly found in the literature, is stated by Schlesinger (1979). Validation is the *"substantiation that a computerized model within its domain of applicability possesses a sat-*

isfactory range of accuracy consistent with the intended application of the model" (Schlesinger, 1979).

The community around the Department of Defence (DoD) in the United States and the OR community, or organizations like the Institute of Electrical and Electronics Engineers (IEEE) and the International Organization for Standardization (ISO), have their own V&V definitions and methods (W. Oberkampf *et al.,* 2000). The ISO defines verification as the *"confirmation of a claim (...), through the provision of objective evidence, that specified requirements have been fulfilled"* (ISO, 2019) and validation as the *"confirmation of a claim (...), through the provision of objective evidence, that the requirements for a specific intended future use or application have been fulfilled"* (ISO, 2019). The ISO V&V definition, which is similar to the definition of the IEEE's one, is more general than definitions in other communities and is the most dominant definition of V&V worldwide (W. L. Oberkampf *et al.,* 2012). The unclear ISO definition for simulation model V&V, the number of available different possible definitions for V&V, and the sometimes inappropriate interchangeable use of the meaning of V&V can lead to confusion in the V&V process (W. L. Oberkampf *et al.,* 2012).

The definitions of the American Institute of Aeronautics and Astronautics (AIAA) and American Society of Mechanical Engineers (ASME) present a more specific and intuitive definition (W. Oberkampf *et al.,* 2000). Verification is *"the process of determining that a computational model accurately represents the underlying mathematical model and its solution"* (ASME, 2006) and validation is *"the process of determining the degree to which a model is an accurate representation of the real world from the perspective of the intended uses of the model"* (ASME, 2006).

W. L. Oberkampf *et al.* (2012) collected further existing definitions of V&V and discussed them. In this thesis, the ASME V&V definition will be used. The following words are defined to avoid misinterpretation:

- System: "a set of physical entities that interact and are observable, where the entities can be a specified quantity of matter or a volume in space." (W. L. Oberkampf *et al.,* 2012)
- Model: "a representation of a physical system or process intended to enhance our ability to understand, predict, or control its behaviour." (W. L. Oberkampf *et al.,* 2012)
- Simulation: "the exercise or use of a model to produce a result." (W. L. Oberkampf *et al.,* 2012)

Verification

According to Sargent (1998), verification ensures that the simulation is error-free and properly implemented. Standard software development philosophies should be applied in an object oriented design or modular manner to assist an error-free implementation (Sargent, 1998). The goal of verification is to recognize errors, reduce them, quantify their impact on the solution, and prove the stability and robustness of the code (W. L. Oberkampf *et al.,* 2003). W. Oberkampf

et al. (2000) added that verification determines whether the implemented model fits to the conceptual model. W. L. Oberkampf *et al.* (2012) divided verification into two distinct activities, which are based on the work of Roache (1998) and Blottner (1990): (a) code verification and (b) solution verification.

Roache (1998) stated that (a) code verification identifies errors that happen during the code generation, errors in the code instructions or manuals, errors in the problem set up on which the code is based, errors happened in the definition and coding of benchmarks, for example, analytical solutions for comparison reasons, and errors occurred in the interpretation of the results. W. L. Oberkampf *et al.* (2003) defined the goal of code verification is first, to ensure that numerical algorithms are implemented correctly and their solutions should be in the desired range of accuracy. Second, software quality assurance (SQA) is assessed. SQA deals with implementing correct code, which includes the use of version control, code architecture, documentation, testing methods, or configuration management. SQA further ensures that the code is robust, can produce repeatable solutions, and meets its requirements in the view of a software product.

(b) Solution verification estimates numerical errors of the calculation of the PDE's based on its analytical solution and quantifies the accuracy of the solution (W. L. Oberkampf *et al.,* 2003).

Figure 3.1 shows the V&V process of the ASME guide. Experiments on the real world system are part of the V&V process, like the model and its implementation and simulation. The verification process takes place in the implementation and execution or calculation phase of the model. After the verification, uncertainty quantification of the results must be done and the simulation outcome can be compared and validated with the experimental outcome.

Validation

Balci (1994) stated that model validation substantiates that the model shows the same behaviour as the real world system. The model is executed with the same input conditions as the real world system. Afterwards, the real world output and the model output, the behaviour and the accuracy are compared. W. Oberkampf *et al.* (2000) stated that the error and uncertainty of the model are quantified and the agreement between the measured data and the model data is evaluated. This approach does not assume that the recorded data is more accurate than the computed one but that the recorded data is the most reliable source for validation (W. L. Oberkampf *et al.,* 2003). W. L. Oberkampf *et al.* (2008) summarized three key goals of validation: First, the model output is compared to the experimental data and its accuracy is examined, second the model is examined on its capability to predict future states and third the estimated accuracy of the previous steps must fulfil the stated conditions and the desired accuracy. The validation takes part at the end of the experiments of the real world system and after the verification and the simulation outcome, seen in Figure 3.1. If the agreement between the simulation and the experimental data is not in an acceptable range, the model has to be revised. This may result in new models, a new V&V process, and new experiments. The whole simulation building process is iterative.

The purpose of V&V is to prevent three major errors. Type I Error is refusing a credible

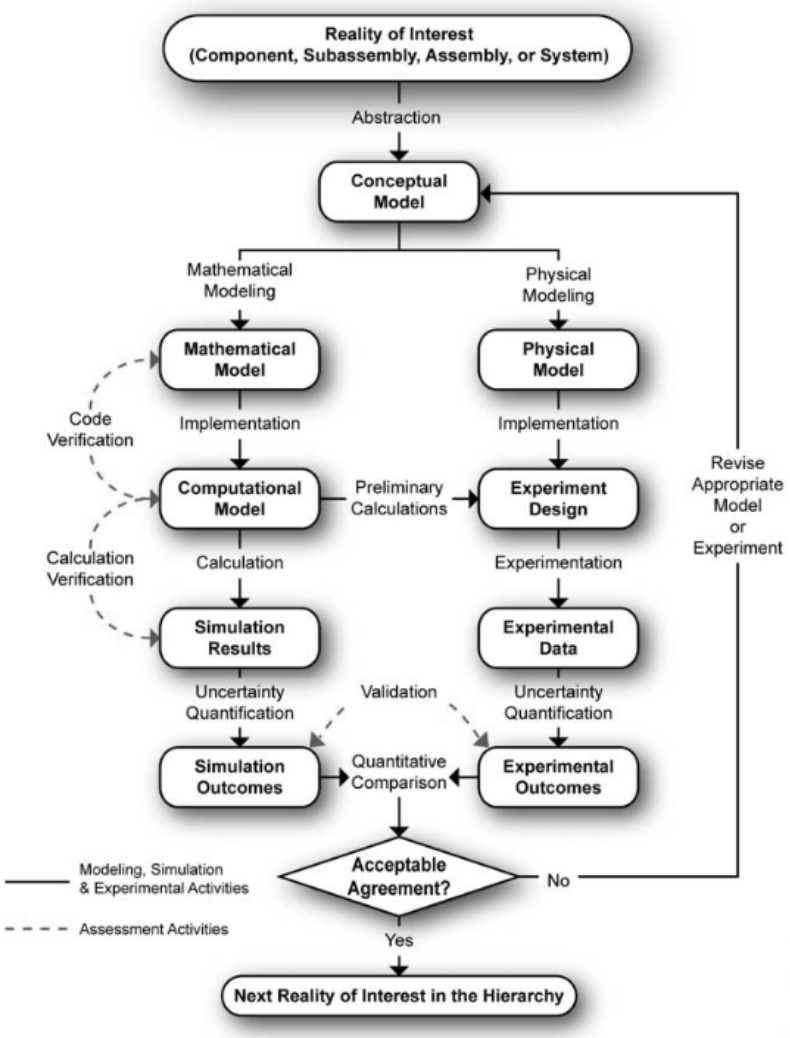

Figure 3.1: The simulation building process with the V&V activities (ASME, 2006).

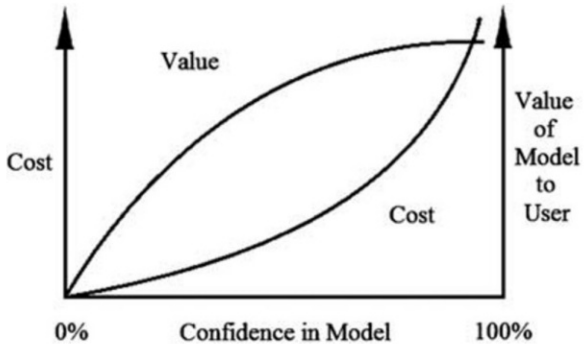

Figure 3.2: Course of the 'Cost' and the 'Value of Model to User' as a function of the 'Confidence in Model' (Anshoff *et al.,* 1972).

model called the model builder's risk (Balci *et al.,* 1981). Type II Error is accepting a refused model, which is called the model user's risk (Balci *et al.,* 1981). Solving the wrong problem with a model is a Type III Error (Balci *et al.,* 1985). Balci *et al.* (1981) argued that the model user's risk or Type II Error, should be kept small in the validation process because wrong and expensive decisions based on inaccurate models could cause high losses. Greig (1979) showed that a Type II error's costs could be higher than a Type I Error and developed a decision basis on how much validation is needed to reduce the expected Type I or II Error loss to a minimum. Balci *et al.* (1981) stated a methodology for constructing a relationship between the Type I and II Error risk, the acceptable range of validity, the budget, and the sample size of observations on the model and the real world system. These parameters influence each other and an acceptable range for each parameter must be chosen. The result is a trade-off between the degree of validation and the costs of validation. Figure 3.2 shows the relation of the "Confidence in Model" to the "Cost" and the "Value of Model to User" as stated in Anshoff *et al.* (1972). The relation shows that at some point of the V&V process, the value compared to the cost rise low and the costs rise exponentially with more V&V activities.

Oreskes *et al.* (1994) noted that V&V sometimes has an either / or characteristic, which means that a model is valid or not, is principally not possible. The reasons are limitations by the data, limitations of the possibility of the observations of the phenomenon, the assumptions are made, the hypothesis which is set on, or the dynamic a system is exposed. In practice, few models are entirely valid or not. Shannon (1975) stated that validation is not a binary decision but calculates a degree of validity. Further, the validity of a simulation model can only be evaluated as meaningful and varies by the context of its purpose (Balci, 1990). The model should reflect the characteristics of a studied process and V&V produces an acceptable level of confidence (Robinson, Nov. 1997). Landry *et al.* (1993) stated that validation results depend on the participants of the validation process and the research activity of the involved social organization because of the social character of the V&V process. Carson (1989) pointed out that V&V cannot be done by the modeller alone. A client that could be the management, the users, or engineers, should pass judgement on the validity of the model. Gass *et al.* (1981) summed up that confidence in a model is the result of the collected information of a model

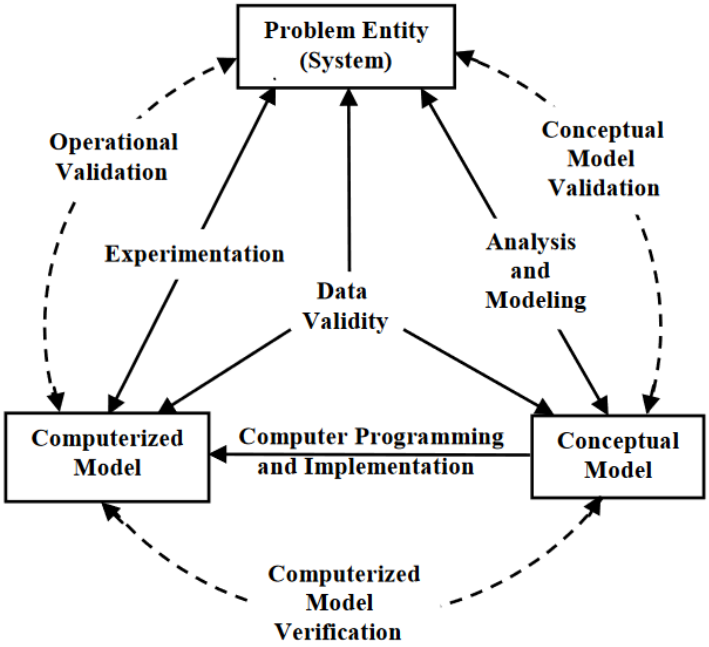

Figure 3.3: The life cycle of a simulation study (Sargent, 1981).

gained through the validation process.

Figure 3.3 shows the life cycle of a simulation study. It is an iterative process that should be applied throughout the whole life cycle of a simulation (Balci, 1990). Oval symbols are phases, dashed arrows describe the sequence of the process, and solid arrows describe the credibility dependence between the phases. In each step of the modelling process, V&V takes place. It is no static process but continuous (Shannon, 1975).

Data validation is the basis for all phases in the simulation process. Adequate data is needed to build the conceptual model, the computerized model, and validate the model. The data must be in an appropriate, accurate, and sufficient form available. Sargent (1998) defined that measured data must be examined whether it is consistent, if there are outliers and errors, and must be preprocessed if needed for the further V&V. Data from defined experiments instead of data from the regular production or business are preferred for the V&V, but in most cases, experiments on existing and producing or running plants are not easy or impossible to conduct. Therefore, W. Oberkampf *et al.* (2000) recommended the building block approach: The complexity of the model is divided into four different tiers, with each different availability of experimental data. The complete system is divided into subsystems. The subsystems are divided into benchmark cases and further divided into unit problems (W. Oberkampf *et al.,* 2000). The building block approach provides a strategy to split the validation into small units with well defined validation data sources like experiments, property data taken from engineering handbooks, or scientific results (W. Oberkampf *et al.,* 2000).

V&V should continue until the desired level of confidence is reached (Balci, 1994). This leads to more V&V techniques or more intensive V&V, which raises the costs too. Due to this relation, some V&V techniques must be chosen to meet cost, time, and resource limits. There

are no standard techniques for the V&V process (Davis, 1991; Landry *et al.,* 1993) and techniques are ideally chosen by the model development team together with other involved parties, like the users or the decision makers (Sargent, 1998). Balci (1995) categorized V&V techniques into six different categories: informal, static, dynamic, symbolic, constraint, and formal. The category "informal" is characterized by its reliance on humans. The category "static" contains techniques, which do not execute the simulation but check the semantic or the syntax of the code by automated tools or mental execution. The "dynamic" tools execute the models and examine the behaviour and the output. Tools of the category "symbolic" examine the behaviour of the simulation during its execution. "Constraint" tools assess the correctness of the code concerning the models limits and boundaries, and "formal" techniques assess the correctness of the model by mathematical proofs. Usually, non of the techniques are the basis for a binary validity decision, but each can increase the confidence in the model. Balci (1995) summarized a detailed description of V&V techniques and Banks (1998) identified and described more than 75 V&V techniques.

3.2 Model Predictive Control and Multi-Layer Model Predictive Control

García *et al.* (1989) stated, the control problem of any system must satisfy the following: "On-line update the manipulated variables to satisfy multiple, changing performance criteria in the face of changing plant characteristics." (García *et al.,* 1989). According to García *et al.* (1989), Arkun *et al.* (1980) and D. M. Prett *et al.* (1980) stated that the economic minimum of a plant is at the intersection of the control constraints. Furthermore, García *et al.* (1989) stated that a control system must keep the operating point close to the constraints of a plant. The controller must anticipate constraint violations and move the operating point inside the constraints systematically (García *et al.,* 1989). In the process industry, systems with operating points changing over time, processes that are limited by constraints, and non-linear and multivariable processes must be controlled (Qin *et al.,* 2003). The stated requirements can be fulfilled by model predictive control (MPC) (Qin *et al.,* 2003).

The name model predictive control originates from using a plant's model to predict future inputs and their influence on the output (García *et al.,* 1989). García *et al.* (1989) remarked that multivariable and constrained problems are the primary motivation for the MPC development. Further Raković *et al.* (2019) stated that linear quadratic regulator (LQR) is limited by their ignorance of actuator saturation, that is the main argument for the development and the distribution of MPC, instead of using the LQR control. MPC is the only control strategy to handle the model, objective functions, and constraints (García *et al.,* 1989). Compared to MPC, the LQR cannot implement constraints in the design phase. García *et al.* (1989) explained that a common practice is to design a control process and ignore the constraints. During the implementation of the LQR, the controller is adapted to prevent the violation of constraints (García *et al.,* 1989).

Therefore the LQR handles constraints, nonlinearities, and uncertainties inadequately (Mayne *et al.,* 2000). García *et al.* (1989) added that a feasible solution could not be found by the LQR when a disturbance pushes the measured states outside the limits. Another unresolved issue is the tuning of multiple input multiple output (MIMO) systems which can be very complex (García *et al.,* 1989). Computer systems' increased reliability and power further led to digital control technologies as the MPC (Richalet *et al.,* 1978).

Single Layer Model Predictive Control

The following mathematical representation of the models used in MPC is based on Wang (2009), García *et al.* (1989), and Raković *et al.* (2019). The discrete-time linear time-invariant dynamic model, without disturbance and without measurement noise, is presented in Eq. (3.1). The output of the model is calculated in Eq. (3.2). The stated representation is called the state space representation.The mixed-integer linear programming (MILP) representation is introduced from Eq. (3.6) to Eq. (3.11). Other representations as transfer functions are not considered in this review. Further, only linear model predictive control with linear constraint models are considered.

$$\mathbf{x}_{i+1} = \mathbf{A} \cdot \mathbf{x}_i + \mathbf{B} \cdot \Delta\mathbf{u}_i \tag{3.1}$$

$$\mathbf{y}_i = \mathbf{C} \cdot \mathbf{x}_i \tag{3.2}$$

The vector $\mathbf{x}_{i+1}$ is the controlled state vector, $\Delta\mathbf{u}_i$ represents the input vector and $\mathbf{A}$, $\mathbf{B}$, $\mathbf{C}$ are the model matrices where $\mathbf{C}^T \cdot \mathbf{C} > 0$. $\mathbf{y}_i$ is the output of the model. The models can be MIMO and single input single output (SISO). The depicted model in Eq. (3.1) is the receding horizon representation, where the input $\Delta\mathbf{u}_i$ cannot affect the output $\mathbf{y}_i$ at the same time step. Further, a prediction horizon N_p is defined. The MPC calculates the states $\mathbf{x}_i$ and inputs $\Delta\mathbf{u}_i$ from the current time step i to the prediction horizon $i + N_\mathrm{p}$. The stated problem is a quadratic programming (QP) problem (Raković *et al.,* 2019) and the optimal $\Delta\mathbf{u}_i$ is found by minimizing a cost function which is given in Eq. (3.3).

$$J = (\mathbf{Y}_\mathrm{traj} - \mathbf{Y})^T \cdot (\mathbf{Y}_\mathrm{traj} - \mathbf{Y}) + \Delta\mathbf{U}^T \cdot \mathbf{R} \cdot \Delta\mathbf{U} \tag{3.3}$$

J is the 2-norm cost function which is minimized. $\mathbf{Y}_\mathrm{traj}$ is the trajectory of the output and $\mathbf{Y}$ is the predicted output. $\Delta\mathbf{U}$ is the predicted control input deviation vector and $\mathbf{R}$ a symmetric weighting matrix, with $\mathbf{R} > 0$. The error between the output trajectory $\mathbf{Y}_\mathrm{traj}$ and the predicted output $\mathbf{Y}$ is minimized, as well as the predicted input $\Delta\mathbf{U}$. The weighting matrix $\mathbf{R}$ defines, in which relation the minimization of the error between the output and the trajectory, or the input is conducted. Constraints are stated in Eq. (3.4) and Eq. (3.5). The states and inputs are constrained to prevent damages to the real world system, prevent the MPC from calculating

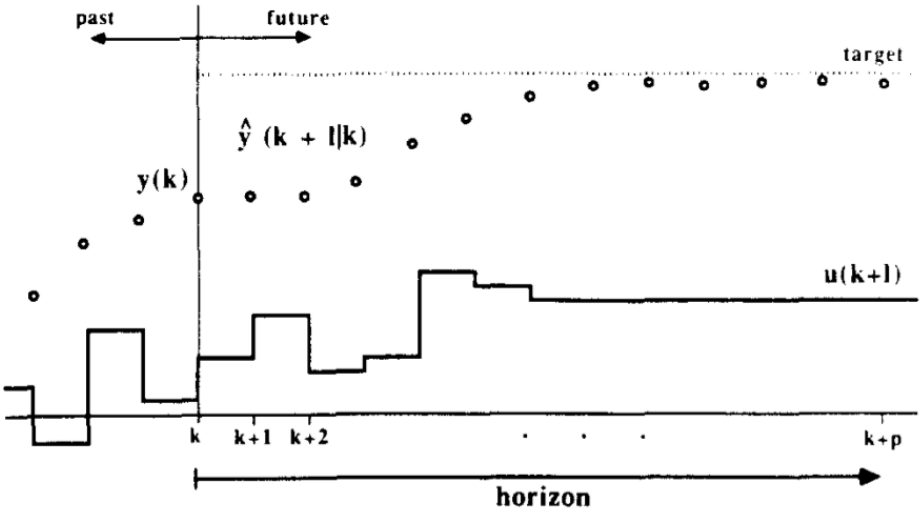

Figure 3.4: In the receding horizon control concept the output $\hat{y}$ and the input u is predicted for the prediction horizon from the actual step k to the prediction horizon $k+N_\mathrm{p}$. The MPC optimizes a QP problem and minimizes the difference between the *target* setpoint and the predicted output $\hat{y}$ (García *et al.,* 1989).

unphysical states, or limit the model according to economic considerations.

$$U_\mathrm{min} \leq \mathbf{U} \leq U_\mathrm{max} \tag{3.4}$$

$$X_\mathrm{min} \leq \mathbf{X} \leq X_\mathrm{max} \tag{3.5}$$

U_min and U_max are the minimum and maximum for the predicted input $\mathbf{U}$. X_min and X_max are the minimum and maximum for the predicted states $\mathbf{X}$. The MPC uses the actually measured states from the real world system and computes the future states and inputs for the prediction horizon based on the defined model. Constraints limit the predicted states and inputs. The difference between predicted states and their trajectory or predicted inputs and their trajectory is minimized. The first value of the N_p calculated inputs $\mathbf{U}_{i=1}$ is applied and in the following sampling step, the MPC calculates optimal inputs for given constraints, objectives, and initial conditions again. Figure 3.4 shows the principles of the MPC, which is interchangeably called receding horizon control. The output y is measured at the current step k. The prediction $\hat{y}$ follows the setpoint trajectory *target*. The predicted input u and the difference between $\hat{y}$ and the *target* is minimized in the prediction horizon $k+N_\mathrm{p}$. Further definitions and explanations of the MPC control design are sated in S. Joe Qin *et al.* (1997), Wang (2009), García *et al.* (1989), or Raković *et al.* (2019).

The problem stated in Eq. (3.1), Eq. (3.2), and Eq. (3.3) can be transformed into a linear programming (LP) problem by reducing the cost function to a linear equation. The general definition of a LP problem is an objective or cost function with a set of equalities and inequalities. A model that does not contain a quadratic feature is called a MILP problem. Further, some or all of the variables are restricted to be integers. The minimizing objective function is stated in

Eq. (3.6). From Eq. (3.7) to Eq. (3.11), the equalities and inequalities are defined.

$$J = \sum_{i=1}^{N} (y_{\text{traj}_i} - y_i + r \cdot u_i) \tag{3.6}$$

$$\mathbf{x}_{i+1} = \mathbf{A} \cdot \mathbf{x}_i + \mathbf{B} \cdot u_i \tag{3.7}$$

$$u_i \geq U_{\min} \tag{3.8}$$

$$u_i \leq U_{\max} \tag{3.9}$$

$$\mathbf{x}_i \geq X_{\min} \tag{3.10}$$

$$\mathbf{x}_i \leq X_{\max} \tag{3.11}$$

r is a weighting factor. The input u_i is optimized for the prediction horizon N_p to minimize the objective function J by a LP algorithm. The process is repeated for each step.

Main concepts of MPC technologies as LP and the moving horizon approach were introduced first in the 1960s (García *et al.,* 1989). One of the first MPC was introduced by Richalet *et al.* (1978), who described a model predictive heuristic control (MPHC). According to Mayne *et al.* (2000), the use of LP for a linear control problem with hard constraints are first used in A.I. Propoi (1963). Optimal control algorithms are summarized in Polak (1997). Wright (1996) and Rao *et al.* (1998) summarized algorithms suitable for solving linear model predictive control problems. Several MPC designs and implementations of MPC exist (Qin *et al.,* 2003; S. Joe Qin *et al.,* 1997). S. Joe Qin *et al.* (1997) collected different MPC design implementations and compared them.

The MPC constraints can be defined on the maximum, minimum, and rate of change of states or inputs, preventing the controller from being unstable or calculating non physical states or inputs (S. Joe Qin *et al.,* 1997). S. Joe Qin *et al.* (1997) stated that MPC constraints are implemented as soft or hard constraints. Soft constraints are allowed to be violated but lead to a penalty, while hard constraints are not allowed to be violated at all (S. Joe Qin *et al.,* 1997). Further, the state or input trajectories are defined as setpoints, zones, reference trajectories, or funnels (S. Joe Qin *et al.,* 1997). Figure 3.5 shows the different possible trajectory definitions with soft constraints, examined by S. Joe Qin *et al.* (1997). The setpoint trajectory are static or changing levels that the states or the input shall reach. The zone trajectory defines a region to which the desired value is limited. The difference between the reference trajectory and the predicted state is tried to keep zero. The funnel is a region between two limits with a decreasing distance to which the states are limited. The soft constraint penalty is active if the value is outside the zone or region between the constraints. The solution is still feasible, although the constraint is violated.

The stability of MPC was tried to reach by tuning costs and changing the prediction horizon parameter (Mayne *et al.,* 2000). Mayne *et al.* (2000) reviewed that Lyapunov value functions can be used for the stability analysis of MPC. According to Mayne *et al.* (2000), Keerthi *et al.* (1988) were the first who establish stability in time varying, constrained, non-linear, discrete

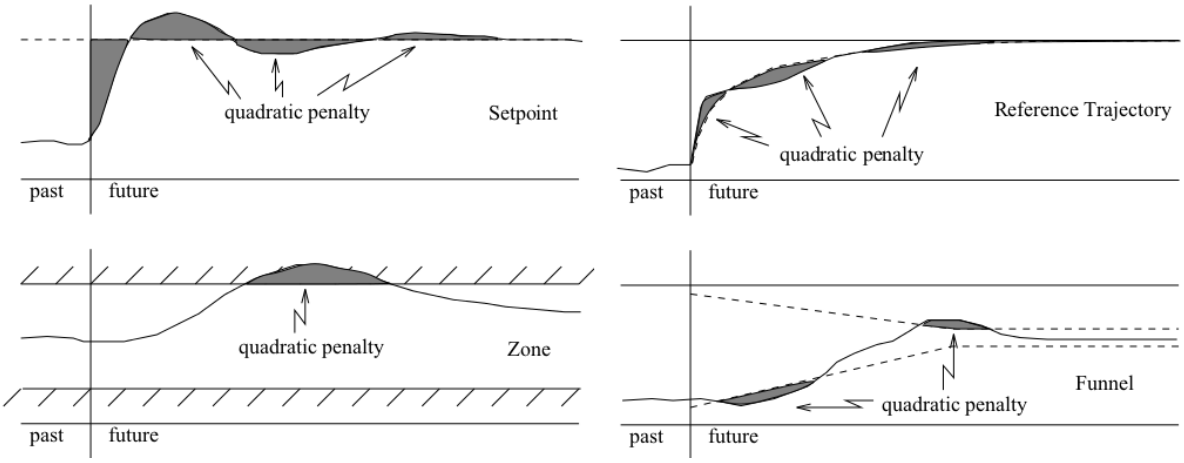

Figure 3.5: Different trajectory techniques with soft constraints and quadratic penalty added to the cost function. In the upper row, costs are added when the prediction does not fit to the trajectory. In the bottom row, costs are added when the prediction cannot be kept between the limits (García *et al.,* 1989).

systems with terminal equality constraints by a Lyapunov value function. The stability of MPC controlled systems can be achieved by setting terminal constraints and terminal costs together (Mayne *et al.,* 2000). Mayne *et al.* (2000) described the process of achieving stability and examined it by four conditions that are sufficient for closed loop stability, although the horizon is finite. Raković *et al.* (2019) stated the stability for an MPC without terminal constraints. MEADOWS *et al.* (1995) stated that MPC could stabilize some systems, continuous feedback controller cannot. Mayne *et al.* (2000) reviewed the stability and robustness of the MPC and presented further literature on techniques accessing stability.

Robustness means that the quality of the MPC and system is preserved, although the dynamic behaviour of the plant differs from the model in the MPC (García *et al.,* 1989). Further uncertainties can influence the robustness of the MPC (Mayne *et al.,* 2000). Raković *et al.* (2019) stated that robustness guarantees that the system is stable, feasible, and performs in the desired way. The MPC is as robust as classic feedback control is, and no general answer to the comparison of the robustness can be stated (García *et al.,* 1989). An unconstrained linear MPC is as robust as the classic feedback control is. The robustness depends on the configuration of the MPC and can be adjusted more easily than in classic feedback control by tuning the weights or constraints (García *et al.,* 1989). The robustness of an unconstrained MPC can be analysed with the available methods for classical feedback control. Raković (2020) summarized different approaches to develop robust MPC with different sets of uncertainties, constraints, and the level of complexity.

Multi Layer Model Predictive Control

The calculation time can exceed acceptable limits for complex optimization tasks even though calculation power has increased over the past decades. Therefore, complex optimization tasks are divided into sub problems and subsystems. If such a system and its subsystems are controlled by several hierarchically distributed layers controlled by MPC, the structure is called a

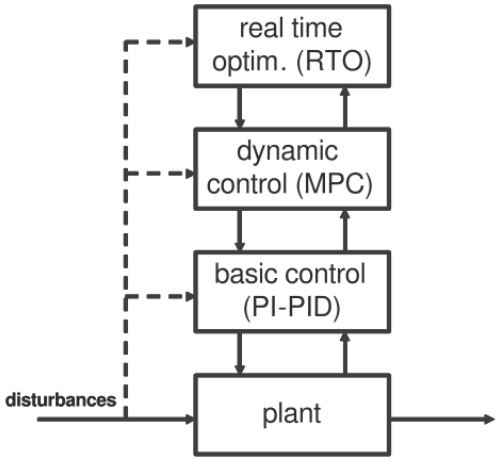

Figure 3.6: A control hierarchy example is shown. The plant or the component directly is controlled by a PID controller which in turn is controlled by an MPC. The MPC tries to follow a trajectory from a plant wide optimization (Scattolini, 2009).

multi-layer model predictive control hierarchy. If such a control hierarchy is implemented, the system components are typically controlled by low-level proportional-integral-derivative (PID) controllers. The PID controller follows setpoints given by the MPC. The first layer executes a plant wide optimization with trajectories for the MPC (Scattolini, 2009). Figure 3.6 shows the structure of an example multi-layer model predictive control architecture. The top level of the hierarchy uses simplified models and solves a long term problem with large time steps, while the middle layer has a higher model and prediction accuracy and solves a short term problem with short time steps. Each layer can consist of multiple controllers.

Systems can be divided into subsystems with separated controllers, called decentralized control (Scattolini, 2009). Sandell *et al.* (1978) discussed the difference between two subsystems controlled separately with a "weak" interaction and subsystems with strong interactions. If the interaction is not negligible, the performance can be decreased (Sandell *et al.,* 1978). Therefore, Sandell *et al.* (1978) introduced the coordinator, which is in contact with both of the systems and controllers. The coordinator's aim is to improve the performance, compared to the case where no coordinator is implemented. Scattolini (2009) stated that few decentralized control systems are developed because the MPC can be implemented centrally with many input and output variables, and stability cannot be as easily analysed in decentralized configurations compared to centralized configurations (Scattolini, 2009). Sandell *et al.* (1978) examined the tasks of the coordinator and the flow between the hierarchies. Sandell *et al.* (1978) concluded that measurements and decisions should be exchanged error-free and delayed. Otherwise, a single controller should be implemented (Sandell *et al.,* 1978). The economic benefit of implementing a sophisticated control hierarchy depends on the higher levels, and optimality depends on the underlying control structure (Richalet *et al.,* 1978).

Scattolini (2009) summarized control hierarchies with different classifications and collected examples of hierarchical MPC system implementations. In Scattolini (2009), the following hierarchical control structures are reviewed:

- *Hierarchical control for coordination*
  The system is divided into different subsystems with interactions among them. The subsystems are controlled by regulators separately, which are themselves coordinated by a coordinator. The coordinator provides the regulators the constraints and optimal prices, which "coincide with the Lagrange multipliers of the coherence constraints in the global optimization problem" (Scattolini, 2009). The optimum of the regulators are calculated locally and send back to the coordinator. At the coordinator, the next global optimization problem is solved and the new constraints are sent back. This iterative process is stopped if the variables satisfy the conditions and constraints.
- *Hierarchical control of multilayer systems*
  Hierarchical multilayer control systems work with different time scales at each layer (Scattolini, 2009)
  - *Hierarchical control of multi time scale systems*
    A system with fast and slow dynamics is controlled by regulators with different frequencies for the output variables. The first controller calculates the output for the slow control input of the system. The second controller calculates the fast control input for the system based on the fast trajectory of the first controller.
  - *Control of systems with hierarchical structure*
    The first layer has a slow dynamic and calculates a long scale optimum. The second layer consists of regulators with faster dynamics. The slow dynamics output is the trajectory of the fast dynamics layer. The stated problem is a cascade feedback control system.
  - *Hierarchical control for plantwide optimization*
    The optimum is calculated concerning economic criterion in the first layer. The underlying layer tries to execute or follow the values from the first layer. The model accuracy can be designed in two ways: In the first layer, a model with higher accuracy than in the following layer is implemented or vice versa.

3.3 Sensible Heat Storage

Beckmann *et al.* (1984) defined a thermal energy storage (TES) as a process which is storing energy during charge and discharge operations. It consists of a vessel, the storage medium, charging and discharging devices, and auxiliaries. Its primary task is to overcome the discrepancy between the energy supply and the energy demand. This discrepancy can be a mismatch of the available time, a mismatch of the location, a mismatch of the kind of the used and provided energy, for example, fluctuate or steady energy supply, or a mismatch of the amount of heat supplied and demanded (Beckmann *et al.,* 1984). The principle process of a TES is the same for all types of TES and includes the following process steps: charging, storing, and discharging (Dincer *et al.,* 2013). Dincer *et al.* (2013) and Dinçer (1997) summarized the use of an Energy

Storage results in:

- Reduced energy costs.
- Reduced energy consumption.
- Improved indoor air quality.
- Increased flexibility of operation.
- Reduced initial and maintenance costs.
- Reduced equipment size.
- More efficient and effective utilization of equipment.
- Conservation of fossil fuels (by facilitating more efficient energy use and/or fuel substitution).
- Reduced pollutant emissions (e.g., CO 2 and chlorofluorocarbons (CFCs)).

Garg *et al.* (1985) categorised TES into two main types: sensible heat storage (SHS) and latent heat storage (LHS). Only the SHS is treated in this thesis. The energy can be stored in a TES by rising or lowering the temperature of a material without a phase change, called a SHS. If the material used for the heat storage is a fluid, it is called heat transfer fluid (HTF). The use of a HTF and a tank design with separate inlets and outlets makes it possible to charge and discharge the SHS simultaneously (Abhat, 1981). If a HTF with a temperature higher compared to the mean tank temperature is pumped into the top of the SHS and a HTF with a lower temperature compared to the tank temperature is pumped into the bottom of the SHS, the difference of the density leads to water layers with different temperatures. The sensible heating is described in Eq. (3.12).

$$H_{\text{load}} = V \cdot \rho \cdot cp \cdot (T_2 - T_1) \tag{3.12}$$

H_{load} is the loaded or unloaded enthalpy of the TES. V is the volume, cp is the heat capacity of the HTF or material or combination of both, ρ is the density, and T_2 is the temperature after the charging and T_1 is the temperature before the charging of the TES. The primary use of the SHS is to buffer and provide the peak demand energy, which the available heat supply cannot provide in the needed period.

4 Methods

The Energy Demand Control System (EDCS) is an online, predictive and holistic, and reconfigurable control system (Windholz, 2018-2021) and was newly developed in the course of the project Energy Demand Control System - PROcess Optimization For industrial low temperature systems (EDCSproof). It is a two-layer hierarchical model predictive control (MPC) that controls the energy supply of a plant. Before applying the EDCS to a plant, its performance and robustness must be validated in simulation studies.

In this thesis, the subsystem of an industrial plant was investigated. The system consists of a heat supply, a sensible heat storage (SHS), and a heat demand. Industrial measurement data was utilized for the modelling and validation process of a simulation. Additional functionality were added to the EDCS, for correcting the heat demand prediction online. Simulation studies were conducted to verify and validate the robustness, stability, correctness of the functionality, and applicability of the EDCS. Furthermore, a simulation study investigated the unpredicted operations of the employees and their consequences on the process quality. The added functionality of the EDCS and its ability to ensure process quality was examined. The performance of the EDCS was quantified by analyzing the effect on the energy consumption and energy cost.

In this thesis, the following research questions are answered:

1. Is it possible to use the measured data to develop a valid simulation model of the plant for testing the EDCS?
2. Can the EDCS be used to control the investigated energy supply system?
3. How robust is the EDCS against unpredicted interactions of human operators?
4. Which influence has the EDCS on the cost and quality of the process?

In the course of this chapter, the methods for the preparation and preprocessing of the measured data are defined and the prediction data are calculated in Section 4.1. The modelling of the simulation model is shown in Section 4.2 and the verification and validation (V&V) methodology of the components and the complete model is presented in Section 4.3. The functionality of the EDCS is explained and its structure is stated in Section 4.4. At last the simulation study is introduced and explained in Section 4.5.

4.1 Data

Due to computation time reasons, constant values were chosen for the material parameters, instead of calculating the parameters for each temperature. Density and heat capacity of water were chosen (VDI, 2013):

- density water at 80°C $\rho_{w80} = 971.8^{kg}/_{m^3}$
- specific heat capacity, water, constant pressure, 80°C $cp_{w80} = 4196^{j}/_{kg \cdot K}$

The measuring devices depicted in Figure 2.1 recorded the following values:

- Q_i: measured heat data, in W
- T_i: measured temperature data, in °C
- G_i: measured valve data, in %
- S_i: measured rotation speed, in rpm

The following meanings apply to the indices:

- measured (meas): This data was measured by a device in the plant.
- prepared (prep): This data was altered through the validation process.
- calculated (calc): This data was calculated by the simulation.
- predicted (pred): This data was used as a prediction for the EDCS.
- real (real): This data was used as the input heat demand data for the simulation and differs from the predicted data.
- reference (ref): This data was used as a reference for the least square (LS) fit.

Where i is an enumeration for the identification of the measurement devices. Variable names without one of the stated indices refer to the measurement device with the corresponding index.

Some of the parameters were taken from the datasheet and some were estimated by a LS fit between the calculated output of the component model and the measured data. Eq. (4.1) and Eq. (4.2) show the problem which was minimized by a LS fit with the trust region approach (Coleman *et al.,* 1996).

$$y_{\text{out}j} = f(\theta, x_{\text{in}j}) \tag{4.1}$$

$$\min_{\theta} \sum_{j=1}^{n} (y_{\text{out}j} - y_{\text{ref}j})^2 \tag{4.2}$$

f is the function which calculates a comparable output $y_{\text{out}j}$ for the reference data $y_{\text{ref}j}$, with the set of parameters θ and the input data for each step $x_{\text{in}j}$. The square error is computed for all steps n. The algorithm minimizes the quadratic error by optimizing the parameters θ.

The model and its V&V depends on the underlying data quality and validity. Therefore data validation was processed first. As reviewed in Section 3.1, data must be prepared and available in the desired accuracy. Measurement imperfections such as outliers were removed and missing data points were interpolated. Due to missing and inconsistent data, a set of trustworthy and consistent data was defined and missing data was calculated with enthalpy balances. The data preparation was done to increase the consistency level. Afterwards the validity and the credibility of the data were examined by a consistency analysis, face validation, and scenario analysis. Prediction data for the heat demand was calculated with the algorithm of Fuhrmann *et al.* (2020) in Subsection 4.1.1.

4.1.1 Heat prediction Q_{189}, Q_{190}, Q_{191}, and Q_{192}

The EDCS needs an accurate prediction of the heat demand $Q_{189}, Q_{190}, Q_{191}$, and Q_{192}. The prediction is used to calculate future states and inputs to the energy supply. The heat prediction was calculated with measured heat data. Fuhrmann *et al.* (2020) presented a calculation of the prediction of pulsed heat load demand. First, the data must fulfil the following assumptions (Fuhrmann *et al.,* 2020):

- The start and end time of the heat demand must be known.
- The desired temperature of the heat demand must be known.
- The integral heat per heat treatment (HT) must be known.
- The heat demand has an initial peak and decreases exponentially.

A prediction can be computed for each HT based on a calculated time constant τ and the integral amount of heat $\dot{Q}_{\mathrm{HT}}$ per HT. The calculation of the HT prediction is presented in Eq. (4.3) (Fuhrmann *et al.,* 2020).

$$\dot{Q}_{\mathrm{HT_{pred}}}(t) = \dot{Q}_{\mathrm{HT}} \cdot (1 - e^{-\frac{t}{\tau}}), 0 < t < t_{\max} \tag{4.3}$$

$\dot{Q}_{\mathrm{HT_{pred}}}$ is the prediction data for one HT and $\dot{Q}_{\mathrm{HT}}$ is the integral amount of heat for one HT. t is the time and τ is the calculated time constant. The parameter $t_{\max}$ was chosen for each HT separately. If the heat $\dot{Q}_{\mathrm{HT_{pred}}}(t)$ function value is lower than 1 W, the parameter $t_{\max}$ is set to the number of the elapsed function values. The rest heat of the exponential function was added equally to all of the generated function values, ensuring that the heat amount is equal to the measured one. The time constant τ was calculated by first choosing the HT's where the usable enthalpy level in the SHS was twice the demanded heat. Second, the time constant τ can be computed with the HT's, which satisfies the stated conditions. In Eq. (4.4), the time constant τ is calculated (Fuhrmann *et al.,* 2020).

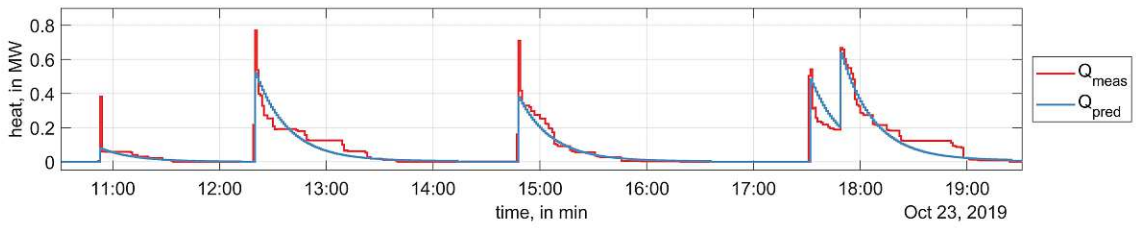

Figure 4.1: The measured heat demand $\dot{Q}_{\text{meas}}$ is compared with the predicted heat demand $\dot{Q}_{\text{pred}}$ as a function of time.

$$\tau = \frac{\sum_{v=1}^{M} \frac{0.95 \cdot \dot{Q}_{\text{HT}_v}}{3}}{M} \tag{4.4}$$

τ is the time constant for the computation of the predicted HT, M is the number of all chosen HT's, and $\dot{Q}_{\text{HT}_\text{v}}$ is one HT. Figure 4.1 compares the calculated heat demand prediction $\dot{Q}_{\text{pred}}$ with the measured heat demand data $\dot{Q}_{\text{meas}}$. The prediction fits reasonably to the measured data with a slight deviation from the measured one. Further analysis of the fit was done in Fuhrmann *et al.* (2020). The integral heat is the same for the prediction and the measured HT.

4.2 Modelling

The modelling process started with defining model requirements. Model requirements were derived from the project goals, respectively, the research questions. They were specified separately for the components and the overall model. Simulation objectives, necessary performance, and structure conditions were stated. Simulation scenarios for the EDCS were defined and had to be executable.

The next activity in the modelling process was the demarcation of the physical system and its components from their environment. The environment was defined and the relationship and uncertainties between the system and its surroundings were identified. System boundaries were chosen based on the measured data and components were separated, to create small logical model units. The usual production environment and scenarios for the simulation were defined.

The physical models were identified by the measured and prepared data and the knowledge of involved system operators of the facility. No experimentation data was available. The main processes, relationships, constraints, variables, and goals were identified, relevant data was collected, and minor dynamics were neglected. Simplifications of the models were made in all three categories: *omission*, *aggregation*, and *substitution*. *Omission* means that physical processes are neglected in the model, as cooling effects, fluid friction, or changing density at changing temperature. *Aggregation* means that physical effects are combined, as the heat transfer between stagnant layers of water and heat transfer by turbulent flow combined with one correction factor. *Substitution* means that known values are substituted by simple ones, for

example, the infinite number of layers in a SHS, which are substituted to a reasonable number. These abstractions and the reduction to the main physical theory follow the principle of Occam's razor. The philosophy is to use a known, limited model rather than a complex model. Complex models require more resources like computation time and V&V costs and lead to few model improvements.

The models are described by physical laws and are mainly partial differential equation (PDE)'s, combined with analytical models. They are deterministic and discrete. Black box or grey box models were not used because the measured data could not meet the requirements for the identification, and universal models, usable for various energy supply systems, were desired. The data was separated into identification data (2/3) and validation data (1/3).

The used PDE's were numerically discrete solved with the explicit Euler method, which meets the prerequisite of the EDCS. The fixed step size was chosen as $t_s = 60$ seconds because the measurement frequency and the standard sampling interval of the EDCS was one minute. The representation of the output data is zero order hold. The model is implemented in the development software Matlab/Simulink 2019b because of the prerequisites of the EDCS (MATLAB, 2019).

From Subsection 4.2.1 to Subsection 4.2.6, the components of the plant are described, delimited from their environment, and equations are defined. Further, parameters and restrictions are stated. The resulting simulation model, its requirements, and input data are defined in Subsection 4.2.7. The modelling of the components follows the same structure:

1. The component is described.
2. The delimited component is presented with its inputs and outputs and the functionality is explained.
3. Parameters are stated.
4. Restrictions of the model are defined.

4.2.1 Sensible Heat Storage

The used model for the SHS is based on Streckiene *et al.* (2011) and Eicker (2005) who described an analytical model of a SHS. The SHS is divided up into several layers with constant volume. The enthalpy balance differential equation for each layer is solved separately. The main features, the charging, the discharging, and the heat loss through the wall, are implemented. Additional internal turbulent flow is represented by a multiplication factor. Figure 4.2 shows the input and output of the SHS model. $\dot{m}_{\mathrm{cold_{in}}}$ and $T_{\mathrm{cold_{in}}}$ are the mass flow and temperature into the buffer storage from the heat exchange, $\dot{m}_{\mathrm{hot_{in}}}$ and $T_{\mathrm{hot_{in}}}$ are the mass flow and temperature into the buffer storage from the heat pump (HP), $T_{\mathrm{hot_{out}}}$ is the temperature out of the SHS to the heat exchange and $T_{\mathrm{cold_{out}}}$ is the temperature out of the SHS to the HP. $\dot{Q}_{\mathrm{loss}}$ is the heat loss of the model through the tank wall.

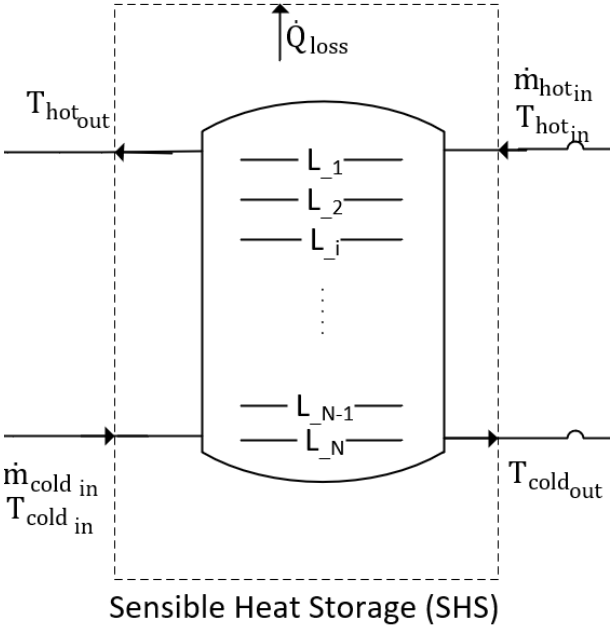

Figure 4.2: The SHS model and its inputs and outputs, set as arrows.

The model equations first calculate the resulting direction for the internal mass flow for the layers, Eq. (4.5). If the resulting mass flow is positive, the water flows from top to bottom. If the resulting mass flow is negative, the water flows from bottom to top. For each layer, the enthalpy balance differential equation is rearranged and the change of temperature $\frac{dT_i}{dt}$ is calculated. Afterwards, the resulting temperature changes are merged by a parameter called mix_{factor}, which maps a turbulent internal flow and leads to tight temperature layers. Eq. (4.6) to Eq. (4.11) shows the differential equations for the layers for both resulting signs of Eq. (4.5). Eq. (4.12) shows the post processing of the change of temperature $\frac{dT_i}{dt}$ with the mix_{factor}.

$$\dot{m}_{\Delta} = \dot{m}_{hot_{in}} - \dot{m}_{cold_{in}} \tag{4.5}$$

1. $\dot{m}_\Delta >= 0$

$$i = 1: \quad \rho \cdot cp \cdot V_\Delta \cdot \frac{dT_1}{dt} = cp \cdot \dot{m}_{\text{hot}_{\text{in}}} \cdot (T_{\text{hot}_{\text{in}}} - T_1) + k \cdot A_\text{h} \cdot \frac{T_2 - T_1}{h_\Delta} + \alpha_\text{w} \cdot A_{\text{l}\Delta} \cdot (T_\text{outside} - T_1) \tag{4.6}$$

$$1 < i < N: \quad \rho \cdot cp \cdot V_\Delta \cdot \frac{dT_i}{dt} = cp \cdot \dot{m}_\Delta \cdot (T_{i-1} - T_i) + k \cdot A_\text{h} \cdot \frac{T_{i+1} - 2 \cdot T_i + T_{i-1}}{h_\Delta} + \alpha_\text{w} \cdot A_{\text{l}\Delta} \cdot (T_\text{outside} - T_i) \tag{4.7}$$

$$i = N: \quad \rho \cdot cp \cdot V_\Delta \cdot \frac{dT_\text{N}}{dt} = cp \cdot \dot{m}_{\text{cold}_{\text{in}}} \cdot (T_{\text{cold}_{\text{in}}} - T_\text{N}) + cp_{\text{w80}} \cdot \dot{m}_\Delta \cdot (T_{\text{N}-1} - T_\text{N}) + k \cdot A_\text{h} \cdot \frac{T_{\text{N}-1} - T_\text{N}}{h_\Delta} + \alpha_\text{w} \cdot A_{\text{l}\Delta} \cdot (T_\text{outside} - T_\text{N}) \tag{4.8}$$

2. $\dot{m}_\Delta < 0$

$$i = 1: \quad \rho \cdot cp \cdot V_\Delta \cdot \frac{dT_1}{dt} = cp \cdot \dot{m}_{\text{hot}_{\text{in}}} \cdot (T_{\text{hot}_{\text{in}}} - T_1) + cp_{\text{w80}} \cdot \dot{m}_\Delta \cdot (T_1 - T_2) + k \cdot A_\text{h} \cdot \frac{T_2 - T_1}{h_\Delta} + \alpha_\text{w} \cdot A_{\text{l}\Delta} \cdot (T_\text{outside} - T_1) \tag{4.9}$$

$$1 < i < N: \quad \rho \cdot cp \cdot V_\Delta \cdot \frac{dT_i}{dt} = cp \cdot \dot{m}_\Delta \cdot (T_i - T_{i+1}) + k \cdot A_\text{h} \cdot \frac{T_{i+1} - 2 \cdot T_i + T_{i-1}}{h_\Delta} + \alpha_\text{w} \cdot A_{\text{l}\Delta} \cdot (T_\text{outside} - T_i) \tag{4.10}$$

$$i = N: \quad \rho \cdot cp \cdot V_\Delta \cdot \frac{dT_\text{N}}{dt} = cp \cdot \dot{m}_{\text{cold}_{\text{in}}} \cdot (T_{\text{cold}_{\text{in}}} - T_\text{N}) + k \cdot A_\text{h} \cdot \frac{T_{\text{N}-1} - T_\text{N}}{h_\Delta} + \alpha_\text{w} \cdot A_{\text{l}\Delta} \cdot (T_\text{outside} - T_\text{N}) \tag{4.11}$$

N is the number of constant volume layers in the SHS. V_Δ is the SHS volume divided by the number of layers N. $\dot{m}_{\text{hot}_{\text{in}}}$ is the hot mass flow and $\dot{m}_{\text{cold}_{\text{in}}}$ is the cold mass flow into the SHS. T_i is the temperature of the layer j. h_Δ is the height of one layer. A_h is the horizontal area of the cylindrical SHS. $A_{\text{l}\Delta}$ is the lateral area of the SHS. α_w is the heat transfer coefficient of the wall of the SHS. k is the thermal conductivity of water.

$$\frac{dT}{dt} = \frac{dT}{dt} - (T - \frac{\sum_{i=1}^{N} T_i}{N} \cdot mix_\text{factor}) \tag{4.12}$$

$\frac{dT}{dt}$ is the calculated change of temperature for each layer, T is the temperature of the previous step of each layer and mix_factor is a factor tightening the temperature layers.

The dimensions of the SHS are:

- Diameter: 1.9m

- Volume: 12.7m³

For the model, five equidistant layers with constant volume and various temperatures, distributed over the height of the SHS, were chosen. The computed temperatures could be compared to the temperature data of the five temperature sensors, which were distributed over the height of the SHS in the plant.

The heat transfer coefficient α_w, which describes the heat loss through the wall of the SHS, was computed by the loss of enthalpy H_Δ, during periods in time with no charge or discharge of the SHS. 51 periods with only heat loss through the wall could be identified in the chosen period from Section 4.2. They were divided into an identification and a validation part. The first 34 periods were used for the identification part and the last 17 periods were used for the validation part. The change of enthalpy H_{Δ_k} in each time step j was calculated from the measured temperature difference data and a resulting heat transfer coefficient α_w for each time step was computed. The resulting heat transfer coefficient α_w is the mean of the coefficients of each time step. Eq. (4.13) shows the change of enthalpy for one time step and Eq. (4.14) shows the equation of the heat transfer coefficient α_w.

$$H_{\Delta_j} = \sum_{i=1}^{N} (T_{(j+1)_i} - T_{j_i}) \cdot cp_{w80} \cdot \rho_{w80} \cdot \frac{V}{N} \tag{4.13}$$

$$\alpha_w = \frac{1}{n} \cdot \sum_{j=1}^{n} \frac{H_{\Delta_j}}{60s \cdot A_{l\Delta} \cdot \sum_{i=1}^{N} (T_{\text{outside}_j} - T_{j_i})} \tag{4.14}$$

H_{Δ_j} is the change of enthalpy in the SHS for one time step, j is the index for one time step and i is the index for the Layer. T_{j_i} is the temperature for a time step and a Layer and T_{outside_j} the temperature outside the tank. $A_{l\Delta}$ is the lateral area of one Layer of the SHS. α_w is the heat transfer coefficient for the wall of the SHS and n is the number of measured values.

The coefficient for the thermal conductivity of water k between the layers, was chosen by Eicker (2005) as 0.644 $^W/_{m \cdot K}$. The specific heat capacity cp and the density ρ were chosen in Section 4.1. The following parameters for the SHS were chosen:

- $N = 5$
- $V_\Delta = 2.54m^3$
- $h_\Delta = 0.8959m$
- $A_h = 2.835m^2$
- $A_{l\Delta} = 6.4815m^2$
- $\alpha_w = 1.6528\ ^W/_{m^2 \cdot K}$
- $k = 0.644\ ^W/_{m \cdot K}$
- $mix_{\text{factor}} = 5.85984 \cdot 10^{-4}$

In further calculations, the state of charge (SOC) of the SHS, which describes the enthalpy in the SHS, was used. The SOC is calculated by subtracting the enthalpy level at the minimum allowed temperature from the measured enthalpy with reference to 0°C. Eq. (4.15) calculates the enthalpy level at the minimum allowed temperature and Eq. (4.16) calculates the SOC of the SHS.

$$H_{\min} = T_{\min} \cdot cp_{\mathrm{w80}} \cdot \rho_{\mathrm{w80}} \cdot V \tag{4.15}$$

$$SOC = \sum_{i=1}^{N} (T_i - T_{\min}) \cdot cp_{\mathrm{w80}} \cdot \rho_{\mathrm{w80}} \cdot V/N \tag{4.16}$$

$H_{\min}$ is the minimum enthalpy level allowed in the SHS. $T_{\min}$ is the minimum allowed temperature in the SHS and T_i is the actual temperature of one layer in the SHS.

Simplifications were made in the model. Internal flows which can influence the mixture of the layers are approximated. The convective heat transfer is neglected. Five layers were chosen for comparison reasons which was an approximation to the real layer distribution. The model is technically not restricted to non-physical states but restrictions for its use are stated. It is not allowed to exceed the temperature above the boiling temperature of water (100°C) and lower the temperature below the freezing temperature of water (0°C). The layer temperatures are calculated with the heat capacity and the density of water at a temperature of 80°C. The SHS model causes a one step delay from its input to its output.

4.2.2 Heatpump

A HP can be used in two ways: First, heating up the heat sink to a desired temperature by enough heat supply at the heat source, called HP. Second, cooling down the heat source to a desired temperature by heat exchange at the heat sink, called chiller. In this thesis, only the HP configuration was used.

The used HP model in this thesis is a model from the AIT (2020). It was designed and developed in Modelica from Dymola (Dassault Systèmes, 2020; Modelica Association, 2020) and was packed as a functional mockup unit (FMU), a format to exchange models between different development software. The model was allowed in this work to be used explicitly.

The HP is used to provide the heat for the heat demand by charging the SHS. Figure 4.3 shows the model with its input and output. The HP is grouped with a valve G_{120} at the heatsink and a valve G_{130} at the heatsource with two correspondent constant mass flow pumps P10 and P11, ensuring the designed mass flow for the heat exchangers. The valves G_{120} and G_{130} are PID controlled and shall ensure a desired temperature difference for the heat exchangers by opening and closing the valve between 0% and 100% and feedback the outlet of the heat exchanger. $\dot{m}_{\mathrm{sink_{out}}}$ and $T_{\mathrm{sink_{out}}}$ are the mass flow and temperature out of the HP model, at the heat sink, controlled by the valve G_{120}. $\dot{m}_{\mathrm{source_{out}}}$ and $T_{\mathrm{source_{out}}}$ are the mass flow and temperature out of the HP model, at the heat source, controlled by the valve G_{130}. $T_{\mathrm{sink_{in}}}$ is the temperature into the HP at the heat sink and $T_{\mathrm{source_{in}}}$ is the temperature into the HP at the heat source. U_{HP} is

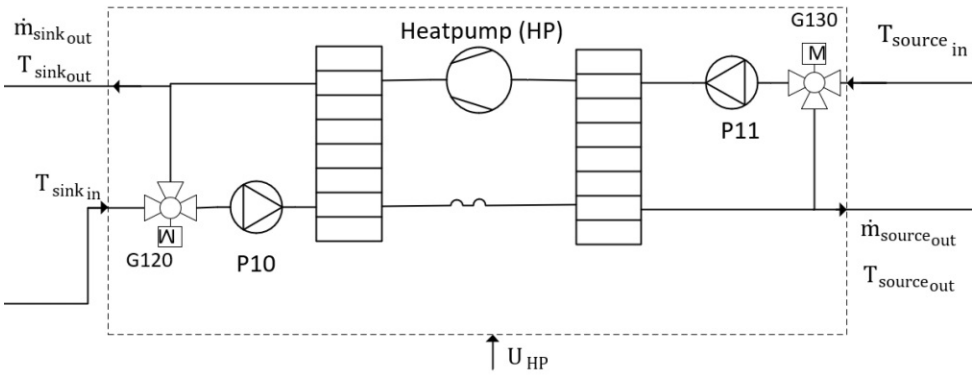

Figure 4.3: The HP model and its inputs and outputs, set as arrows. The included components are grouped.

the input for the power of the compressor in %. The valves and pumps at the heat sink and the heat source are integrated into the model. The following parameters can be adjusted: the desired temperature difference at the heat sink dT_{sink}, the desired temperature difference at the heat source dT_{source}, the desired output temperature at the heat sink $Tset_{\text{sink}_{\text{out}}}$ and the desired power at the heat sink $\dot{Q}_{\text{sink}_{\text{design}}}$. The parameter cs is the compressor scaling and reduces the design power to a level between 0% and 100%.

dT_{sink}, dT_{source} and $Tset_{\text{sink}_{\text{out}}}$ were chosen from the datasheet. The FMU is designed for the design values. The design power value of $\dot{Q}_{\text{sink}_{\text{design}}}$ is 206 kW according to the datasheet but the compressor power was reduced to 78%. The power of the real plant HP heat at the heat sink decreases not linearly with the reduction in percent, but exact curves were not known. Therefore the $\dot{Q}_{\text{sink}_{\text{design}}}$ had to be fitted to the data. Because of stability reasons of the FMU model, it was not possible to optimize the heat power by a least square fit. The metric value normalized root mean squared error (NRMSE) defined in Section 4.3 between the measured heat and the simulated heat at the heat sink was minimized to a value of 0.3098 by manually setting the compressor scaling cs and ensuring stability at the chosen value. The following parameters were chosen:

- $dT_{\text{sink}} = 5.52$ K
- $dT_{\text{source}} = 5.9$ K
- $Tset_{\text{sink}_{\text{out}}} = 84$ °C
- $\dot{Q}_{\text{sink}_{\text{design}}} = 206$ kW
- $cs = 0.78$

The model is technically restricted to physical states. Therefore it is impossible to exceed the heat sink or heat source temperature above the cooking temperature of water (100°C) and lower the temperature below the freezing temperature of water (0°C). Further restrictions are implemented for the internal refrigerant temperature and pressure. The model interrupts if the heat supply temperature is too low or the input U_{HP} is set between $0\% < U_{\text{HP}} < 30\%$ for an

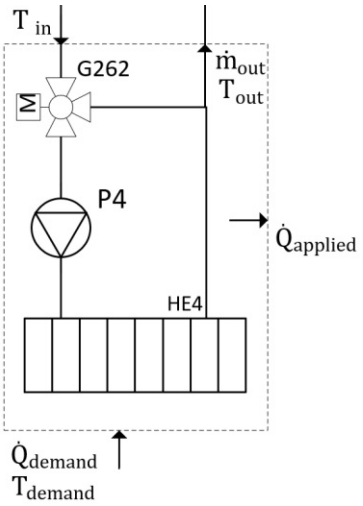

Figure 4.4: The heat exchange model and its inputs and outputs, set as arrows. The included components are grouped.

undefined duration which can cause nonphysical states internally. The start behaviour of the HP is not modelled and cannot be simulated. The HP model causes a one step delay from its input to its output.

4.2.3 Heat exchange

Figure 4.4 shows the heatexchange model with its input and output. The heat exchanger model is grouped with a constant mass flow pump Pxx and a valve G_{xxx} which is proportional-integral-derivative (PID) controlled. The PID controller applies a desired difference temperature between the input and the output temperature by changing the valve's position between 0% and 100%. The valve influences the input and output mass flow $\dot{m}_{\text{out}}$ of the model and leads to a maximum mass flow at 100%. The constant mass flow of the pump ensures the desired mass flow through the heat exchanger.

The input of the heat exchanger model is the heat demand $\dot{Q}_{\text{demand}}$ and the demand temperature T_{demand}. The demand temperature is the HT minimum temperature at which a heat exchange in the correct direction is possible. T_{in} and T_{out} are the input and output temperatures of the model. $\dot{Q}_{\text{applied}}$ is the applied heat and can differ from $\dot{Q}_{\text{demand}}$ if the input temperature T_{in} falls below the demand temperature T_{demand}. The difference heat between $\dot{Q}_{\text{applied}}$ and $\dot{Q}_{\text{demand}}$ of the current step will be added as $\dot{Q}_{\text{integrator}}$ to the next step heat demand $\dot{Q}_{\text{demand}}$. The following parameters can be adjusted: the heat capacity of the used fluid cp, the maximum mass flow of the pump $\dot{m}_{\text{max}}$, the maximum exchangeable heat $\dot{Q}_{\text{max}}$, and the desired temperature difference of the heat exchanger ΔT. Eq. (4.17) to Eq. (4.27) shows the calculation of the mass flow $\dot{m}_{\text{out}}$ and the temperature T_{out}.

$$\dot{Q}_{\text{demand}} + \dot{Q}_{\text{integrator}} < \dot{Q}_{\max} \qquad \dot{Q}_{\text{applied}} = \dot{Q}_{\text{demand}} + \dot{Q}_{\text{integrator}} \tag{4.17}$$

$$\dot{Q}_{\text{demand}} + \dot{Q}_{\text{integrator}} > \dot{Q}_{\max} \qquad \dot{Q}_{\text{applied}} = \dot{Q}_{\max} \tag{4.18}$$

$$\dot{m}_{\text{tar}} = \frac{\dot{Q}_{\text{applied}}}{\Delta T_{\text{tar}} \cdot cp} \tag{4.19}$$

$$\dot{m}_{\text{tar}} > \dot{m}_{\max}: \qquad \dot{m}_{\text{tar}} = \dot{m}_{\max} \tag{4.20}$$

$$\Delta T = \frac{\dot{Q}_{\text{applied}}}{\dot{m}_{\text{tar}} \cdot cp} \tag{4.21}$$

$$T_{\text{in}} > T_{\text{demand}}: \qquad T_{\text{out}} = T_{\text{in}} - \Delta T \tag{4.22}$$

$$\dot{Q}_{\text{applied}} = \dot{Q}_{\text{applied}} \tag{4.23}$$

$$\dot{m}_{\text{out}} = \dot{m}_{\text{tar}} \tag{4.24}$$

$$T_{\text{in}} < T_{\text{demand}}: \qquad T_{\text{out}} = T_{\text{in}} \tag{4.25}$$

$$\dot{Q}_{\text{applied}} = 0 \tag{4.26}$$

$$\dot{m}_{\text{out}} = 0 \tag{4.27}$$

$\dot{Q}_{\text{demand}}$ is the heat demand and T_{demand} is the necessary minimum temperature for the heat demand. $\dot{Q}_{\text{applied}}$ is the applied heat of the model, which can differ from the demand. $\dot{Q}_{\text{integrator}}$ is the heat amount that was not exchanged and is added to the heat in the next step. $\dot{Q}_{\max}$ is the maximum possible heat that can be exchanged in one step. cp is the heat capacity of the fluid, ΔT_{tar} is the desired temperature difference between the input and the output temperature and $\dot{m}_{\text{tar}}$ is the target mass flow with the temperature difference ΔT_{tar}. $\dot{m}_{\text{tar}}$ differs from $\dot{m}_{\text{out}}$ because the model pump is limited to a maximum and minimum mass flow $\dot{m}_{\max}$ and $\dot{m}_{\min}$. ΔT is the applied temperature difference depending on the mass flow $\dot{m}_{\text{tar}}$. T_{out} is the output temperature and $\dot{m}_{\text{out}}$ the output mass flow.

The parameter ΔT_{tar} had to be fitted to the measured data because there was no datasheet for the heat exchangers HE1, HE2, HE3, and HE4. A LS fit, described in Section 4.1, was used to find the parameter by comparing the simulation output T_{out} to the measurement temperature T_{33}. Each of the heat exchangers was fitted separately. HT identification data for the input for each heat exchanger, when only the heat exchanger of interest is active, were collected and the parameter ΔT_{tar} was fitted.

The fitted temperature ΔT_{tar} for the heat exchangers HE1, HE2, HE3, and HE4 was 5.16K on average. Due to the fact that similar heat exchangers were used and for simplification reasons, the value 5K was used. The output mass flow $\dot{m}_{\max}$ is limited by a valve in the output pipe. The first heat exchanger HE1 has a smaller dimension and lower parameters compared to the others.

The model's heat capacity was chosen as the heat capacity of water at 80°C. The maximum possible heat exchange $\dot{Q}_{\max}$ was set to 1MW for each component. The desired temperature difference ΔT_{tar} was set to 5K for each component. The maximum mass flow of the heat exchange component HE1 was set to $4.3^{kg}/_{s}$. The maximum mass flow of the heat exchange

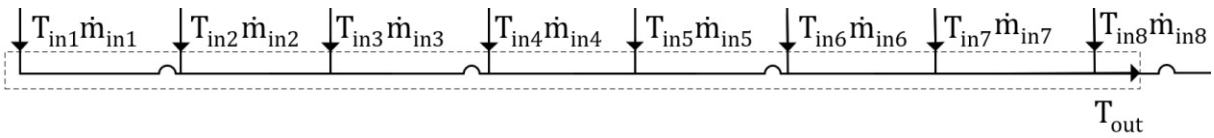

Figure 4.5: The mixing pipe model and its inputs and outputs, set as arrows.

components HE2, HE3, and HE4 was set to $8.5^{kg}/_{s}$

The model restricts the possible heat $\dot{Q}_{\text{demand}}$ to the maximum heat $\dot{Q}_{\text{max}}$. If the input temperature T_{in} is higher than the demand temperature T_{demand}, the heat $\dot{Q}_{\text{demand}}$ can be exchanged, although a limitation occurs in the real world system at high heat values $\dot{Q}_{\text{demand}}$ caused by the heat exchanger design or the temperature of the batch consumer (BC). The limitation to the maximum heat and mass flow leads to a maximum temperature difference of 28K. The heat exchange model causes a one step delay from its input to its output which corresponds to the observed behaviour in the data from Subsection 5.1.1.

4.2.4 Mixing Pipe

Several pipes can be connected to one pipe in hydraulic systems, which can be called distributor pipes. In the plant, distributor pipes are installed to merge the mass flow of the different heat exchanger flows. The mixing pipe model merges the temperatures relative to their mass flows. Eight pipes can be connected. Figure 4.5 shows the model with eight inlets $T_1 - T_8$ and $\dot{m}_1 - \dot{m}_8$ and one outlet T_{out}. Eq. (4.28) shows the calculation of the output temperature.

$$T_{\text{out}} = \frac{\sum_{i=1}^{8} T_{\text{in}_i} \cdot \dot{m}_{\text{in}_i}}{\sum_{i=1}^{8} \dot{m}_{\text{in}_i}} \tag{4.28}$$

T_{in_i} and $\dot{m}_{\text{in}_i}$ are the temperatures and the mass flow of one inlet and T_{out} is the temperature of the outlet.

The heat loss through the pipe wall, a possible delay and turbulent flow are neglected. The outgoing mass flow is not used. Instead of, the calculated mass flow of the connected pump is used because of the hydraulic balancing.

4.2.5 Pump

The variable mass flow pump is configured to ensure a constant differential pressure of nearly zero bar. If a connected pump-valve combination changes the valve position, the mass flow changes. The constant differential pressure pump raises the mass flow to ensure the desired mass flow and ensure a pressure of nearly zero bar. The connected pumps are, according to the valve position, supplied by enough pressure. A minimum mass flow ensures a differential pressure of nearly zero bar if no heat exchange valve is open. The desired differential pressure is usually configured as low as possible just to overcome the friction of the pipe system.

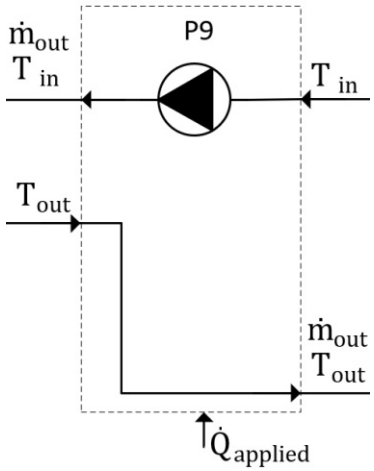

Figure 4.6: The pump model and its inputs and outputs, set as arrows.

The inputs to the model are the applied heat of the heat exchanger, the input temperature, and the output temperature of the connected system. The temperatures are necessary to calculate the mass flow with the enthalpy balance. Figure 4.6 shows the variable mass flow pump model with its inputs and outputs. T_{in} is the incoming temperature which is feed through to the outlet with the mass flow $\dot{m}_{\text{out}}$. T_{out} is the temperature after the heat exchange and is feed through to the output with the mass flow $\dot{m}_{\text{out}}$. $\dot{Q}_{\text{applied}}$ is the heat that is applied by the connected heat exchangers. The pump is active if heat $\dot{Q}_{\text{applied}}$ is exchanged. The variable mass flow pump is connected to the SHS with the inlet T_{in}. Further, it is connected to several heat exchangers, supplied with the temperature T_{in} and the mass flow $\dot{m}_{\text{out}}$. The pump model receives the applied heat $\dot{Q}_{\text{applied}}$ from the heat exchange models with the corresponding temperature T_{out} and calculates the mass flow $\dot{m}_{\text{out}}$ and T_{out}. The following parameters can be adjusted: the heat capacity of the used fluid cp, the maximum mass flow of the pump $\dot{m}_{\text{max}}$, and the minimum mass flow $\dot{m}_{\text{min}}$ of the pump if it is active. Eq. (4.29) shows the calculation of the mass flow.

$$\dot{m}_{\text{out}} = \frac{\dot{Q}_{\text{applied}}}{cp \cdot (T_{\text{out}} - T_{\text{in}})} + \dot{m}_{\text{min}} \tag{4.29}$$

cp was chosen in Section 4.1 and $\dot{m}_{\text{max}}$ was chosen from the datasheet and cannot be exceeded. The minimum mass flow $\dot{m}_{\text{min}}$ is equal to the identified minimum pump mass flow $\dot{m}_{\text{P9}_{\text{min}}}$ from Subsection 5.1.3. The calculated mass flow cannot fall below this minimum if the pump is active. The following parameters were chosen for the pump P9:

- $cp = cp_{\text{w80}}$
- $\dot{m}_{\text{max}} = 13.5 {}^{kg}/_{s}$
- $\dot{m}_{\text{min}} = 1.5056 {}^{kg}/_{s}$

The pump model is only active if heat is applied. The model neglects that the pump is active if

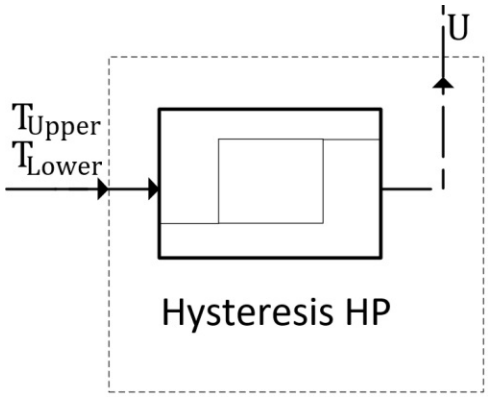

Figure 4.7: The hysteresis controller model and its inputs and outputs, set as arrows.

the HP is active. The model causes no delay. If the enthalpy balance, calculated with the applied heat and the temperature difference, does not result in a mass flow between its minimum and maximum, the mass flow is limited and a new output temperature T_{out} is calculated with the limited mass flow.

4.2.6 Hysteresis Controller

A hysteresis controller controls the HP. It is active if the measured temperature in the SHS falls below a defined threshold and stops working until another measured temperature reaches another threshold. The used hysteresis can activate or deactivate the component. It is not possible to run the component in partial load mode. Figure 4.7 shows the model with its input and output. The input temperature T_{upper} is connected to the top temperature T_{19} in the SHS, which is compared to the upper limit where the hysteresis output U switches to zero. The input temperature T_{lower} is connected to the bottom temperature T_{23} in the SHS, which is compared to the lower limit, where the hysteresis output U switches to one. The parameters T_1 and T_2 define the upper and lower limit of the hysteresis and must be set.

Measurement data for the runtime of the HP and the input temperatures into the hysteresis controller were available. The model output was compared to the measured runtime data and the parameters were identified by a LS fit. The following parameters were identified for the hysteresis controller and chosen as the lower and the upper limit:

T_{upper} is connected to the SHS bottom layer
T_{lower} is connected to the SHS top layer

- $T_{\text{upper}}, limit = 82°\text{C}$
- $T_{\text{lower}}, limit = 78°\text{C}$

4.2.7 Plant

The plant and the process were described in Chapter 2. The resulting simulation model must meet the following criteria:

- A simulation duration of 24 hours must be executed in less than 1 minute. The simulation is executed without the EDCS.
- The error between the simulation and the measured data is not allowed to exceed 10% except short periods and the error must not exhibit any trend.
- The simulation must be stable and must not interrupt during the whole simulation time.
- The main dynamics of the system, like charging and discharging the SHS, heat loss through the wall of the SHS, the heat supply via the HP, and the heat transfer through the heat exchangers, must be mapped by the simulation.
- The main scenarios: 'the SOC is below the lower limit', 'more heat demand than heat supply' and 'run the system after a pause of up to seven days with no heat demand' must be mapped by the simulation correctly.
- The simulation must be developed and deployable in Matlab/Simulink (MATLAB, 2019).
- The simulation must be applicable for the EDCS Framework and usable with its controllers.
- The inputs and outputs of the simulation must be usable by the EDCS.
- The simulation states and outputs must be readable by the EDCS.

The main components of the plant are modelled: the HP, heat exchanger, SHS, mixing pipe, and pump. The components are connected via their out- and inputs. Four heat exchange models are connected to the mixing pipe model connected to the pump model. Together these components are the heat demand part of the plant. The model is connected to its surrounding by the heat exchangers, the heat loss of the SHS, and the connection of the HP to the internal heat network. Therefore the input data for the simulation consists of the heat demand, the temperature outside the building for the SHS, and the temperature of the fluid of the internal heat network. The SOC of the SHS is the comparable output of the simulation for the validation. The plant is schematically depicted in Figure 2.1.

The main dynamics of the system can be depicted with the model. The following simplifications were made:

- The pipes and their influence on the heat loss and delay are neglected.
- The warm-up of the components during startup is neglected.
- The logical condition that the pump P9 is active if the HP is active is neglected.

One step delays are induced by the HP, the SHS, and the heat exchange model. Some parameters were calculated by a LS fit based on the biased data.

The combined model is restricted by the maximum number of active HT's. It is not allowed to start more than two HT's simultaneously because the supply pump P9 cannot ensure the necessary mass flow. Further, the heat transfer fluid (HTF) water must not exceed the temperature range between 5°C and 95°C.

4.3 Verification and Validation

The model and V&V phase is an iterative process where simulation results influence the V&V and vice versa. The following software principles were applied and tools were used to assist an error-free development of the simulation:

- Central definition of units
- Documentation
- Component-based software developing
- Version control
- Use of a high level programming language
- Architectural design

The following verification techniques were applied:

- *Desk checking* is a process where a second person examines the work of the developer to find errors, ensure completeness, consistency, and clearness of code.
- *Face validation* means that potential users, engineers, team members, developers, or supervisors together judge whether the model and its results meet the desired accuracy and objectives.
- *Compiling the code* means checking the code against syntax errors.
- *Automatic static analysers* are often executed by the compiler and try to find incorrect, inefficient, or inconsistent use of code the compiler cannot see.
- *Defect testing* is executing the code to detect errors in code. Small pieces of code like components or units are executed just like the complete simulation and known output is compared to the calculated one.
- *Simple tests* verify whether the code meets a defined behaviour. A conservation test that ensures that the net energy flux in and out of a component must be zero is applied.

Verification techniques like the walkthrough, the review, the inspection, or the Turing test were not applied because of the limited personnel and time resources.

The following validation techniques were applied:

- *Building-block approach* divides the system into subsystems, subsystems into components, and components into units. The number of included physical effects and the complexity decrease from top to bottom. For each of them, specific validation data can be used for validation.
- *Face validation* is the judge of whether a model reaches the desired accuracy and intention, done together by the development team, potential users, and knowledgeable people. The model output and the dynamics are examined based on the intuition and subjective experience of each member.
- *Graphical comparison* is creating graphs and figures for comparing the model results with the real world data. Trends, periodicities, behaviour inconsistency, phase shift, constant errors, etc., are tried to uncover.
- *Submodule testing* is testing, verifying, and validating all of the simulation modules before the connected simulation model is tested.
- *Sensitivity analysis* is the systematically changing of the input and the internal parameters and examining their output effect of the model. This technique reveals the information about inputs that impact the result and parameters that change the model's behaviour if they are little altered. Before the sensitivity analysis is conducted, an uncertainty analysis separates parameters into well defined and uncertain values. The uncertain parameters are of special interest for sensitivity analysis.
- *Comparison of means* is valuing the agreement between the measured data and the simulated data. A metric based on statistical values can not be developed because of the lack of experimental data. Eq. (4.30) to Eq. (4.32) calculates the NRMSE, which values the agreement between the measured and the calculated data.

$$\varepsilon_{\text{error}_j} = y_{\text{meas}_j} - y_{\text{sim}_j} \tag{4.30}$$

$$\bar{y}_{\text{meas}} = \frac{1}{n} \cdot \sum_{j=1}^{n} y_{\text{meas}_j} \tag{4.31}$$

$$NRMSE = 1 - \frac{\sqrt{\sum_{j=1}^{n} \varepsilon_{\text{error}_j}^2}}{\sqrt{\sum_{j=1}^{n} (y_{\text{meas}_j} - \bar{y}_{\text{meas}})^2}}; \quad -INF < NRMSE < 1 \tag{4.32}$$

  $\varepsilon_{\text{error}_j}$ is the difference between one measured and one simulated value, y_{meas_j} is one measured value and y_{sim_j} is one simulated value simultaneously. $\bar{y}_{\text{meas}}$ is the mean value of all measured values y_{meas_j} and n is the number of simulated values. $NRMSE$ is the fit value that indicates a perfect fit if the value is zero.
- *Scenario analysis* tests the model by running several chosen scenario inputs and examining their output and the model behaviour about their validity.
- *Historical data validation* divides the available data into two groups: The first group, the larger sample, is used to examine and build the model and identify parameters. The

second part of the data is used to validate the model. The first 2/3 of the data is used for the identification and the last 1/3 of the data for the validation.

Hypothesis testing is a method to accept or refuse a model or make a decision between two different models. In computational physics, hypothesis testing is rarely used because the underlying phenomenon is well understood, models exist, and the fit to the measured data is examined. Therefore no hypothesis testing was applied. The V&V methods were chosen concerning their applicability in the development team, the available data, and the available resources.

For each component, the V&V was conducted. Components with a higher complexity were conducted with more V&V activities and components with a lower complexity were conducted with fewer V&V activities. The V&V was conducted with the last 1/3 of the data, which is called the validation part. The NRMSE was used as a validation parameter for comparing simulation output to the measured data. After the components V&V, the complete connected model controlled by the hysteresis controller was examined. The V&V of the components followed the same structure:

1. The model's purpose was defined.
2. Sources of uncertainty were identified and analysed.
3. Scenario analysis was done to identify the influence of the input, the behaviour of the model, and identify errors in the code.
4. The model output was compared to measured data.
5. Sensitivity analysis was done.
6. A conclusion was presented from the V&V process.

4.4 EDCS

The EDCS is an online, predictive and holistic and reconfigurable control system (Windholz, 2018-2021) and was newly developed in the course of the project EDCSproof. In this thesis, the EDCS was used to control the heat supply of the plant under study with a heat demand prediction. Its implementation leads to access to the flexible power price market. Therefore, a flexible power price was utilized by the EDCS to reduce power costs while ensuring process quality with optimal heat supply. The EDCS was used with a configuration applicable in future research when additional components enhance the plant under study.

4.4.1 Controller Structure

The EDCS is a multi-layer model predictive control concept which consists of two layers called: Operation Planner (OP) and MPC. Further, an observer is implemented for the state

estimation, the calculation and adaptation of the prediction data, and the calculation of the minimum SOC.

The OP calculates trajectories based on linearized models, objectives, constraints, and prediction for chosen plant in- and outputs for heat supply components or states of components in a facility. It optimizes a long term problem with large time steps and long execution time. The prediction accuracy is lower than the prediction of the MPC. The OP is used with the most important constraints, objectives, and predictions.

The MPC is connected to the heat supply components. It calculates the input for the heat supply components by following the trajectory of the OP, based on linearized models, objectives, constraints, and prediction. The prediction accuracy is higher compared to the OP and the MPC optimizes a short term problem with small steps and short execution time. The calculated output from the MPC differs from the trajectory because the layers are calculating results based on different information. The provided data from the observer is used as the initial value for calculating the prediction of the OP and the MPC. The MPC is used with detailed constraints, objectives, and prediction data of the connected components.

The same model functions are used for the OP and the MPC. Active constraints and cost functions can be chosen for the OP and the MPC independently. They are added as equalities and inequalities component wise. Several model functions, constraints, and cost functions can be added per component. Basic thermodynamic laws are stated to connect the components. The equations are used to calculate future states and inputs. A cost function is minimized by optimizing the input to the heat supply. The resulting mathematical problem is called a mixed-integer linear programming (MILP) problem. The EDCS uses the solver Gurobi for solving the problem (Gurobi Optimization, 2021).

The observer of the EDCS executes the following tasks:

- Actualize the current states (SOC, exchanged heat at the heat exchanger, and supplied heat from the HP) of the OP and the MPC.
- Prepare the prediction data for the OP.
- Adapt the heat load prediction utilizing measurement data.
- Calculation of the SOC_{min} limit.

In the configuration of this thesis, the OP calculated the trajectory for the SOC of the SHS for the next 96 hours, $N_{\text{pOP}} = 96$, for every 15 minutes, $t_{\text{stepOP}} = 15$. Every 60 minutes, the OP recalculated the SOC trajectory. The 15 minutes interval between the trajectory values reduces the computation time and provides the OP enough time to calculate the SOC trajectory, especially if more components of the facility are added. The prediction of the OP consisted of the prediction of the power price and the prediction of the heat demand.

The MPC had a prediction horizon of 45 minutes, $N_{\text{pMPC}} = 45$, and calculated a value every minute, $t_{\text{stepMPC}} = 1$. The output of the MPC was the input U for the HP in percent between 0% and 100%. The prediction of the MPC consisted of the heat demand.

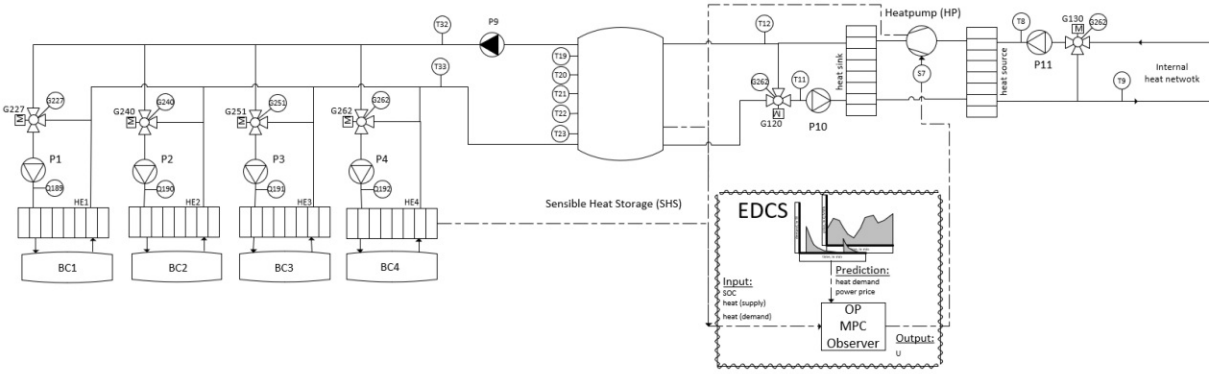

Figure 4.8: The implementation of the EDCS in the plant under study schematically. The hysteresis controller is replaced by the EDCS.

Figure 4.8 shows the implementation of the EDCS in the simulation model. Dashed lines show the input to the EDCS processed by the observer and the output to the HP processed by the MPC.

4.4.2 Linearized Models and Parameters

The OP calculates the prediction for the trajectory of the SOC. The MPC calculates the prediction for the power control input U for the HP. The calculation of the prediction is based on the prediction data, model functions, constraints, and objectives. The plant's main components are implemented as linearized and optimized model functions and their mathematical definitions can be solved analytically. The following optimized models are implemented:

- *storage* for the SHS
- *heat_pump* for the HP
- *demand* for the heat exchanger

The components pump and mixing pipe of the simulation model are neglected. Both of the layers, the OP and the MPC, use the same optimized models with different configurations. For each optimized model, the definitions, the used constraints, model equations, and objectives are stated for the OP and the MPC. Further, the balance equation for the EDCS is stated.

EDCS storage model

The optimized model *storage* is an integrator model for the stored energy and a simplification of the model stated in Subsection 4.2.1. The constraints define the allowed energy level of the SOC between a maximum and a minimum level. The model equations describe the load and unload of the SHS with energy and a constant and a variable loss of energy over time. The objectives are the costs for the deviation between the measured and the trajectory SOC. Further, the exceeding of the limits is added by a slack variable. From Eq. (4.33) to Eq. (4.36), the

constraints for the *storage* are stated:

OP:

$$\mathbf{SOC}_{\text{min}} < \mathbf{SOC}_{\text{pred}} < \mathbf{SOC}_{\text{max}} \tag{4.33}$$

MPC:

$$\mathbf{SOC}_{\text{min}} < \mathbf{SOC}_{\text{pred}} + \mathbf{SOC}_{\text{slack}} \tag{4.34}$$

$$\mathbf{SOC}_{\text{pred}} - \mathbf{SOC}_{\text{slack}} < \mathbf{SOC}_{\text{max}} \tag{4.35}$$

$$\mathbf{SOC}_{\text{slack}} >= 0 \tag{4.36}$$

The $\mathbf{SOC}_{\text{min}}$ is a vector and defines the minimum energy level of the SHS or the minimum energy level which is needed by a HT. The $\mathbf{SOC}_{\text{max}}$ is a vector and defines the maximum energy level of the SHS and the $\mathbf{SOC}_{\text{pred}}$ is a vector with the predicted SOC of the SHS. The $\mathbf{SOC}_{\text{slack}}$ is a vector with the values exceeding the limits $\mathbf{SOC}_{\text{min}}$ and $\mathbf{SOC}_{\text{max}}$.

From Eq. (4.37) to Eq. (4.44), the model equations for the *storage* are stated:

OP:

$$\mathbf{SOC}_{\text{L}} = \mathbf{SOC} \cdot (1 - \frac{t_{\text{stepOP}}}{60} \cdot SOC_{\text{varloss}}) - \frac{SOC_{\text{fixloss}}}{60} \cdot t_{\text{stepOP}} \tag{4.37}$$

$$\mathbf{SOC}_{\text{Cmwh}} = \frac{t_{\text{stepOP}}}{60} \cdot \mathbf{C}_{\text{MWH}} \tag{4.38}$$

$$\mathbf{SOC}_{\text{Dmwh}} = -\frac{t_{\text{stepOP}}}{60} \cdot \mathbf{D}_{\text{MWH}} \tag{4.39}$$

$$\mathbf{SOC}_{\text{pred}} = \mathbf{SOC}_{\text{L}} + \mathbf{SOC}_{\text{Cmwh}} + \mathbf{SOC}_{\text{Dmwh}} \tag{4.40}$$

MPC:

$$\mathbf{SOC}_{\text{L}} = \mathbf{SOC} \cdot (1 - \frac{t_{\text{stepMPC}}}{60} \cdot SOC_{\text{varloss}}) - \frac{SOC_{\text{fixloss}}}{60} \cdot t_{\text{stepMPC}} \tag{4.41}$$

$$\mathbf{SOC}_{\text{C}} = \frac{t_{\text{stepMPC}}}{60} \cdot \mathbf{C}_{\text{MWH}} \tag{4.42}$$

$$\mathbf{SOC}_{\text{D}} = -\frac{t_{\text{stepMPC}}}{60} \cdot \mathbf{D}_{\text{MWH}} \tag{4.43}$$

$$\mathbf{SOC}_{\text{pred}} = \mathbf{SOC}_{\text{L}} + \mathbf{SOC}_{\text{Cmwh}} + \mathbf{SOC}_{\text{Dmwh}} \tag{4.44}$$

$\mathbf{SOC}_{\text{L}}$ is a vector with the constant and the variable loss of energy of the *storage* over time. The $\mathbf{SOC}_{\text{C}}$ and $\mathbf{SOC}_{\text{D}}$ are vectors with the charge and discharge energy flow of the *storage*. The $\mathbf{SOC}_{\text{pred}}$ is initialized with the SOC_{init} of the SHS calculated by the observer at the corresponding t_{step}. SOC_{fixloss} is a parameter describing the constant loss of energy of the SHS and SOC_{varloss} is a parameter describing the variable loss of energy of the SHS. t_{stepOP} and t_{stepMPC} are the intervals between two calculated prediction values of the OP respectively MPC. $\mathbf{C}_{\text{MWH}}$ and $\mathbf{D}_{\text{MWH}}$ are vectors for the charge and discharge of the *storage* based on the *heat_pump* and

demand values.

No objectives are used in the *storage* model of the OP. From Eq. (4.45) to Eq. (4.46) the objectives for the *storage* model of the MPC are stated:
MPC:

$$O_{\text{traj}} = \Theta_{\text{traj}} \cdot \sum_{j=1}^{N_{\text{pMPC}}} SOC_{\text{pred}_j} - SOC_{\text{traj}_j} \tag{4.45}$$

$$O_{\text{slack}} = \Theta_{\text{slack}} \cdot \sum_{j=1}^{N_{\text{pMPC}}} SOC_{\text{slack}_j} \tag{4.46}$$

O_{traj} is the cost for the deviation between the measured and the trajectory SOC and O_{slack} is the cost of exceeding the SOC limits by a slack. N_{pMPC} is the prediction horizon of the MPC. SOC_{pred_j} is one predicted SOC and SOC_{traj_j} is the corresponding trajectory SOC in time. Θ_{traj} is a parameter that scales the deviation between the measured and the trajectory SOC to the maximum price per MWh. SOC_{slack_j} is the exceeding of the SOC limits in one time step and Θ_{slack} is a parameter that scales the slack to the maximum price per MWh.

EDCS heat_pump model

The optimized model *heat_pump* is a heat supply model and a simplification of the model stated in Subsection 4.2.2. The constraints limit the heat to the maximum and minimum possible heat supply. The model equations calculate the predicted input for the HP. The objectives are the costs for the power consumption in MWh at the actual price, the costs for the startup of the HP, and the costs for the deviation of the input of the HP. From Eq. (4.47) to Eq. (4.48) the constraints for the *heat_pump* are stated:
OP and MPC:

$$U_{\text{min}} < \mathbf{U} < U_{\text{max}} \tag{4.47}$$

If the HP is active the input to the HP must be between the minimum U_{min} and the maximum U_{max}. $\mathbf{U}$ is a vector for the predicted input to the HP between zero and one. Further the HP must be active after its start for a desired minimum time and inactive after shutdown for a desired minimum time.

In Eq. (4.48) the model for the *heat_pump* is stated:
OP and MPC:

$$\dot{\mathbf{Q}}_{\text{sink}} = \mathbf{U} \cdot \dot{Q}_{\text{sink}_{\text{HPmax}}} \tag{4.48}$$

$\dot{\mathbf{Q}}_{\text{sink}}$ is a vector for the predicted heat supply of the *heat_pump* and $\dot{Q}_{\text{sink}_{\text{HPmax}}}$ is the maximum heat supply possible by the HP.

From Eq. (4.49) to Eq. (4.52) the objectives for the *heat_pump* are stated:

OP:

$$O_{\text{costs}} = \frac{t_{\text{stepOP}}}{60} \cdot \sum_{j=1}^{N_{\text{pOP}}} P_{\text{HP}j} \cdot p_j \tag{4.49}$$

$$O_{\text{SU}_{\text{OP}}} = \Theta_{\text{SU}} \cdot \sum_{j=1}^{N_{\text{pOP}}-1} \mathbf{U}_{\text{start}_{\text{OP}}} \tag{4.50}$$

MPC:

$$O_{\text{dU}} = \Theta_{\text{dU}} \cdot \sum_{j=1}^{N_{\text{pMPC}}-1} |\dot{Q}_{\text{sink}_{j+1}} - \dot{Q}_{\text{sink}_j}| \tag{4.51}$$

$$O_{\text{SU}_{\text{MPC}}} = \Theta_{\text{SU}} \cdot \sum_{j=1}^{N_{\text{pMPC}}-1} \mathbf{U}_{\text{start}_{\text{MPC}}} \tag{4.52}$$

O_{costs} is the cost for the predicted power consumption $P_{\text{HP}j}$ at the predicted price per MWh p_j. O_{dU} is the cost for the predicted change of the input to the HP. Θ_{dU} scales the rate of change of the input to the maximum price per MWh and a desired maximum rate of change. $\mathbf{U}_{\text{start}_{\text{OP}}}$ and $\mathbf{U}_{\text{start}_{\text{MPC}}}$ are vectors indicating if the HP starts and Θ_{SU} scales the startup costs to the maximum price per MWh and a desired minimum HP active time. $O_{\text{SU}_{\text{OP}}}$ and $O_{\text{SU}_{\text{MPC}}}$ are the costs for the predicted startup and shutdown of the HP.

EDCS demand model

The optimized model *demand* is an energy sink model. No model constraints, equations and objectives are set. $\dot{Q}_{\text{SV}}$ is the predicted heat of one heat exchanger.

The EDCS minimizes the scalar O_{OP} and O_{MPC} which are calculated from Eq. (4.53) to Eq. (4.54):
OP:

$$O_{\text{OP}} = O_{\text{costs}} + O_{\text{SU}_{\text{OP}}} \tag{4.53}$$

MPC:

$$O_{\text{MPC}} = O_{\text{traj}} + O_{\text{slack}} + O_{\text{dU}} + O_{\text{SU}_{\text{MPC}}} \tag{4.54}$$

O_{OP} and O_{MPC} are the summation of the objectives for each layer which are minimized by the EDCS separately.

EDCS balance equation

The energy balance for the components are stated in Eq. (4.55). The energy balance must be fulfilled in each step and connects the models.

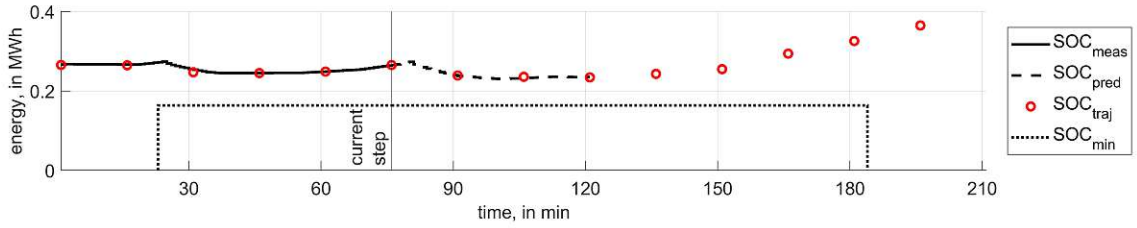

Figure 4.9: An EDCS operating example. The MPC prediction SOC_{pred} follows the trajectory SOC_{traj} of the OP. The SOC_{meas} is constrained by its lower level with the SOC_{min}.

$$\dot{\mathbf{Q}}_{\text{sink}} + \mathbf{SOC}_{\text{D}} = \dot{\mathbf{Q}}_{\text{SV}_1} + \dot{\mathbf{Q}}_{\text{SV}_2} + \dot{\mathbf{Q}}_{\text{SV}_3} + \dot{\mathbf{Q}}_{\text{SV}_4} + \mathbf{SOC}_{\text{C}} \tag{4.55}$$

4.4.3 Main functionality

The OP calculates a long term prediction trajectory and the MPC tries to follow the trajectory with a more accurate prediction of the HT's but with no information about the power price. Figure 4.9 shows the operation principle of the EDCS.

The solid black line is the measured enthalpy of the simulation SOC_{meas}. The red circles are the trajectory of the OP SOC_{traj} and the dashed black line is the predicted SOC of the MPC SOC_{pred}. The dotted black line is the minimum SOC_{min} which is not allowed to undercut. The measured SOC differs from the predicted one due to the linearisation of the models used in the EDCS and the difference between the predicted and the input heat demand data. The prediction of the MPC differs from the trajectory because of different constraints and objectives, which are active only for the MPC or the OP, the MPC's higher accuracy of the heat prediction, and because the power price prediction data is only available for the OP. The SOC is charged whenever possible in periods with low costs. The MPC starts the HP if the deviation to the trajectory becomes too large and the heat prediction demands a higher energy level in the SHS. Further, the SOC must not fall below the SOC_{min}.

4.4.4 Observer functionality

In this thesis, the functionality of the observer was extended by a real-time HT prediction manipulation. The aim of the functionality is to increase the performance and flexibility of the EDCS and ensure sufficient heat supply when the HT start time prediction is disturbed. This is accomplished by raising the energy level in the SHS in periods with no heat demand to ensure a minimum energy level for unpredicted HT's. Further, measured applied heat is used to adapt the heat demand prediction in real-time. The following three functions were implemented in the observer:

- The observer can extend the SOC_{min} to the future and the past to raise the energy level.

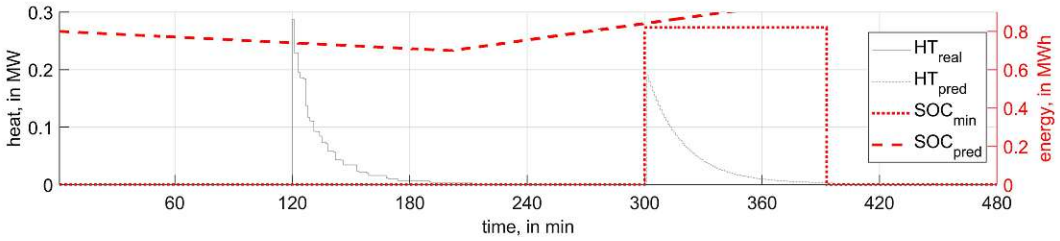

Figure 4.10: The OP prediction of the SOC, the prediction of the HT with its $SOC_{\min}$, and the real HT, starting earlier than predicted.

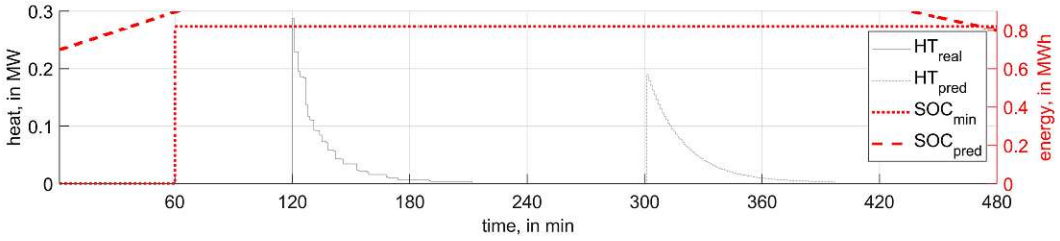

Figure 4.11: The OP prediction of the SOC with the extended $SOC_{\min}$ of the predicted HT. The real HT starts earlier than predicted.

- The observer can move the HT's to another time in the prediction horizon in case of disturbed start time predictions.
- The observer measures the applied heat of the heat exchangers and reduces too much predicted heat or adds too little predicted heat in the future.

Each function is described below.

EDCS SOC minimum extension

Due to HT start prediction errors, the SOC can fall below the $SOC_{\min}$, causing production quality problems by an insufficient heat supply. The observer can be configured to extend the $SOC_{\min}$ to reduce the risk of the SOC falling below the $SOC_{\min}$. Figure 4.10 shows the prediction of the SOC, which falls below the $SOC_{\min}$ because the start time of the HT prediction is in the future.

The observer can extend the $SOC_{\min}$ to the future and the past by the parameter t_{safety}. Figure 4.11 shows the extension of the $SOC_{\min}$ and the new prediction of the trajectory of the OP. The SOC does not fall below the $SOC_{\min}$ because of the extension.

The extension of the $SOC_{\min}$ can increase the production safety by a trajectory that remains at a higher SOC level.

EDCS heat treatment movement

The start of a HT is identified utilizing the measured heat applied at the heat exchangers. When a difference between real and predicted start time is detected, the observer moves the prediction data to the time when the heat is measured. Further, it cuts off the $SOC_{\min}$ if no heat

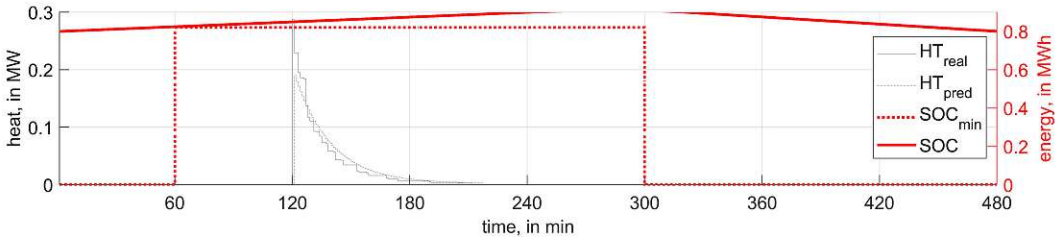

Figure 4.12: The HT prediction is moved to the measured start of the HT and the extension of the $SOC_{\min}$ is cut off by the observer. Further the heat prediction was altered during the execution with the difference between predicted and measured heat data.

can be measured anymore. Figure 4.12 shows the movement of the heat prediction data and the cut off of the $SOC_{\min}$ by the observer.

EDCS heat treatment distribution

The prediction of the heat demand is not perfect. Therefore the observer measures a difference between the predicted and measured heat applied at the heat exchangers. If the integral heat of the prediction fits to the applied prediction reasonably well and only the course of the HT differs, it is reasonable to distribute the measured difference to the ongoing HT prediction. The observer calculates the difference between measured heat and predicted heat at the actual time and distributes the difference heat to the ongoing prediction by reducing the future prediction heat or increasing the future prediction heat. This functionality improves the accuracy of the prediction in real-time by correcting the prediction of the integral heat in every step.

4.5 Simulation Study

The aim of the simulation study was to examine the influence of unpredicted interactions of human operators on the production process. In the examined partial automated process, employees start the processes of the HT's manually. Therefore, it was presumed that HT's start earlier or later than planned ones. If the prediction of the start time is not exactly known, it was expected that the provided heat by the SHS might be insufficient for the heat demand in some cases. The SOC falls below the minimum desired energy level of the HT $SOC_{\min}$ and might influence the product quality negatively. Figure 4.13 shows the SOC below the $SOC_{\min}$ with extended heat exchange duration caused by insufficient heat supply. The heating up process time increases and might harm the product quality. Therefore the SOC must be prevented from falling below the $SOC_{\min}$.

Furthermore, the robustness of the EDCS against unpredicted HT start times was examined. The frequency of the SOC falling below the $SOC_{\min}$ can be reduced by the observer parameter t_{safety} introduced in Section 4.4.4. It extends the $SOC_{\min}$ to the past and the future and increases the prediction's minimum energy level. Further, the HT movement and the HT distribution functionality introduced in Section 4.4.4 were used. They increase the prediction accuracy and

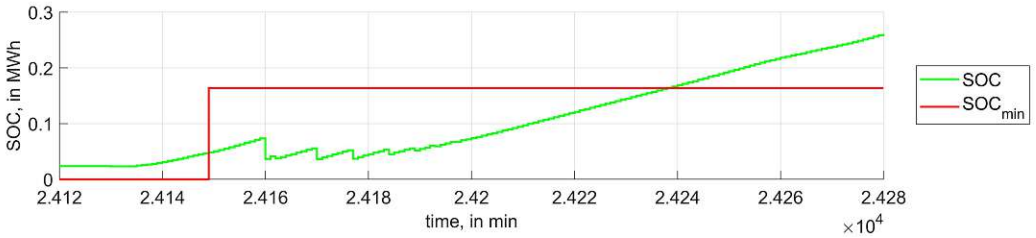

Figure 4.13: An example of insufficient heat when the SOC is below the $SOC_{\min}$ in case of unpredicted HT start times..

the robustness of the EDCS in real-time.

The simulation study compared different controller configurations of the EDCS and its influence on the undercut of the $SOC_{\min}$. The parameter t_{safety} was set to the following three values: 0, 4, and 8 hours. The simulation study was conducted with measured data from October 2019. The prediction data of the HT's were created by an exponential function, described in Fuhrmann *et al.* (2020) and calculated in Subsection 4.1.1. The start time of the prediction data was shifted to the past or the future by a maximum of eight hours. A normal distribution calculated the time shifted values. The normal distribution was chosen because the planned HT start was known and the assumption was made that the employees can decide whether to start a HT earlier or later, representing a normally distributed start time. The prediction data represented the planned production and the real heat data represented the deviation from the planned production start time. The simulation was repeated 36 times with each parameter value and normally distributed prediction start time deviations for the heat prediction. The simulation model is deterministic and the uncertainty of the output was induced only by the prediction data. For comparison reasons, the simulation was executed once with the hysteresis controller. The output of this reference simulation execution is called hysteresis benchmark. The influence of the heat supply of the internal heat network was neglected and it was assumed that the internal heat network supplies enough heat at all times.

The simulation meets the following criteria, which are necessary for comparing the data:

- The simulation is a terminating simulation with a fixed ending.
- The single simulation executions use the same initialization rules, with independent and identically distributed inputs.
- The runtime is the same for each execution.
- The independence of the different runs is accomplished by using random numbers for the normal distribution.
- The variable of interest is comparable between the different runs.

The evaluation of the output is depicted by error bars, a Pareto front and point estimators for the mean $\bar{X}$, the estimator for the variance S^2 and an approximate $100(1-\alpha)$ percent $0 < \alpha < 1$ confidence interval. The values can be compared via means and theirs confidence intervals because the output is independent and identically distributed. The t distribution for the confidence

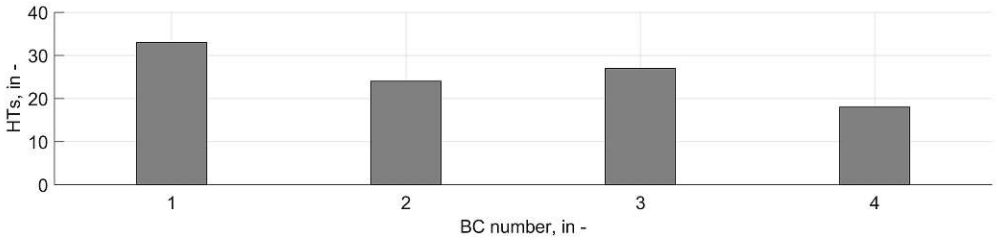

Figure 4.14: The number of applied HT's of each BC.

interval calculation can be used because the sample size is large enough to apply the central limit theorem.

4.5.1 Data

The applied heat input data for the simulation study was the measured data from the plant from October 2019. 102 HT's were conducted. HT's started between 5 a.m. in the morning and midnight with the main working time between 6 a.m and 18 a.m. The distribution among the BC's of the HT's was shown in Figure 4.14. The most HT's were applied on the BC with the index one and the fewest HT's were applied on the BC with the index four. The integral of the heat of each HT per BC is shown in Figure 4.15. The different heat amount per applied HT, shows that different HT programs were conducted on the BC's and that the programs were not distributed equally.

The prediction of the price per MWh is shown in Figure 4.16. The price varies between 57€ and 105€. The price data was measured data from the year 2019 and represents a variable power price market price. In the simulation study, the price prediction was equal to the input price of the simulation.

The HT's prediction data for the EDCS is calculated as described in Subsection 4.1.1. The unpredicted behaviour of the employees leads to start times which are not exactly known, so the start time of the exponential prediction data was moved to the future and the past by a maximum shift of eight hours. The time shift is normally distributed with the parameters: $\mu = 0$ and $\sigma = 4$ *hours*. Figure 4.17 shows a prediction data example with a disturbed start time. 78% of the time shifts were less than 4 hours due to the normal distribution.

4.5.2 Evaluation

The output of the simulation study was evaluated by summarizing the output of the 36 executions with each parameter and comparing the three output summary values to each other. The hysteresis benchmark was added to the graphs.

X_i are mean values from the different simulation runs i, which are calculated with the output data of the simulations. Eq. (4.56) shows the calculation of the mean price per MWh per simulation run. The following two equations calculate how often and how long the SOC felt below the $SOC_{\min}$. Eq. (4.57) shows the calculation of the mean affected HT's per simulation execution

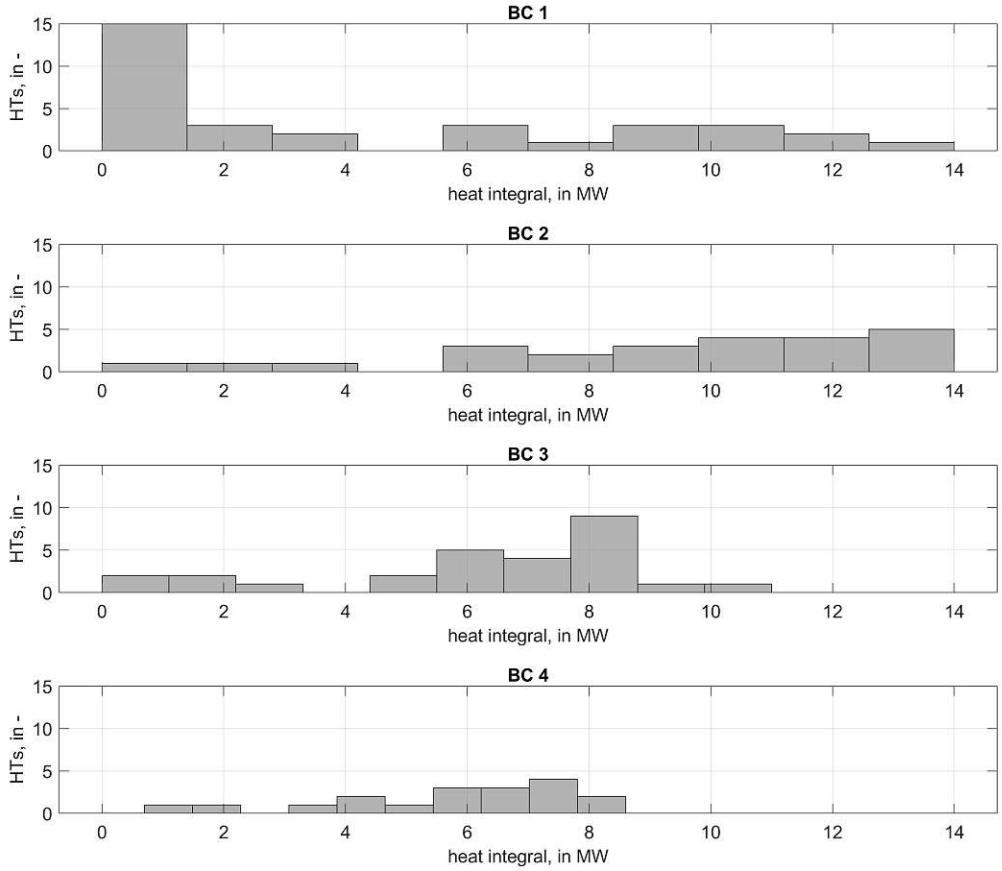

Figure 4.15: The number of HT's per integral heat demand and BC.

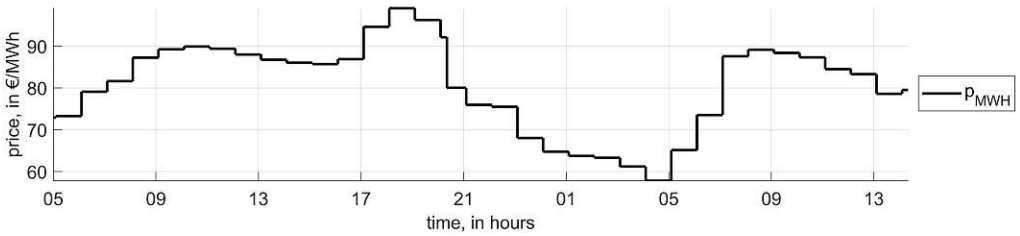

Figure 4.16: The prediction of the price per MWh over 32 hours.

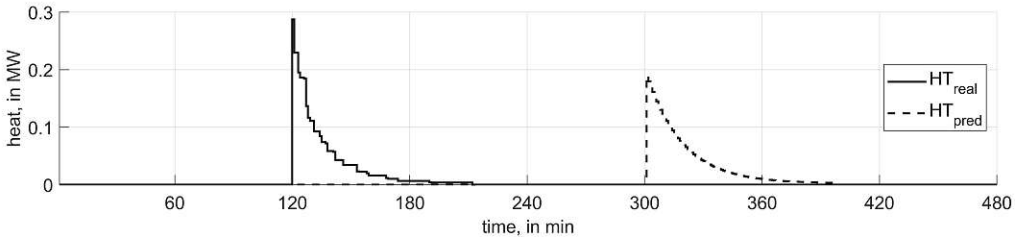

Figure 4.17: The prediction of a HT compared to its real heat demand with a delayed start time.

and Eq. (4.58) calculates the mean time the SOC was below the SOC_{min} per execution.

$$X_{i\_\text{mean\_price}} = \frac{\sum_{j=1}^{n} p_j \cdot P_{\text{HP}j}}{\sum_{j=1}^{n} P_{\text{HP}j}} \tag{4.56}$$

$$X_{i\_\text{mean\_aff\_HTs}} = \frac{n_{\text{HT\_aff}}}{n_{\text{HT}}} \tag{4.57}$$

$$X_{i\_\text{mean\_time\_per\_aff\_HT}} = \frac{t_{\text{SOC}_{\text{undercut}}}}{n_{\text{HT\_aff}}} \tag{4.58}$$

The mean values are calculated as $X_{i\_\text{mean\_price}}$ for the price, $X_{i\_\text{mean\_aff\_HTs}}$ for the affected HT's, and $X_{i\_\text{mean\_time\_per\_aff\_HT}}$ for the mean time the HT's are below the SOC_min. They are calculated for $i = [1,...,W]$ for each parameter set. W is the number of executions per parameter set. p_j is the price per MWh and $P_{\text{HP}j}$ the correspondent power consumption of the HP. $n_{\text{HT\_aff}}$ is the number of the HT's affected by an insufficient SOC and n_{HT} the number of each simulated HT per execution. $t_{\text{SOC}_{\text{undercut}}}$ is the time the SOC is below the SOC_{min} per execution. The point estimator for the mean μ is calculated in Eq. (4.59), and the variance σ^2 is calculated in Eq. (4.60). An approximate $100(1-\alpha)$ percent $0 < \alpha < 1$ confidence interval is calculated in Eq. (4.61).

$$\bar{X}(W) = \frac{\sum_{i=1}^{W} X_i}{W} \tag{4.59}$$

$$S^2(W) = \frac{\sum_{i=1}^{W} (X_i - \bar{X}(W))^2}{W-1} \tag{4.60}$$

$$\bar{X}(W) \pm t_{\text{critical}} \cdot \sqrt{S^2(W)/W} \tag{4.61}$$

$\bar{X}(W)$ is the point estimator of the mean value and $S^2(W)$ is the point estimator for the variance of the measured data. t_{critical} is the critical t-value of the t distribution. 0.95 was set as α for a 95% confidential interval.

5 Results and Discussion

This chapter analyses the results of the data preparation and its validation in Section 5.1. Further, the model validation results are discussed in Section 5.2. The results of the Energy Demand Control System (EDCS) implementation are stated in Section 5.3. The output of the simulation study is shown and interpreted in Section 5.4.

5.1 Data Preparation and Validation

5.1.1 Heat measurement Q_{189}, Q_{190}, Q_{191}, and Q_{192}

The heat consumption measurements $Q_{189}, Q_{190}, Q_{191}$, and Q_{192}, for the heat exchangers HE1, HE2, HE3, and HE4, show the characteristic batch heat consumption. There is a peak heat consumption at the beginning of every heat treatment (HT), which is exponentially decreasing. At the beginning, the measured heat peaks should result in the temperature drop of the heat exchangers inflow temperature T_{32} to its outflow temperature T_{33}. Figure 5.1 shows the measurement devices for the validation of the heat demand data.

In the measured data, the heat consumption peak occurs one step before the temperature drop measurement in T_{33}. This shift might result from a one step delay caused by the physical distance of the temperature measurement devices, the inertia of the sensor, or measurement errors and not by the heat exchanger component. Therefore, the heat demand data was shifted one step into the future. The shift was implemented in the model to ensure a correct depiction of the plant. Figure 5.2 shows in the top graph the inflow T_{32} and outflow T_{33} temperature of the heat exchangers and the bottom graph the sum of the measured heat consumption $Q_{\text{sum}_{\text{meas}}}$,

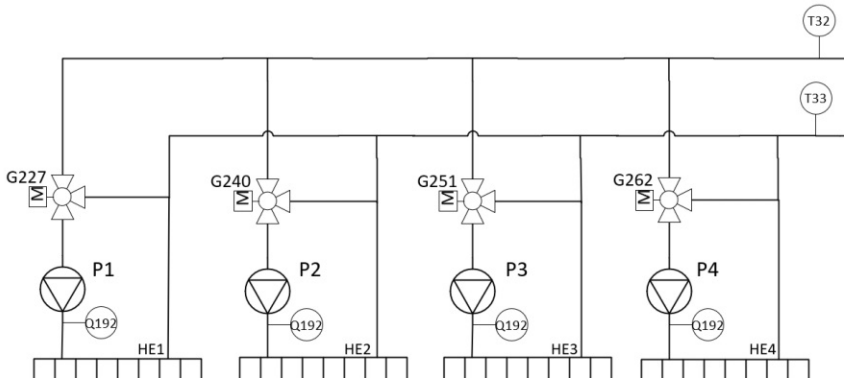

Figure 5.1: The necessary measurement devices for the heat demand data validation are depicted.

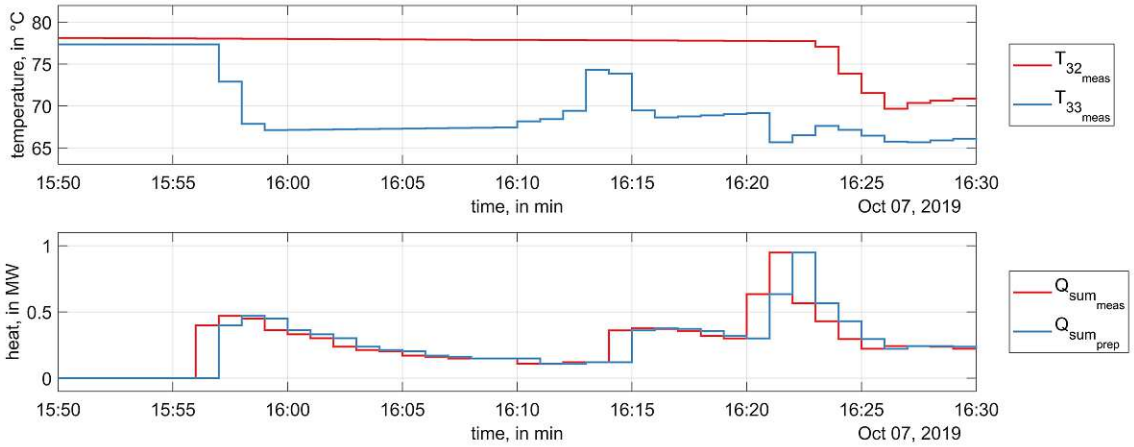

Figure 5.2: The top graph shows the measured input $T_{32_{\text{meas}}}$ and output $T_{33_{\text{meas}}}$ temperature of the heat demand. The bottom graph shows the heat consumption $Q_{\text{sum}_{\text{meas}}}$ and the shifted heat consumption $Q_{\text{sum}_{\text{prep}}}$ of the heat demand.

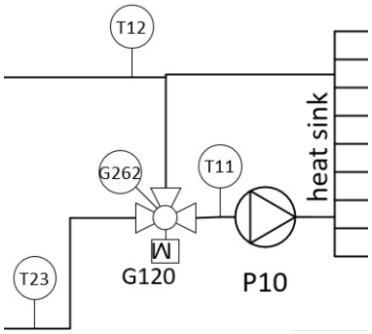

Figure 5.3: The necessary measurement devices for the validation of the G_{120} valve data.

and its right shifted sum $Q_{\text{sum}_{\text{prep}}}$. In further calculations, the shifted heat demand data will be used.

5.1.2 Mass flow valve G_{120}

The mass flow out of the heat pump (HP) at the heat sink side had to be extracted from the valve position G_{120} because no mass flow data was recorded. The valve position in % and the constant mass flow pump P10, define the mass flow out of the HP. It was assumed that the pump P10 is active if the valve is open. The surrounding temperature data of the valve was used to evaluate the consistency of the valve position. The output temperature T_{11} is the mixing temperature of T_{12} and T_{23}. T_{23} is the bottom layer temperature of the sensible heat storage (SHS) and is used as the input temperature for the valve because no other measurement device has been installed. Figure 5.3 shows the measurement devices for the validation of the valve position.

T_{11}, T_{23}, and T_{12} were used to calculate the valve position in Eq. (5.1). The valve position is limited between $0\% < G_{120_{\text{prep}}} < 100\%$.

$$\mathbf{G}_{120_{\text{prep}}} = \frac{\mathbf{T}_{11} - \mathbf{T}_{12}}{\mathbf{T}_{23} - \mathbf{T}_{12}} \cdot 100 \tag{5.1}$$

$\mathbf{G}_{120_{\text{prep}}}$ is the valve position calculated by the input temperatures $\mathbf{T}_{23}$ and $\mathbf{T}_{12}$ and the output temperature $\mathbf{T}_{11}$. The temperatures T_{11}, T_{12}, and T_{23}, the rotation speed of the HP S_7, valve position $G_{120_{\text{meas}}}$, and the newly calculated valve position $G_{120_{\text{prep}}}$ are shown in Figure 5.4. The top graph shows the temperature measurements around the valve T_{12}, T_{23}, and T_{12}, the second graph shows the rotation speed of the HP $S_{7_{\text{meas}}}$, and the bottom graph shows the measured and the prepared valve data $G_{120_{\text{meas}}}$ and $G_{120_{\text{prep}}}$.

The temperature T_{11} is consistent with the temperature T_{12}, which is indicated by a constant temperature difference induced by a constant heat supply. If the valve is completely open, indicated by a measured valve position of 100%, the temperature T_{23} should be equal to the temperature T_{11}, which is not the case. Further, the temperature T_{11} is not a value between the temperature T_{23} and the temperature T_{12} in every step, although it must be. This error might be the result of the temperature measurement device position T_{23} in the SHS. It measures the layer temperature and the ingoing fluid temperature of the heat demand side.

The HP rotation speed is consistent with the temperature rise and therefore defines when the valve should be open. The measured valve position rises before the start of the HP. The initial steep rise of the valve data $G_{120_{\text{meas}}}$ at the HP start does not lead to a temperature difference between the measured temperatures T_{12} and T_{11}. When the HP starts, a closed valve would be expected.

The identified inconsistency is a result of the missing temperature measurement device at the inflow to the valve and the inaccurate measured valve data. The prepared valve starts and stops together with the HP rotation speed and is more consistent with the temperature data compared to the measured valve data. Therefore, the prepared valve data $G_{120_{\text{prep}}}$ was used. A consistency error remains if the temperature T_{23} is higher than the temperature T_{11} because of the limitation of the prepared valve data to 100%.

The constant mass flow of the pump P10 $\dot{m}_{\text{P10}}$ was chosen from the datasheet of the pump as $13.5^{kg}/_{s}$. The mass flow out of the HP is calculated in Eq. (5.2).

$$\dot{\mathbf{m}}_{\text{HP}_{\text{out}}} = \dot{m}_{\text{P10}} \cdot \mathbf{G}_{120_{\text{prep}}} \tag{5.2}$$

$\dot{\mathbf{m}}_{\text{HP}_{\text{out}}}$ is the mass flow out of the HP.

5.1.3 Variable mass flow pump P9

There was no recorded data for the variable mass flow of the supply pump P9. Therefore the mass flow and the pump runtime had to be identified. Figure 5.5 shows the measurement devices for the identification and validation of the pump data.

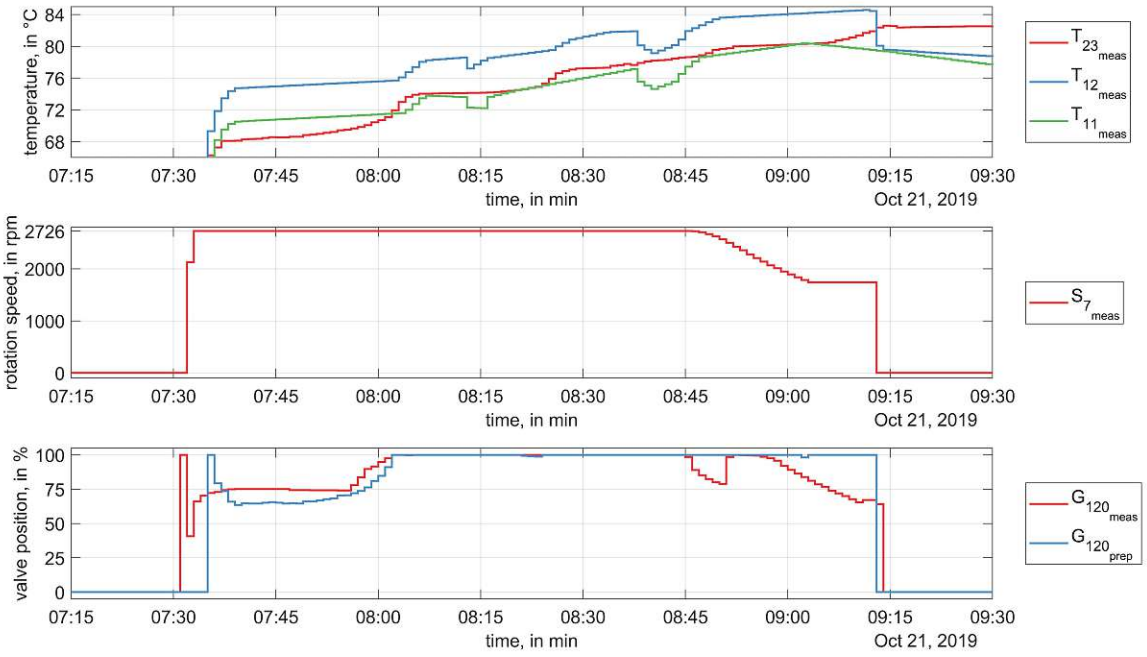

Figure 5.4: The top graph shows the ingoing and outgoing measured temperatures of the valve G_{120}. The second graph shows the measured rotation speed of the HP. The bottom graph shows the newly calculated valve data $G_{120_{\text{prep}}}$ compared to the measured valve data $G_{120_{\text{meas}}}$. The HP data and the temperature data were used for the validation of the valve data.

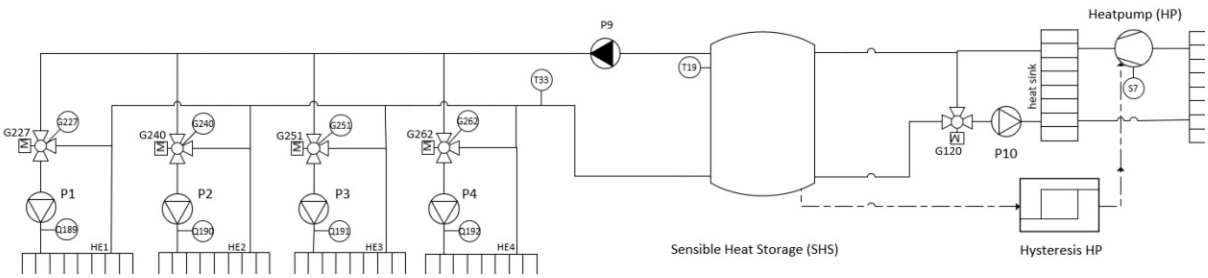

Figure 5.5: The necessary measurement devices for the identification and validation of the pump P9 data.

Rules were derived from the measurement data to indicate the activity of the pump P9. The pump is active if one of the following conditions are true:

- The temperature T_{33} decreases with a gradient larger than $1^{\circ C}/_{min}$.
- The HP is active.
- The heat demand at the heat exchangers HE1, HE2, HE3, or HE4 is > 0.
- One or more of the valves G227, G240, G251, or G262 are open.

The mass flow of the pump is variable and the pump is configured to hold a constant differential pressure of nearly zero bar. The pressure difference of the hydraulic system depends on the pump height, which depends on the length and position of the pipes and the valve position data G227, G240, G251, or G262. The mass flow is calculated utilizing energy conservation law because no pressure information was available. The variable mass flow is calculated from Eq. (5.3) to Eq. (5.5). In Eq. (5.3), the prepared heat data is summarized and in Eq. (5.4), the conservation of energy is stated.

$$\dot{\mathbf{Q}}_{\text{sum}_{\text{prep}}} = \mathbf{Q}_{189_{\text{prep}}} + \mathbf{Q}_{190_{\text{prep}}} + \mathbf{Q}_{191_{\text{prep}}} + \mathbf{Q}_{192_{\text{prep}}} \tag{5.3}$$

$$\dot{\mathbf{Q}}_{\text{sum}_{\text{prep}}} = cp_{\text{w80}} \cdot (\mathbf{T}_{33} - \mathbf{T}_{19}) \cdot \dot{\mathbf{m}}_{\text{P9}} \tag{5.4}$$

$$\dot{\mathbf{m}}_{\text{P9}} = \frac{\dot{\mathbf{Q}}_{\text{sum}_{\text{prep}}}}{cp_{\text{w80}} \cdot (\mathbf{T}_{33} - \mathbf{T}_{19})} \tag{5.5}$$

$\dot{\mathbf{Q}}_{\text{sum}_{\text{prep}}}$ is the sum of the heat for all heat consumers, cp_{w80} is the specific heat capacity for water at 80°C, $\mathbf{T}_{19}$ is the temperature in the top layer of the SHS and $\mathbf{T}_{33}$ is the outflow temperature of the heat exchangers. $\dot{\mathbf{m}}_{\text{P9}}$ is the variable pump mass flow of the pump P9.

Whenever the pump is active, it ensures a minimum mass flow even though there is no heat measured. The unknown minimum mass flow was calculated with a least square (LS) fit. The enthalpy of the SHS was calculated with the ingoing and outgoing enthalpy and the difference to the measured enthalpy in the SHS was minimized. The outgoing enthalpy was calculated with the mass flow $\dot{m}_{\text{P9}}$ and the temperature difference T_{19} and T_{33}. The minimum mass flow $\dot{m}_{\text{P9}_{\text{min}}}$ was added to the mass flow $\dot{m}_{\text{P9}}$ and was optimized by the LS fit. The optimized minimum mass flow of the pump P9 is $1.5056^{kg}/_{s}$.

The minimum mass flow $\dot{m}_{\text{P9}_{\text{min}}}$ is added whenever the pump P9 is active. The maximum mass flow of the pump was chosen from the datasheet as $13.496^{kg}/_{s}$. The mass flow is limited by its minimum and maximum value. Figure 5.6 shows in the top graph the pump mass flow $\dot{m}_{\text{P9}}$, in the second graph the inflow temperature T_{19} and outflow temperature T_{33}, in the third graph the heat demand sum $\dot{Q}_{\text{sum}_{\text{prep}}}$, and in the bottom graph the rotation speed of the HP $S_{7_{\text{meas}}}$. The pump P9 is active whenever one of the stated conditions is active. Between 08:30 and 09:45, the minimum mass flow $\dot{m}_{\text{P9}_{\text{min}}}$ is active. This is induced by the heat demand $\dot{Q}_{\text{sum}_{\text{prep}}}$ and the difference between the temperatures T_{33} and T_{19}, which demand a lower mass flow calculated with an energy balance.

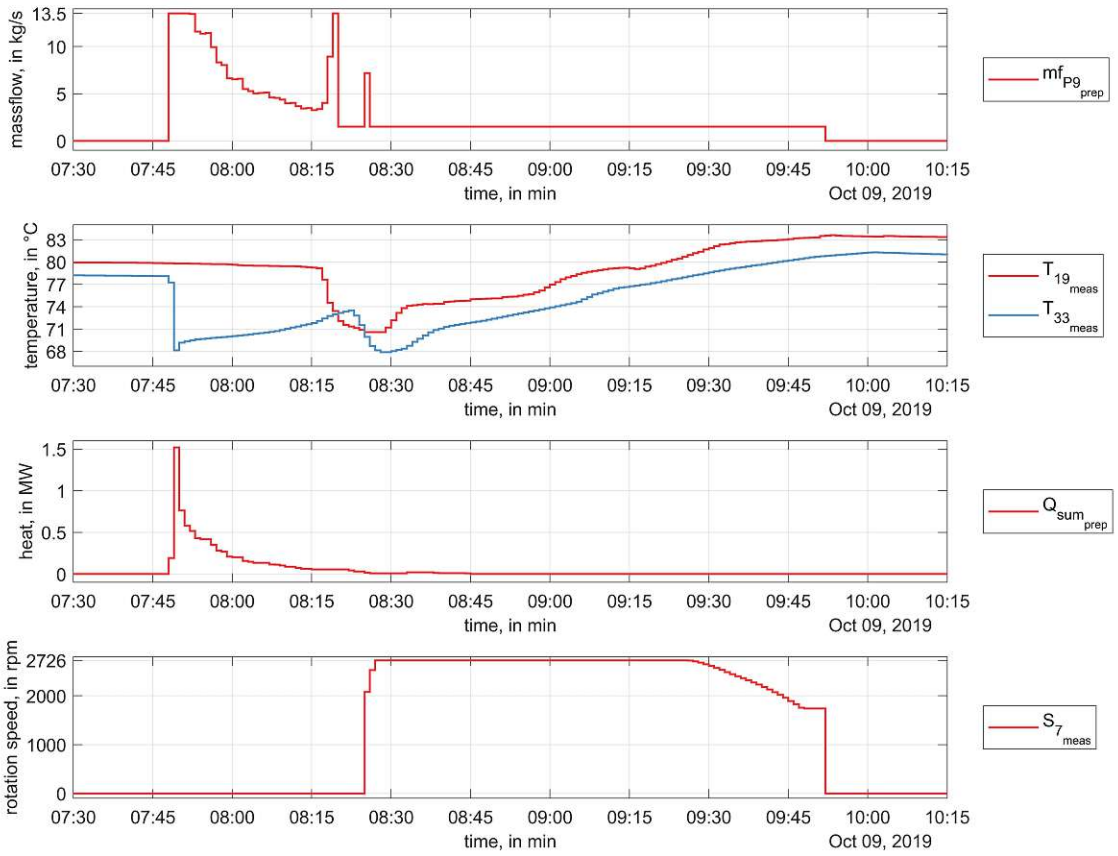

Figure 5.6: The top graph shows the calculated mass flow of the pump P9 $\dot{m}_{\mathrm{P9_{prep}}}$. The second graph shows the ingoing T_{19} and outgoing T_{33} measured temperatures of the heat demand which is connected to the pump P9. The third graph shows the prepared heat consumption of the heat demand. The bottom graph shows the measured rotation speed of the HP.

5.1.4 Enthalpy balance SHS

The prepared data was validated by the enthalpy balance around the SHS. The sum of the ingoing and outgoing enthalpy minus the heat loss through the wall of the tank was calculated and compared to the measured enthalpy. From Eq. (5.6) to Eq. (5.8), the enthalpy in and out of the SHS and the enthalpy loss are calculated. From Eq. (5.9) to Eq. (5.12), the absolute enthalpy in the SHS the state of charge (SOC) and the error between the measured and the calculated enthalpy, divided by the minimum usable enthalpy level, are calculated. The identification of the heat loss is shown in Subsection 4.2.1.

$$\mathbf{h}_{\text{in}} = \frac{\mathbf{G}_{120_{\text{prep}}}}{100} \cdot \dot{m}_{\text{P10}} \cdot cp_{\text{w80}} \cdot (\mathbf{T}_{12} - \mathbf{T}_{23}) \tag{5.6}$$

$$\mathbf{h}_{\text{out}} = \dot{\mathbf{m}}_{\text{P9}} \cdot cp_{\text{w80}} \cdot (\mathbf{T}_{33} - \mathbf{T}_{19}) \tag{5.7}$$

$$\mathbf{h}_{\text{loss}} = \alpha_{\text{w}} \cdot A_{\text{l}} \cdot (\mathbf{T}_{\text{outside}} - \mathbf{T}_{\text{SHS}}) \tag{5.8}$$

$\mathbf{h}_{\text{in}}$ is the calculated enthalpy into the SHS, $\mathbf{h}_{\text{out}}$ is the calculated enthalpy out of the SHS and $\mathbf{h}_{\text{loss}}$ is the calculated loss of enthalpy through the wall of the SHS. α_{w} is the heat transfer coefficient for the wall of the SHS and A_{l} is the area of the wall of the SHS. $\mathbf{T}_{\text{outside}}$ is the measured temperature outside of the SHS and $\mathbf{T}_{\text{SHS}}$ is the measured temperature inside the SHS.

$$\mathbf{SOC}_{\text{meas}} = cp_{\text{w80}} \cdot V \cdot \rho_{\text{w80}} \cdot \mathbf{T}_{\text{SHS}} \tag{5.9}$$

$$\mathbf{SOC}_{\text{calc}} = (\mathbf{h}_{\text{in}} + \mathbf{h}_{\text{out}} + \mathbf{h}_{\text{loss}}) \cdot t_{\text{s}} \tag{5.10}$$

$$SOC_{\text{min}} = cp_{\text{w80}} \cdot V \cdot \rho_{\text{w80}} \cdot T_{\text{SHS}_{\text{min}}} \tag{5.11}$$

$$\mathbf{SOC}_{\text{error}} = \frac{\mathbf{SOC}_{\text{meas}} - \mathbf{SOC}_{\text{calc}}}{SOC_{\text{min}}} \tag{5.12}$$

$\mathbf{SOC}_{\text{meas}}$ is the calculated absolute enthalpy with the measured temperature in the SHS and $\mathbf{SOC}_{\text{calc}}$ is the calculated enthalpy with the ingoing and outgoing enthalpy and the loss of enthalpy through the wall. SOC_{min} is the minimum usable enthalpy level calculated with the minimum usable temperature $T_{\text{SHS}_{\text{min}}}$. $\mathbf{SOC}_{\text{error}}$ is the difference between the measured and calculated enthalpy divided by the minimum enthalpy. V is the volume of the SHS and t_{s} is the discretization time which is 60 seconds. The enthalpy was calculated to the reference of 0°C.

Figure 5.7 shows in the top graph the calculated enthalpy SOC_{calc} compared to the measured enthalpy SOC_{meas} in the SHS. The bottom graph shows the difference between the measured and the calculated enthalpy divided by the minimum usable enthalpy level as the error SOC_{error}. The graph depicts the constant loss of energy and the constant error during the operation free periods. Therefore the loss of energy is modelled accurately and the measured data shows the behaviour of a thermal energy storage (TES) with energy loss during the charging free periods. The dynamic behaviour of the data is not consistent and leads to a constant error during the energy loss periods. The error is up to 20 % during the execution time without a trend.

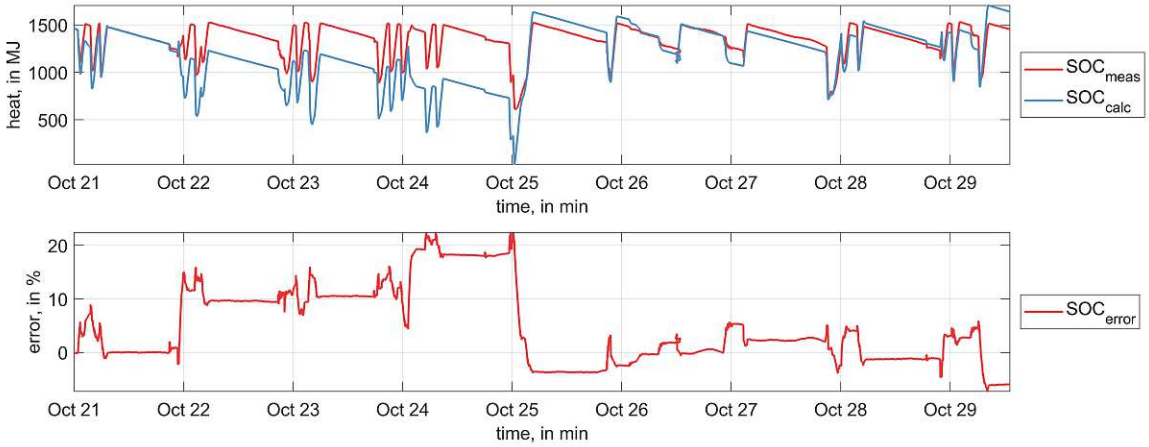

Figure 5.7: The measured enthalpy of the SHS SOC_{meas} is compared to the enthalpy balance of the ingoing and outgoing enthalpy flow SOC_{calc} in the top graph. The difference between them is divided by the minimum enthalpy level in the SHS and depicted as the error SOC_{error} in the bottom graph.

5.1.5 Conclusion

The following data was prepared and added:

- $Q_{189}, Q_{190}, Q_{191}$ and Q_{192} were replaced by their right shifted version.
- The prepared valve data was used to calculate the mass flow through the valves G120 $\dot{\mathbf{m}}_{\text{HP}_{\text{out}}}$.
- The conservation of energy equation was used to calculate the P9 pump mass flow data $\dot{\mathbf{m}}_{\text{P9}}$.

The prepared heat demand, the added mass flow, the HP power and rotating speed, and the measured temperatures were used for the modelling and validation. There was no information about the precision, possible interferences, or range of accuracy of the measurement devices that keep the data in an unknown range of accuracy and no range of error could be stated.

The consistency of the prepared data by an enthalpy balance is given in Figure 5.7 and shows that some dynamics cannot be depicted consistently. The error has no trend, but constant errors arise after dynamic operations. This might be caused by the missing mass flow data, the result of configurations of the plant which were not known and could not be identified with the data, or manual interactions at the plant. Further, startup behaviour at the plant was not examined and not used for the consistency analysis. The data trustworthiness is sufficient because the main dynamics are depicted without a trend and the error is small enough for a comprehensible analysis. The data was used for the modelling and verification and validation (V&V) process.

5.2 Model Validation

The first question in this thesis was: 'Is it possible to use the measured data to develop a valid simulation model of the plant for testing the EDCS'. The validation results answer the

research question by several V&V methods chosen in Section 4.3. The V&V results are given from Subsection 5.2.1 to Subsection 5.2.7.

5.2.1 Sensible Heat Storage

The purpose of the SHS model is to simulate the following operations:

- Charging and discharging the SHS by the mass flow and temperature into and out of the model.
- Heat loss through the wall.
- Heat transfer between the temperature layers.

The following uncertainties were identified:

- Parameter: heat transfer coefficient of the wall α_w
  The parameter α_w estimation was done in Subsection 4.2.1. The mean normalized root mean squared error (NRMSE) for the calculated heat loss in the validation periods is 0.0827. The error between the calculated and the measured data during the heat loss periods is constant with deviations up to 1°C for each layer. The real value for the parameter α_w depends on the geometry and the insulating material.
- Parameter: the specific heat capacity cp and the density of water ρ
  A fixed specific heat capacity and a fixed density of water at 80°C and a pressure of 1 bar were chosen for all calculations because of saving computation time. The temperature range of the SHS is between 60°C and 90°C. In the stated temperature range, the specific heat capacity of water rises with the temperature increase and vice versa. The density decreases with the increase of the temperature and vice versa. The difference between the energy level in the SHS calculated with the IF-97 standard values and the fixed chosen values divided by the IF-97 standard values is at every temperature level between 60°C and 90°C lower than 0.01146%.
- Model behaviour: internal flow
  The model cannot simulate internal turbulent flow. Temperature changes caused by internal turbulent flow cannot be simulated and their influence on the temperature distribution in the SHS was not examined. The mix_{factor} tightens the temperature distribution over the volume layers and represents the turbulent flow in a simple way.

The scenario analysis was executed with several charging and discharging scenarios. The analysis of the SHS model is shown in Figure 5.8. The applied mass flow and temperature inputs are shown in Table 5.1.

In (1), the layer temperatures tend to the temperature with the higher mass flow. The temperature of the top layer decreases slower compared to the other layers. It asymptotically reaches 70°C, which is the analytical temperature output for the chosen input values in the top volume

Table 5.1: Input mass flow and input temperatures of the SHS scenario analysis.

number	$\dot{m}_{\text{hot}_{\text{in}}}$, *in* $^{kg}/_{s}$	$T_{\text{hot}_{\text{in}}}$, *in* °C	$\dot{m}_{\text{cold}_{\text{in}}}$, *in* $^{kg}/_{s}$	$T_{\text{cold}_{\text{in}}}$, *in* °C
1	5	80	10	60
2	0	-	10	60
3	10	80	5	60
4	0	-	10	60
5	10	70	0	-
6	10	80	0	-

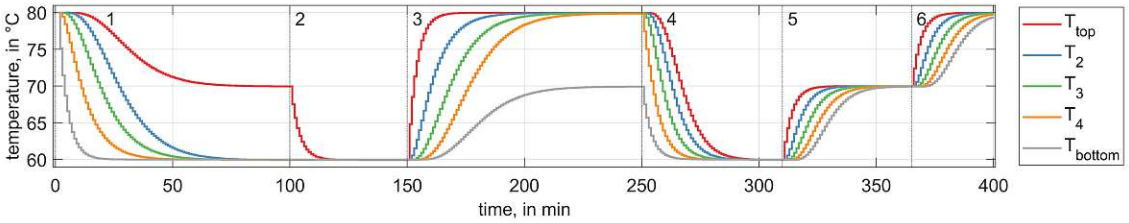

Figure 5.8: The scenario analysis output temperatures of the SHS for several charge and discharge scenarios. The constant input sections are separated by vertical lines.

layer. In (2), the mass flow $\dot{m}_{\text{hot}_{\text{in}}}$ changes to zero resulting in layers with the same temperature. (3) shows the same behaviour as in (1) vice versa. In (4), the pure unload of the SHS is shown, which takes up to 48 minutes in the simulation. The analytical calculation of the unload time with a constant output temperature of 70°C is about 41 minutes. The difference between analytical and simulated discharging time is caused by the differential equations of the model, which reduce the heat transfer at lower temperature differences. In (5) and (6), a piecewise load of the SHS is shown. The scenario analysis output is comprehensible and depicts the expected behaviour.

The simulation was executed with the validation data to evaluate the fit between the measured and the calculated data. The inputs to the model were the measured mass flow and the corresponding temperatures. The temperature layers of the model were compared to the measured temperatures of the SHS. Figure 5.9 shows the temperature of the layers of the SHS from top to bottom. The top graph shows the measured temperatures, the second graph shows the calculated temperatures, and the bottom graph shows the absolute difference between the temperatures. The heat loss can be simulated with an error of less than 1°C, which is indicated by the horizontal temperature difference in the bottom graph. The dynamic of the charging and discharging is depicted with an absolute temperature error up to 6°C, which is caused by a more and faster change of temperature in the measured data caused by initial cold water in the pipes, data inaccuracies, or short circuits between the HP and the heat demand circuits through the SHS. In addition, the temperature measurement devices react more sensitive to the incoming mass flow, while the temperature in the volume layer can differ from the measured one.

Figure 5.10 shows the enthalpy of the simulation compared to the measured enthalpy. The

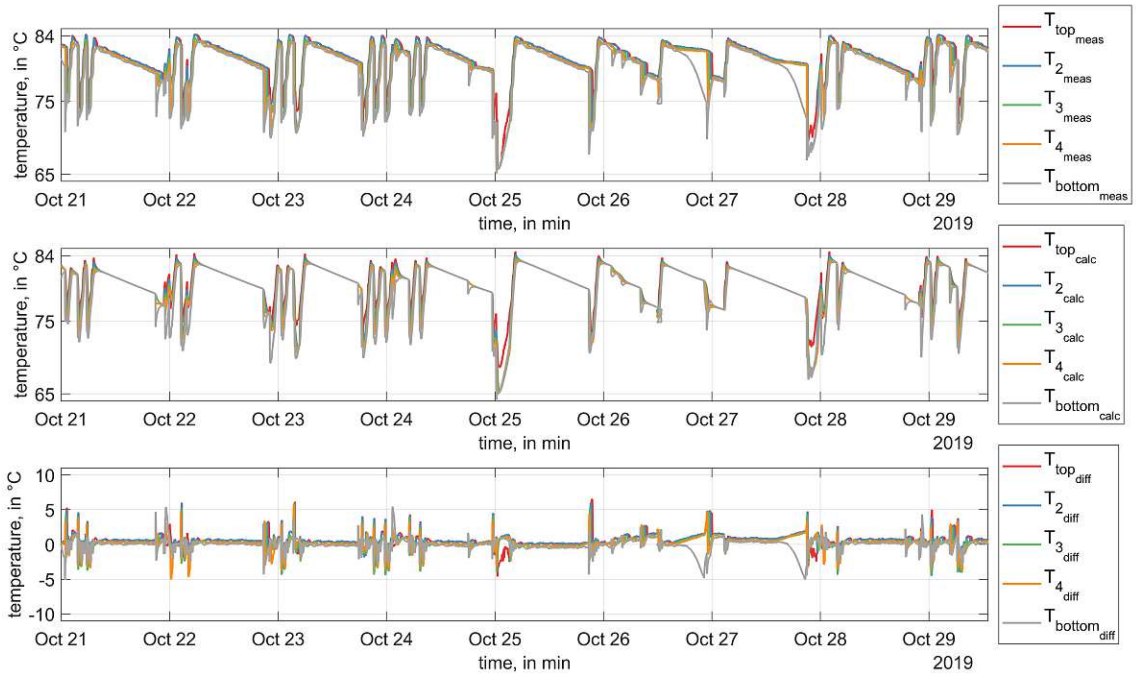

Figure 5.9: The measured temperatures of the SHS are shown the top graph and the calculated temperatures of the SHS model conducted with measured input are shown the second graph. The differences between the measured and the calculated temperatures are depicted in the bottom graph.

top graph shows the comparison between the measured and the calculated enthalpy. The bottom graph shows the enthalpy difference divided by the minimum usable enthalpy. The NRMSE is 0.2074. The maximum error in one time step is less than 5%.

The sensitivity analysis was conducted with the following parameters:

- The heat transfer coefficient α_{w}.
- The mixing factor mix_{factor}.

Both parameters were examined by simulating a reference SOC with the original parameter and comparing the new SOC with the reference SOC. The error is calculated in Eq. (5.13).

$$SOC_{\mathrm{err}} = \frac{SOC_{\mathrm{ref}} - SOC_{\mathrm{new\_parameter}}}{SOC_{\mathrm{ref}}} \tag{5.13}$$

The SOC_{err} is the error compared to a reference SOC_{ref} in percent.

The sensitivity analysis for the heat transfer coefficient α_{w} was conducted with two different values. The original value for the heat transfer coefficient α_{wref}, which is set in the simulation, is 1.6528 $W/m^2 \cdot K$. One value above and one value below the original value, with a deviation of 0.1 $W/m^2 \cdot K$, were chosen and executed in the sensitivity analysis. The output temperature was set to a constant value of 10°C for each run. Figure 5.11 shows the SOC of the SHS with different values for the heat transfer coefficients α_{w1} and α_{w2} and the error of the SOC compared to the SOC_{ref}. The error was calculated as stated in Eq. (5.13). The error is approximately symmetric

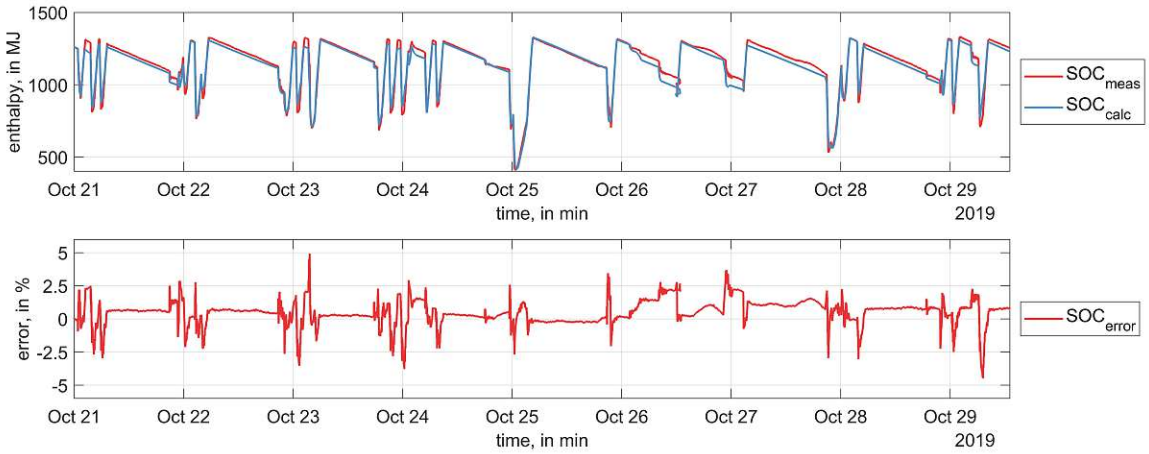

Figure 5.10: The measured enthalpy level of the SHS and the enthalpy level of the SHS model conducted with measured input is compared in the top graph. The difference between the measured and the calculated enthalpy is divided by the minimum usable energy level and depicted as the error in the bottom graph.

for both α_w values and leads to a negative or positive trend during the loss of energy periods when no heat load process is active. If the parameter α_w is not evaluated exactly, the dynamic behaviour of the load process of the SOC is influenced only in its beginning. The start level of the increase of energy is affected. The deviation to the reference SOC caused by an incorrectly chosen α_w leads to more or less energy loss in the SHS, which has an increased affect if the idle period of the HP is long. The error after 20 hours idle period is approximately 0.005%. Therefore a deviation of $\pm 0.1\ {}^{W}/_{m^2 \cdot K}$ for the parameter α_w can affect the reliability but seems not to decrease the simulation performance if the idle period of the HP is in the range of 24 hours. If the idle time gets longer, an inaccurate chosen parameter causes a significant trend in the calculated enthalpy data.

The sensitivity analysis for the mixing factor mix_{factor} was conducted with two different values. The original value for the mixing factor mix_{factor} set in the simulation is $5.8598 \cdot 10^{-4}$. One value above and one value below the original value, with a deviation of $4 \cdot 10^{-4}$ were chosen and executed in the sensitivity analysis. The output temperature was set to a constant value of 10°C for each run. Figure 5.12 shows the SOC of the SHS with different values for the mixing factor $mix_{\text{factor\_1}}$ and $mix_{\text{factor\_2}}$ and the error of the SOC compared to the SOC_{ref}. The error was calculated as stated in Eq. (5.13). The error is approximately symmetric for both mix_{factor} values and leads to a constant offset during the loss of energy periods when no heat charge process is active. Unlike the influence of the parameter α_w, the mix_{factor} influences the dynamic behaviour during the charge and discharge process. A deviation of the parameter mix_{factor} by $4 \cdot 10^{-4}$ results in the same error range as the deviation chosen for the parameter α_w. Therefore the parameter mix_{factor} has more influence and must be chosen more carefully. An inaccurate chosen parameter mix_{factor} leads to a constant error during the HP idle time and a dynamic error with changing signs during the charge and discharge process.

The model SHS depicts the main dynamics measured in the data with an adequate level of

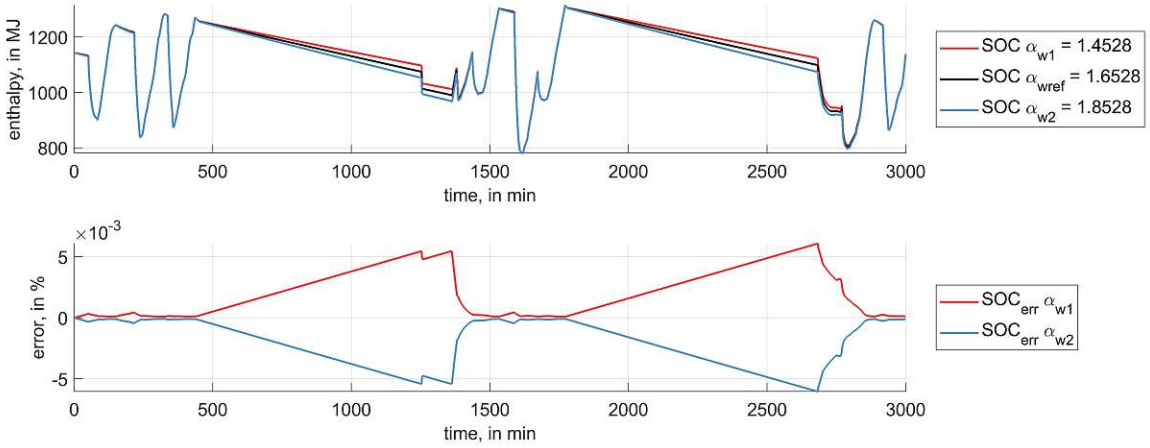

Figure 5.11: The SHS model is executed with measured data and different heat transfer coefficients α_w. The SOC of each run is compared to the SOC with the original heat transfer coefficient in the top graph. In the bottom graph the SOC is divided by the SOC calculated with the original parameter and depicted as error.

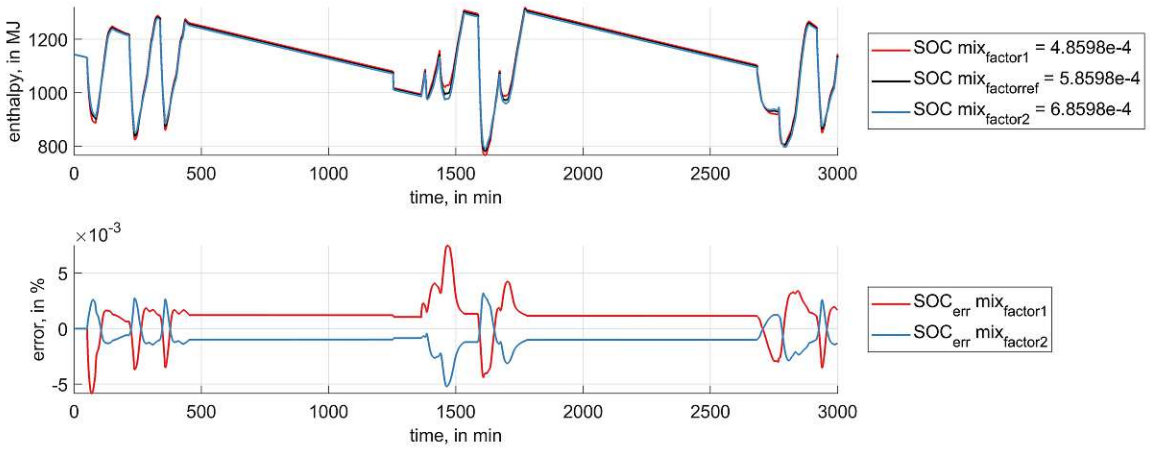

Figure 5.12: The SHS model is executed with measured data and different mixing factor mix_{factor}. The SOC of each run is compared to the SOC with the original mixing factor in the top graph. In the bottom graph the SOC is divided by the SOC calculated with the original parameter and depicted as error.

error. The model leads to no trend or offset in the data. Several parameters are defined by the geometry or the fluid, which should be chosen as exact as possible while others must be identified. The influence of deviations of the parameters was examined.

5.2.2 Heatpump

The purpose of the HP model is to simulate the heat supply for the SHS. The HP transports heat from its heat source to its heat sink. The ingoing water at the heat sink side shall be heated up to a desired temperature.

The following uncertainties were identified:

- Parameter: CompressorScaling
  The actual configuration of the HP in the plant during October 2019 was not exactly known. Some parts were replaced and in October the rotation speed was reduced leading to less heat supply at the heat sink which does not decrease linearly with the rotation speed. The design values are not reached in the data, so plausible parameters were chosen during the modelling process to depict the measured power. The available model cannot depict the heat supply data exactly.
- Model behaviour: Variable mass flow and temperature level
  The installed HP in the plant has two proportional-integral-derivative (PID) controlled mixing valves for the output temperature. The used model either supplies a constant mass flow with variable temperature output or a constant temperature output with a variable mass flow if enough heat is supplied at the heat source side. The behaviour depends on the inlet temperature and does not reflect the behaviour of the controller in the plant.
- Model behaviour: Start behaviour
  The model does not simulate the start behaviour of the HP. Therefore, more heat is available at the model startup compared to the real component since a startup behavior with a heating-up process is expected in the first few minutes.

The scenario analysis was conducted with different sets of constant inputs to the HP model. The inputs U, $T_{\text{sink}_{\text{in}}}$ and $T_{\text{source}_{\text{in}}}$ were altered. Figure 5.13 shows the input and the output of the HP executed with the scenario analysis values. The top graph shows the heat supply at the sink $\dot{Q}_{\text{sink}}$ and the heat source $\dot{Q}_{\text{source}}$ side of the model. The second graph shows the mass flow at the heat sink side $\dot{m}_{\text{sink}}$. The mass flow at the source side is approximately constant in the examined range of operation conditions. The third graph shows the input temperatures to the heat sink and the heat source side $T_{\text{sink}_{\text{in}}}$ and $T_{\text{source}_{\text{in}}}$. The output temperature at the heat sink is the constant design output temperature 84°C. The bottom graph shows the input U to the model. In each interval, only one parameter was changed and its influence was examined.

In (1), the HP reaches its steady state. From (2) to (5) the input is changed from $U = 0.25$ to $U = 1$ in 0.25 steps. The power at the heat sink side corresponds to the input U linearly and the HP model takes up to three minutes to reach a new steady state. In (6) and (7), the input

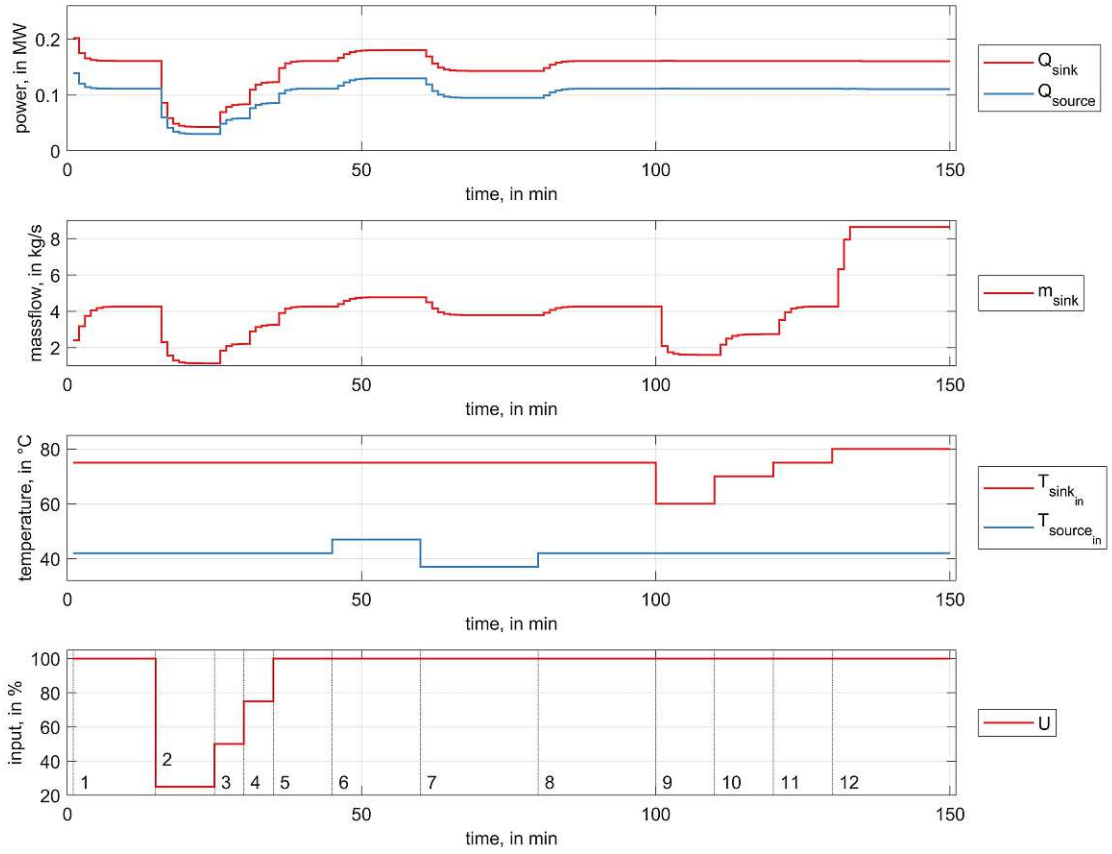

Figure 5.13: The scenario analysis of the model HP is conducted several constant input data. The output heat is shown in the top graph. The output mass flow is shown in the second graph. The input temperatures are shown in the third graph. The input U to the HP is shown in the bottom graph. The constant input sections are separated by vertical lines.

temperature at the heat source side is changed, which has a significant influence on the heat supply at the heat sink side. A temperature change of 5°C leads to an approximate increase or decrease of heat of 12%. In (8), design values are applied and in (9), the temperature $T_{\text{sink}_{\text{in}}}$ is set to 60°C and rises from (10) to (12) up to 80°C. The maximum mass flow of the connected pump of $\dot{m}_{\text{sink}_{\text{out}}} = 9.897 {}^{kg}/_{s}$ cannot be reached at a temperature of 80°C. The maximum mass flow will be reached at a temperature of 84°C. From (11) to (12) temperature steps of 5°C are added to the temperature $T_{\text{sink}_{\text{in}}}$. This leads to the most mass flow increase, compared to the other temperature steps which indicates a non-linear behaviour of the model if the temperature difference at the sink side is lower than the design values.

The HP model was executed with the validation data. The power of the HP was reduced to 78% in the measured configuration. Therefore a deviation to the nominal power of 207kW at the heat sink side of the HP was expected during the validation simulation and must be simulated by the model. Figure 5.14 shows the simulation of the HP compared to the measured data. In the top graph, the calculated power $\dot{Q}_{\text{calc}}$ is compared to the measured power $\dot{Q}_{\text{meas}}$ of the

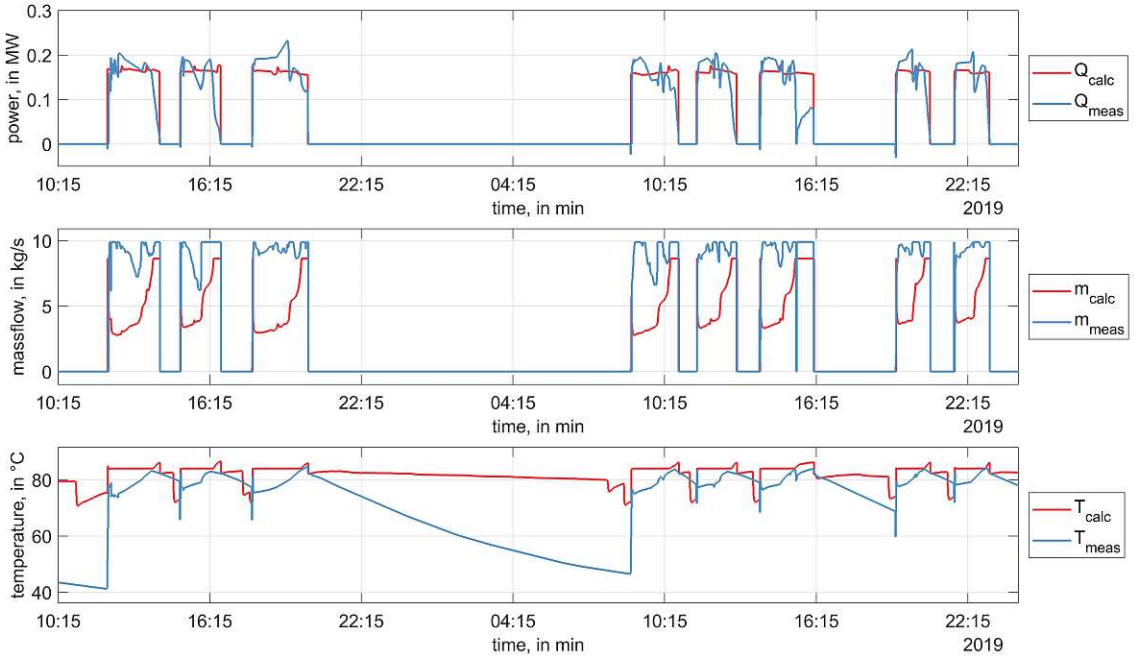

Figure 5.14: The HP model is conducted with measured input. The output of the HP at the heat sink side is compared to the measured values. In the top graph the heat is compared. In the second graph the output mass flow is compared. In the bottom graph the output temperatures are compared.

HP at the heat sink side. The second graph shows the calculated mass flow $\dot{m}_{\text{calc}}$ compared to the measured mass flow of the HP $\dot{m}_{\text{meas}}$ and the bottom graph shows the calculated output temperature T_{calc} compared to the measured temperature T_{meas} of the HP at the heat sink side. The calculated power stays at an approximately constant value compared to the measured power. The difference of the sum of the heat between the calculated heat and the measured heat is approximately 9.32 MW in 7 days and the error is about 0.023%, Eq. (5.14) to Eq. (5.17). The calculated mass flow of the HP is higher compared to the measured mass flow. The calculated temperature of the HP is constant until the maximum mass flow is reached.

$$\dot{Q}_{\text{sink}_{\text{meas}}} = 407.55MW \tag{5.14}$$

$$\dot{Q}_{\text{sink}_{\text{calc}}} = 416.88MW \tag{5.15}$$

$$\dot{Q}_{\text{sink}_{\text{diff}}} = |\dot{Q}_{\text{sink}_{\text{meas}}} - \dot{Q}_{\text{sink}_{\text{calc}}}| = 9.32MW \tag{5.16}$$

$$\dot{Q}_{\text{sink}_{\text{err}}} = \frac{|\dot{Q}_{\text{sink}_{\text{meas}}} - \dot{Q}_{\text{sink}_{\text{calc}}}|)}{\dot{Q}_{\text{sink}_{\text{meas}}}} = 0.023\% \tag{5.17}$$

$\dot{Q}_{\text{sink}_{\text{calc}}}$ is the integrated calculated heat and $\dot{Q}_{\text{sink}_{\text{meas}}}$ is the integrated measured heat at the heat sink side of the executed time. $\dot{Q}_{\text{sink}_{\text{diff}}}$ is the difference between the measured and the calculated heat and $\dot{Q}_{\text{sink}_{\text{err}}}$ is the difference of the heat divided by the measured heat.

The sensitivity analysis result, shows that the output heat at the sink side decreases linearly

with the input U. The CompressorScaling parameter influences the output heat at the heat sink side linearly too. The heat exchange parameters are design parameters and should be chosen as stated in the datasheet of the HP and were not examined.

The model HP can depict the main dynamics. The behaviour of the model differs from the measured data as the model output temperature and the heat supply at the heat sink side are constant, and the output mass flow is dynamically rising until the desired temperature difference at the heat sink side is reached. The mass flow at the heat sink side is lower than the measured one until the designed temperature is reached. The error of the integrated heat during the execution is reasonably low.

5.2.3 Heat exchange

The purpose of the heat exchange model is to simulate the following operations:

- Calculate an output temperature and mass flow based on the input temperature, the heat demand, the demand temperature, and the model limitations.
- Prevent the heat exchange if temperatures are below the demand temperature.
- Integrate not exchanged heat to the following steps.

The following uncertainties were identified:

- Parameter: the desired temperature difference ΔT_{tar}
  The design parameter ΔT_{tar} was not known. It was fitted with a LS fit for each heat exchanger separately. The mean value of the ΔT_{tar} temperature for each of the four heat exchangers was chosen as a parameter for the models. The real temperature difference parameter might be different. The exact behaviour of the heat exchanger could not be identified because a mixing valve limits the ingoing mass flow to the heat exchanger and a ball valve limits the outgoing mass flow and the control design was not exactly known.
- Parameter: the maximum heat exchange is limited to the parameter $\dot{Q}_{\text{max}}$
  The chosen value for the maximum heat exchange is one MW. The chosen value is the maximum heat exchange value in the measured data. The real maximum value depends on the maximum possible temperature difference between the two fluids, the mass of the batch consumer (BC) tanks, and the connected hydraulic components.
- Model behaviour: output temperature
  The temperature of the BC's are not used. Instead of the biased heat measurement data was used which does not reflect the exact heating process. Therefore, the output temperature is biased.
- Model behaviour: controller behaviour
  The heat exchanger output temperature and mass flow are influenced by an ingoing PID controlled valve and an outgoing ball valve. The behaviour of the PID controller can be

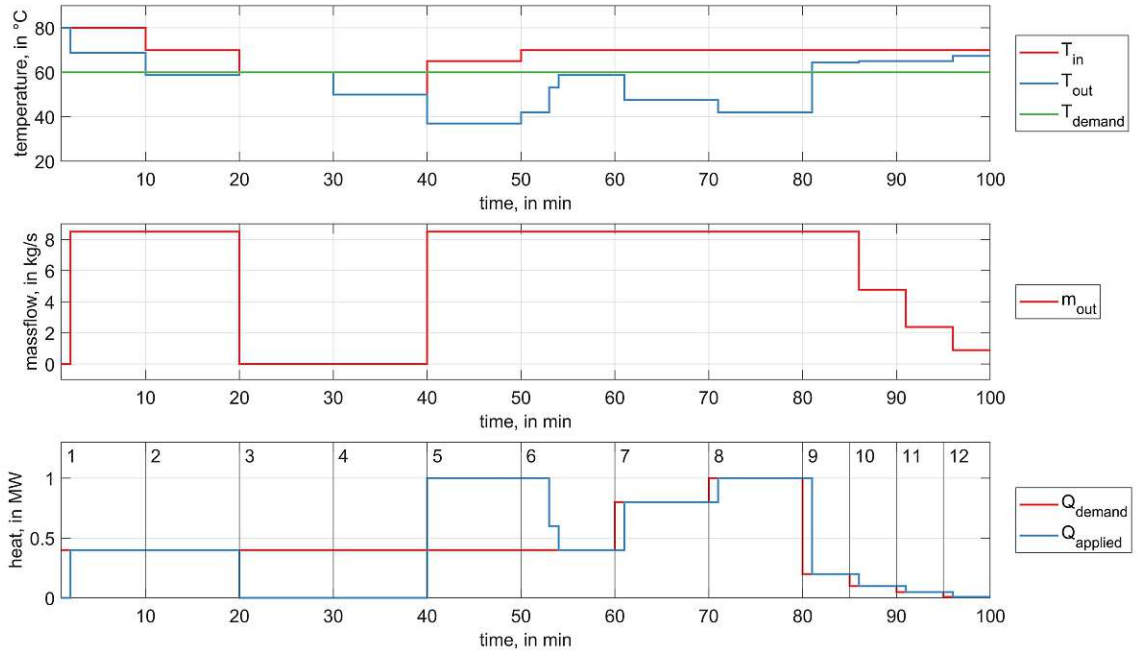

Figure 5.15: In the scenario analysis, several constant input values are applied on the heat exchange model. The top graph shows the input, output, and demand temperature. The second graph shows the mass flow out of the model and the bottom graph shows the the heat demand compared to the heat applied.

traced in the measured valve data, but the complete identification of the controller structure is not possible. Therefore, the model does not depict the complete control behaviour.

The scenario analysis was conducted for one heat exchange model. The input temperature T_{in} and the demand heat $\dot{Q}_{\text{demand}}$ were altered. Figure 5.15 shows the output of the heat exchange model executed with the scenario analysis values. The top graph shows the input and output temperatures T_{in} and T_{out} of the model and the demand temperature T_{demand}. The second graph shows the mass flow out of the model $\dot{m}_{\text{out}}$ and the bottom graph shows the heat demand $\dot{Q}_{\text{demand}}$ and heat applied $\dot{Q}_{\text{applied}}$ to the model.

From (1) to (4), the input temperature T_{in} decreases from 80°C to 50°C in 10°C steps. The heat cannot be exchanged if the input temperature is below the demand temperature T_{demand}. From (5) to (6), integrated heat from the previous and the actual steps are exchanged because the input temperature T_{in} is above the demand temperature T_{demand}. The maximum heat of $\dot{Q}_{\text{max}} = 1MW$ is exchanged because of the integrated heat. From (7) to (8), the heat demand increases to 0.8 MW and 1 MW, resulting in a wider difference between the output and the input temperature. From (9) to (13) the heat demand decreases in the following steps: 1MW, 0.3MW, 0.2MW, 0.1MW, 0.05MW and 0.01MW. The decrease of the heat demand leads to the desired model parameter temperature difference between the input and output temperature and a decreased mass flow. This behaviour was identified in the measured data if measured heat decreases and the valve closes to ensure the desired temperature difference.

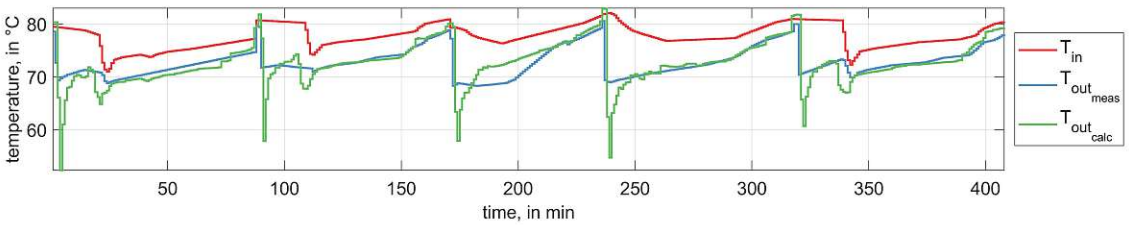

Figure 5.16: The heat exchange model is executed with measured data. The graph shows the temperatures into and out of the model. The measured output temperature is compared to the calculated output temperature.

The model was executed with the validation data. The second heat exchanger and its measured data were chosen and data segments were selected and combined, where only the chosen heat exchanger was active. Figure 5.16 shows the execution of the model with the measured data. The graph shows the input and output temperatures T_{in} and $T_{\text{out}_{\text{calc}}}$ and the measured output temperature $T_{\text{out}_{\text{meas}}}$ of the heat exchanger. At the beginning of a HT, the calculated temperature decreases sharply compared to the measured one, which is a consequence of the pulsed heat demand data. This behaviour indicates an approximately stable heat exchange where the tank and its surrounding mass is heated up, which cannot be depicted in the model. The ongoing calculated temperature fits to the measured data reasonably well. Five different measured HT's were used for the validation.

The heat exchange models are used in the simulation as a combination of four heat exchangers, connected to the mixing pipe and the pump model. The combined model was executed with the validation data. The input temperature, the heat demand, and the temperature demand for the four heat exchangers were the input to the combined model. Figure 5.17 shows the execution of the combined model. The top graph shows the heat demand $\dot{Q}_{\text{demand}}$ and the bottom graph shows the input temperature T_{in}, the calculated output temperature $T_{\text{out}_{\text{calc}}}$ and the measured output temperature $T_{\text{out}_{\text{meas}}}$. The output temperature of the combined model fits reasonably well to the measured temperature if the heat demand is above 0.1MW. If the measured heat demand is below 0.1MW, the minimum constant mass flow of the pump P9 is active and a decreasing temperature difference between the input and the output temperature is calculated by the model. This might be a consequence of the missing information of the controller settings, the missing mass flow data of the heat sink models, biased heat demand data, biased temperature measurement data, or heat loss through the pipes, which are not modelled. The temperature and the mass flow during a heat demand above 0.1MW can be simulated with small deviations. The temperature drop at the beginning of a HT cannot be simulated correctly.

The sensitivity analysis shows that a lower chosen $\dot{Q}_{\text{max}}$ value changes the exponential characteristic of the heat demand data by limiting the maximum values, which was not desired. Its main function is to prevent the uncontrolled rise of the heat in the heat exchange in the model by the integrator caused by insufficient heat supply of the SHS.

The heat exchanger model analysis and its execution with the validation data showed that the main dynamics were simulated with a significant bias at the beginning of a HT caused by the

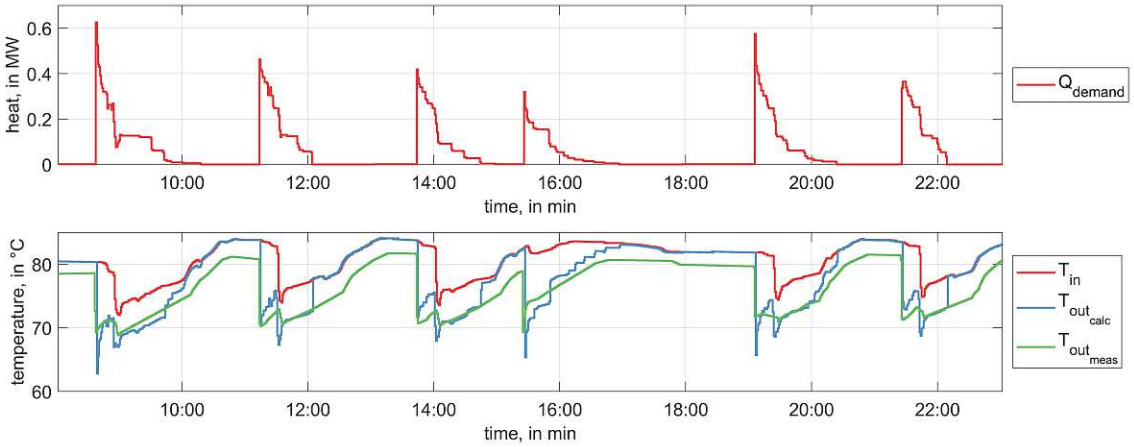

Figure 5.17: Four heat exchange models are grouped with the mixing pipe model and the pump model. They are executed with measured data. The top graph shows the measured heat demand as input data to the model and the bottom graph shows the temperatures into and out of the model. The measured output temperature is compared to the calculated output temperature.

use of the heat data instead of the temperature data. The combined model leads to a decrease of the fit if the heat demand is below 0.1 MW, by a reduced temperature difference between the output and the input temperature. This is caused by the minimum pump mass flow and missing additional data. The model can exchange the heat demand consistently and comprehensibly.

5.2.4 Mixing Pipe

The purpose of the model mixing pipe is to mix the connected inlets into one outlet. The calculated outlet mass flow and temperature are proportional to the inlets' mass flow and their corresponding temperatures. The pipe simulates no temperature loss over time and no losses caused by friction or turbulent flow.

No sources of uncertainty could be identified. The scenario analysis showed the expected proportional behaviour. The comparison of measured data with the simulation output was not possible because no measured data was available for this purpose. No parameters can be altered, so no sensitivity analysis was conducted. The output was compared with an analytical solution and is reliable for its purpose.

5.2.5 Pump

The purpose of the model pump is to simulate the summarized variable mass flow demanded by all of the heat demand models. It further limits the heat exchange to the maximum mass flow.

The following uncertainties were identified:

- Model behaviour: the variable mass flow
  The difference pressure height of the system on which the pump is connected was un-

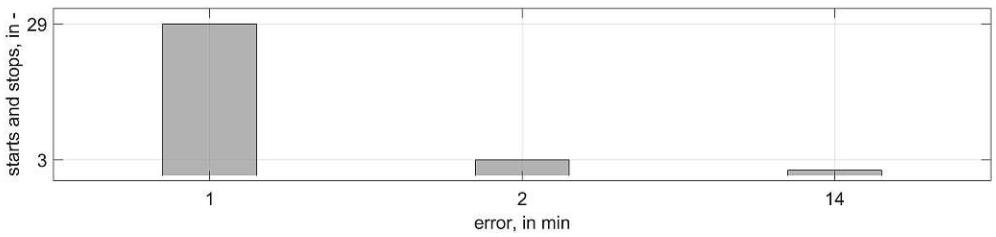

Figure 5.18: The number of start and stop times of the HP model active time compared to the HP measured active time. The difference is depicted as error in minutes.

known. Further, the pressure height depends on the valve of the heat exchangers which was unknown too. An exact mass flow could not be calculated.

Comparing measured data with the model output was not possible because no measured data was available for this purpose. The scenario analysis showed the expected behaviour of the pump if the heat demand and the corresponding temperatures result in a mass flow between the minimum and the maximum mass flow. The pump limits the mass flow to the maximum mass flow if the enthalpy of the heat demand and the temperature difference results in more mass flow than the maximum mass flow. This scenario occurs if more than two heat exchangers start simultaneously. In this case, only limited heat can be exchanged. The limitation to the minimum mass flow happens if the enthalpy of the heat demand and the temperature difference results in a lower mass flow than the minimum mass flow. The output of the model was verified by its analytical solution and is reliable for its purpose. The pump cannot supply the heat demand from more than two heat exchangers simultaneously because of its maximum mass flow, which reflects the current configuration in the plant.

5.2.6 Hysteresis Controller

The purpose of the Hysteresis Controller is to start the HP if a measured value in the SHS is below a defined limit and stops the HP if another measured value in the SHS reaches its configured limit. The HP is started or stopped with the values one and zero without partial control.

The following uncertainties were identified:

- Parameter: The upper and lower limit $T_{\text{upper}}, limit$ and $T_{\text{lower}}, limit$
  The parameters could be identified out of the measured data. Inaccuracies in the measured data of the SHS lead to an uncertainty of the parameters.

The scenario analysis showed that the hysteresis controller starts at the desired temperature and stops if the upper limit temperature is reached. The hysteresis controller was executed with the measured data and its output was compared to the runtime of the HP. The hysteresis controller fits to the implemented controller with start and stop time errors of one and two minutes. Figure 5.18 shows the error of the start time in the validation period.

The hysteresis controller validation showed that the hysteresis parameter can be examined exactly with an error time of about one to two minutes. Imprecise measurement devices in the SHS or measurement inaccuracies in the recording system may cause the evaluated error.

5.2.7 Complete System

The components are connected and controlled with the hysteresis controller. The input to the complete system are the measured heat demand data, temperature data outside the building for the heat loss of the SHS, and measured temperature data of the internal heat network. The simulation was executed with validation data and the simulated SOC of the SHS was compared to the measured SOC. Figure 5.19 shows in the top graph the calculated enthalpy of the SHS SOC_{calc} compared to the measured enthalpy SOC_{meas}. The difference between the calculated and the measured enthalpy divided by the minimum usable enthalpy SOC_{error} is depicted in the bottom graph.

The main dynamics of the system are depicted correctly. The start of a HT leads to an error in the SOC. The HP and the hysteresis controller model lead to an offset error after a charging process of less than 1%. The constant loss of energy during the operation free periods is modelled accurately. The dynamic behaviour of the system can be depicted with an error of up to approximately 10 %. The error might be a result of the missing start behaviour of the pipes, biased heat demand data, or the neglection of the startup behaviour of the HP. It was assumed that the error was not induced by the biased data, but by lack of model functionality because the deviation between the measured and simulated output is larger than the expected measurement errors. Manual actions during the processes are not simulated adequately. There is no trend in the error. The NRMSE between the calculated and the measured SOC is 0.5815. The simulation model is reliable enough for the implementation of the EDCS and fulfils the requirements stated in Section 2.3.

Every component and the assembly were validated. The conducted methods of Section 4.3 led to a trustworthy level of confidence in the simulation. Based on the existing and prepared data, it was possible to identify the plant's most important procedures and configurations. The pipe system and its influence on the startup of the system were neglected. Further, the startup behaviour of the HP and the heat exchanger were not examined and neglected. Essential results for the main components like the scenario analysis, the sensitivity analysis, and the comparison of the output with measured data were shown. The execution of the complete model with measured input data was comprehensible and reliable. The validation is based on the biased available measured data. No range of uncertainty for the measured data for the validation could be stated. The EDCS can be implemented and tested in the simulation.

The simulation was stable and did not interrupt during a simulation runtime of 30 days. Its execution time depends on the used computer, the configuration, and on the HP model, which is an imported functional mockup unit (FMU) and limits the computation time. The execution time for the simulation with the hysteresis controller on an i7-1065g7 CPU 1.30GHz with the operating system Windows 10 2021 took about 5 minutes.

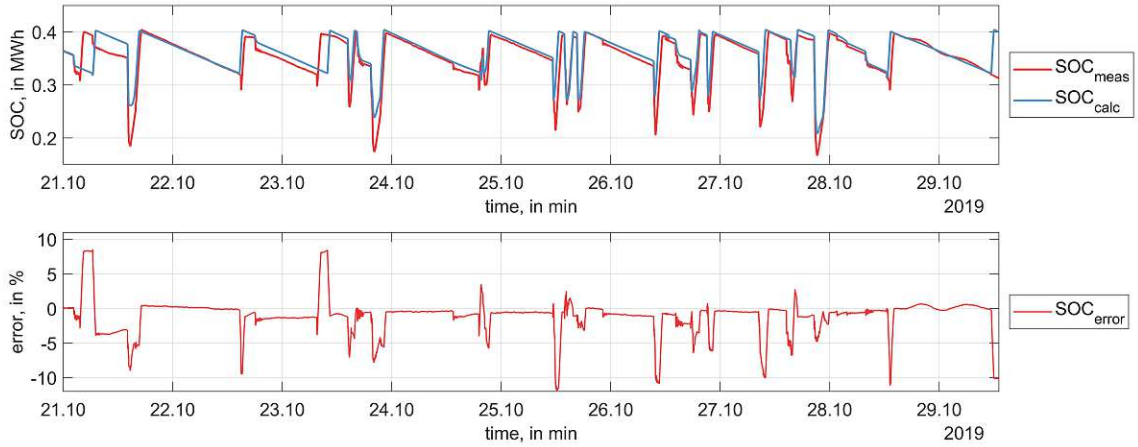

Figure 5.19: The complete model is executed with measured input. In the top graph, the SHS enthalpy SOC_{calc} is compared to the measured SHS enthalpy SOC_{meas}. The bottom graph shows the difference between the measured and the calculated SOC divided by the minimum usable enthalpy level of the SHS SOC_{error}.

5.3 EDCS

The second research question was: 'Can the EDCS be used to control the investigated energy supply system'. This question is answered by the simulation results with the implemented EDCS. The heat demand prediction data from Subsection 4.1.1 was used to execute the simulation of the model with the implemented EDCS and the configuration defined in Section 4.4. The start time of the HT's were moved to the past and the future and differs from the predicted start time. The integral heat data for the HT's was exactly known. The output is presented in Figure 5.20. The simulated enthalpy SOC_{calc} is compared to the SOC trajectory SOC_{traj}. The SOC_{min} of the HT's is shown. The measured SOC differs from its trajectory because the start time and the course of the HT's were not exactly known. The difference between the trajectory and the measured SOC shows that the observer moves the prediction continuously into the future leading to a constant high SOC until the HT starts. The extension of the SOC_{min} prevents the SOC from falling below the SOC_{min}.

The EDCS tries to charge the SHS at times where the power price is low. Figure 5.21 shows that the consumption of *power* at a low power *price* is not always possible. Especially before

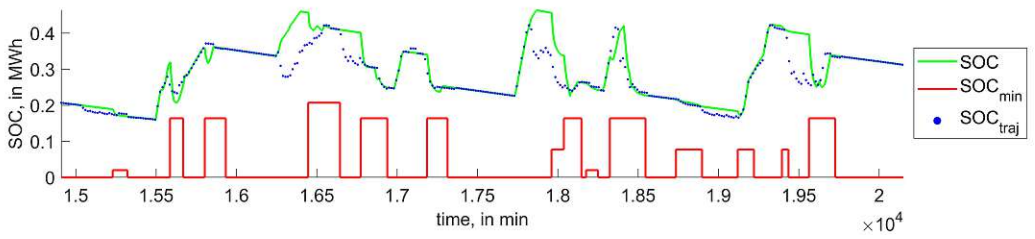

Figure 5.20: The simulated SOC, the SOC_{min} of the heat demand, and the trajectory SOC_{traj} of the Operation Planner (OP). The simulation was executed with the implemented EDCS.

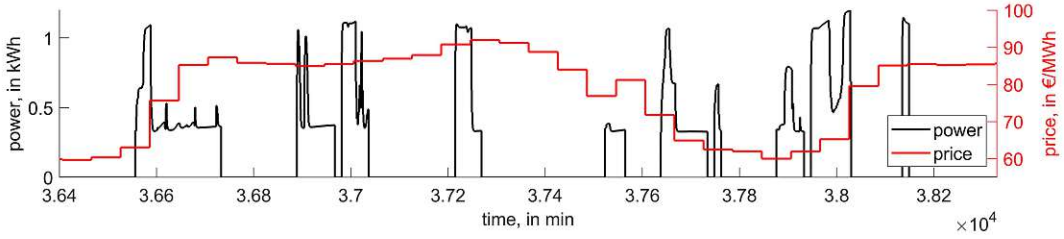

Figure 5.21: The power consumption of the HP is compared to the price per MWh.

the price increases, the power consumption is higher compared to the power consumption after the increase. If heat is demanded and the SHS could not provide the heat demand, the EDCS must start the HP because of constraints, despite the price being high.

The operating example of the EDCS showed that the EDCS can control the heat supply of the plant under study. The flexible power price market was used to charge the SHS in periods with low electricity price. The additional HT observer functionality increases the performance of the EDCS by updating the prediction accuracy in real-time. The movement of the HT prediction corrects imprecise predicted start times. The distribution of heat corrects the course of the HT to ensure a correct integral heat amount for the prediction. The extension of the $SOC_{\min}$ raises the energy level before the HT start and reduces the probability of the undercut of the $SOC_{\min}$. The EDCS can be configured for the desired objectives and its execution produced comprehensible and error-free output. The calculation of the optimization was feasible and the objectives were fulfilled.

The result is restricted by the use of the heat demand data. The heat demand does not reflect the real temperature trajectory, which must be applied to the product. It was assumed that sufficient heat is available for the process if the SOC remains above the $SOC_{\min}$ and the desired temperature trajectory can be applied. Investigations on the real plant are necessary to prove this assumption. Further, the simulation was developed with simplifications. The influence of the simplifications on the performance of the EDCS must be examined.

5.4 Simulation Study

The follwoing two research questions shall be answered by the simulation study: 'How robust is the EDCS against unpredicted interactions of human operators' and 'Which influence has the EDCS on the cost and quality of the process'. The first result is depicted in Figure 5.22, which shows the mean HT's affected by an undercut of the $SOC_{\min}$ and their confidence interval. It is shown, that unpredicted HT start times influence the heat supply of the HT's by inducing an insufficient SOC level. The EDCS reduces the mean affected HT's by approximately 50% to a level lower than 4% in each configuration compared to the hysteresis benchmark. 103 HT's were conducted per simulation execution. The HT movement functionality of the observer ensures sufficient heat supply for each HT which starts later than planned. The parameter t_{safety} reduces the insufficient heat supply of the HT's which start earlier than planned. The mean

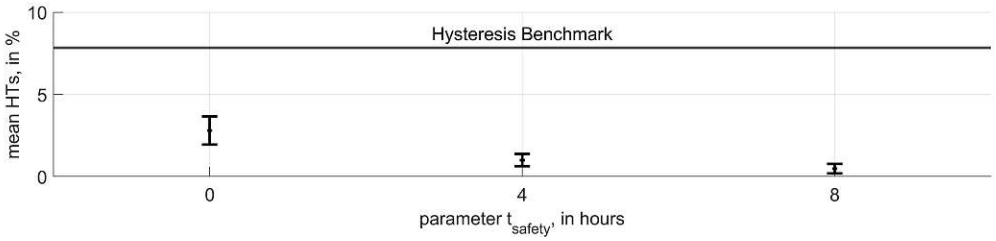

Figure 5.22: The HT's which are affected by an undercut of the $SOC_{\min}$ are evaluated. The mean affected HT's and the confidence interval of the execution with the EDCS and each parameter set is shown. The results are compared to the hysteresis benchmark. $W = 36$ simulation executions for each parameter set.

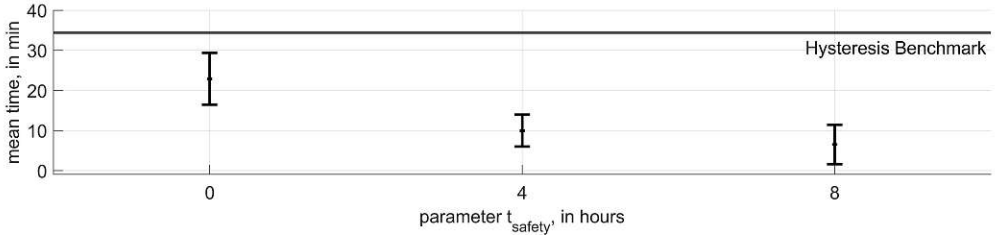

Figure 5.23: The time a HT is affected by an undercut of the $SOC_{\min}$ is evaluated. The mean time per affected HT and the confidence interval of the execution with the EDCS and each parameter set is shown. The results are compared to the hysteresis benchmark. $W = 36$ simulation executions for each parameter set.

affected HT's decrease with the increase of the parameter t_{safety}. Affected HT's with a start time deviation to the planned start time of less than four hours can be reduced to almost zero with the parameter $t_{\text{safety}} = 4hours$.

Analogous to the mean affected HT's, a mean time per SOC undercut can be evaluated. The mean time that the SOC falls below the $SOC_{\min}$ per affected HT decreases with the increase of the parameter t_{safety}. The mean time is below the hysteresis benchmark time in each configuration. This is a result of the appropriate start of the HP when the EDCS recognizes the undercut of the $SOC_{\min}$. Figure 5.23 shows the mean time that the SOC is below the $SOC_{\min}$ and its confidence interval.

The EDCS is able to ensure sufficient heat supply for each HT with a perfect start time prediction. Unpredicted interactions by human operators influence the controllers performance negatively. The deviation of the predicted HT's start time to the real start time can cause the SOC to fall below the $SOC_{\min}$. This influences the production process and the product is not heated up in the desired necessary time, which can harm the product quality. The simulation study showed that the EDCS is a robust control system against unpredicted HT start time deviations. Without the extension of the $SOC_{\min}$, the EDCS can reduce the affected HT's compared to the hysteresis benchmark while ensuring a stable and feasible control. The parameter t_{safety} can increase the EDCS performance further. The higher the parameter t_{safety} is chosen, the lower the probability of the SOC falling below the $SOC_{\min}$. The number of affected HT's and the time duration the SOC is below the $SOC_{\min}$ can significantly be reduced by using the t_{safety}

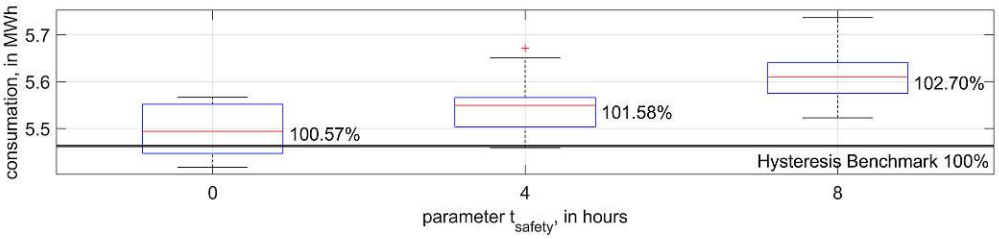

Figure 5.24: The median of the power consumption per parameter set with its percentile and the maximum and minimum values compared to the hysteresis benchmark. $W = 36$ simulation executions for each parameter set.

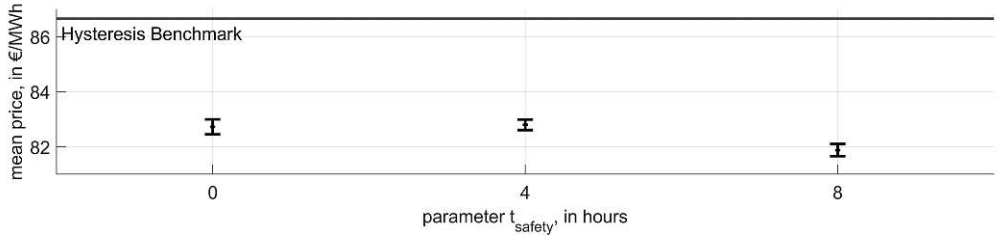

Figure 5.25: The price per MWh is evaluated. The mean price per MWh and the confidence interval of the execution with the EDCS and each parameter set is shown. The results are compared to the hysteresis benchmark. $W = 36$ simulation executions for each parameter set.

parameter.

The influence of the EDCS on the costs of the process can be analysed by the power consumption and the price per consumed MWh. The boxplot of the energy consumption for the executions with the different parameter sets is shown in Figure 5.24. The median consumed energy is higher compared to the hysteresis benchmark in all three cases, although the energy consumption by the HT's is the same for each execution. This indicates more loss of energy in the SHS during the executions with the EDCS. The heat loss is caused by energy that is not used at the appropriate time because the HT start time is shifted to the future. At high energy levels induced by high t_{safety} values, the heat loss is higher compared to low energy levels.

Figure 5.25 shows the mean price per MWh and its confidence interval for the execution of the different parameter sets. The mean price is approximately 4€ per MWh lower compared to the hysteresis benchmark and is the lowest for the parameter $t_{\text{safety}} = 8 hours$. The study shows, that power is consumed at a low price level if possible.

The cost of the power consumption is obtained by multiplying the prices times the consumption. Figure 5.26 shows the boxplot of the costs. The higher the parameter t_{safety} is chosen, the higher are the costs for the execution with the EDCS caused by the high energy consumption induced by the additional loss of energy. The overall costs are lower compared to the hysteresis benchmark. The EDCS reduces the sum of the costs because the cost reduction for charging the SHS during a low price level is higher than the cost of the additional heat loss.

The EDCS can reduce costs and ensure process quality at the same time. The simulation study shows that energy is consumed at low price levels whenever possible. The influence of a flexible power price increases as the price range widens. The use of a photovoltaic system and

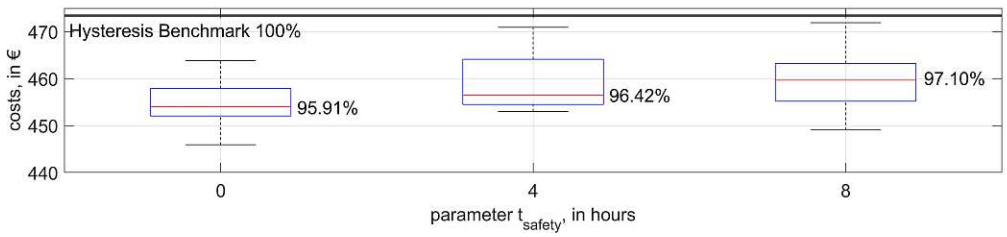

Figure 5.26: The cost of the power consumption is evaluated. The median of the costs per parameter set with its percentile and the maximum and minimum values. The results are compared to the hysteresis benchmark. $W = 36$ simulation executions for each parameter set.

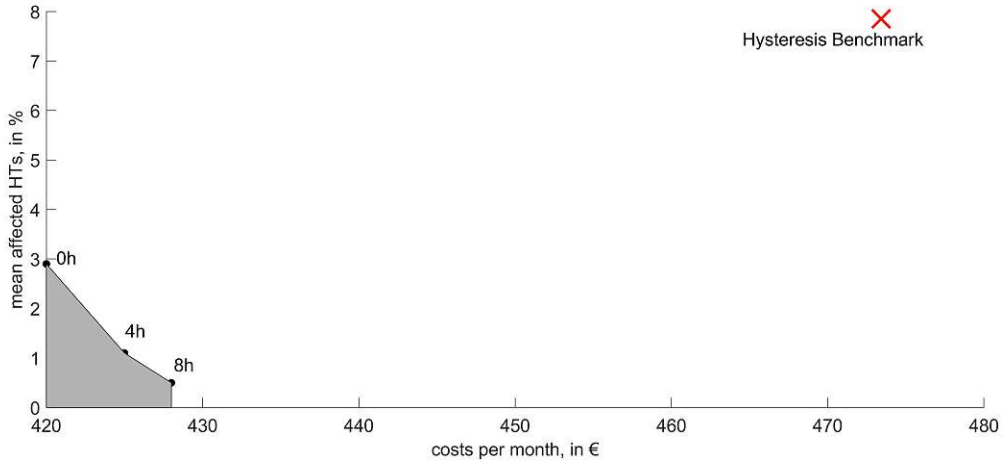

Figure 5.27: The Pareto front shows the correlation between the mean affected HTs and the costs if the parameter $SOC_{\min}$ is adjusted. The values of the execution of the hysteresis is marked as a red cross.

heat recovery can decrease the price per MWh further. At the same time, the EDCS ensures the quality of the production processes by a sufficient heat supply. With the observer functionality disturbances in the prediction of the start times can be managed effectively.

The simulation of the plant controlled with the EDCS reduced the costs and the affected HT's, compared to the hysteresis benchmark. A Pareto front arises in which the desired trade-off between the affected HT's and the costs for the consumed power can be chosen in Figure 5.27. The values for the different parameter sets are shown. The hysteresis benchmark value is added. The economic decision in the Pareto front depends on the consequences the undercut of the SOC has on the product quality. This relation is not examined yet. A valuation of the consequences of harmed products must be done in future research.

6 Resume and Outlook

In this thesis, a simulation model was developed, verified, and validated utilizing measurement data from the plant under study from October 2019. The biased data was prepared to reach the necessary level of confidence and consistency. The main components of the examined plant, the SHS, the HP, and the heat demand, were modelled, verified, and validated. Further minor hydraulic models are added. The connected simulation depicts the main dynamics of the plant. The validation confirmed a reliable simulation model that does not lead to a trend or a constant error compared to the measured data. The processes are mapped comprehensibly and reliably. A valid simulation based on measured data of the investigated plant is available for testing the EDCS (Research Question 1).

The control framework EDCS was implemented in the developed simulation model and executed without errors. The prediction of the EDCS is comprehensible. The execution of the simulation with the EDCS in the examined scenarios was stable, feasible, and the controller achieved the desired objectives. The HT functionality implemented in the observer enhances the performance of the EDCS by improving the prediction quality in real-time. Prediction start time inaccuracies and the integral amount of heat can be corrected in the prediction. It was shown that the EDCS can be used to control the investigated energy supply system (Research Question 2).

The simulation study showed that the EDCS can ensure process safety despite HT start time deviations. The added observer functionality reduces product quality issues effectively. The robustness of the EDCS is validated by the simulation study (Research Question 3). Further, the simulation study shows that the EDCS utilizes the flexible power price to reduce the power costs compared to a hysteresis controller. The EDCS fulfils its aim to optimize the heat supply and simultaneously reducing costs and providing process safety (Research Question 4).

Still, the model error could be further reduced. The accuracy of the models can be improved by simulating the pipe network and its influence on the heat loss and the start up behaviour. Well chosen validation experiments substantiate the validation process. Measurement devices for the mass flow help to increase the simulation accuracy and the validation possibilities. With the knowledge of the precision of the measurement devices, a range of error can be depicted. Nondeterministic model components increase the reliability into the simulation model. Additional parts of the plant can be implemented, verified, and validated. The underlying control structure consists of several PID controlled valves could be investigated and improved.

The EDCS could be tested with and validated on the extended simulation model. The influence of the EDCS on the performance and process quality should be examined further. The

robustness and the stability of the EDCS must be investigated in further examinations. Additional simulation studies could evaluate the influence of an inaccurate predicted power price. The observer functionality and its real-time prediction correction could be investigated with imprecise predicted integral heat amounts per HT.

Future research on the plant and the EDCS should examine the influence of insufficient energy supply on the product quality. The costs of possible harmed products must be evaluated and influence the Pareto optimum. Further, the influence of the EDCS parameters on the process safety and the costs could be examined. A factorial experiment can examine the influence of the parameters on the EDCS. The most influential parameters could be investigated further. The extended simulation model, allows more 'what if' analysis that is worthwhile for the plant operator. The observer can be enhanced by a function that moves the HT's prediction to an earlier start time instead of using the parameter t_{safety}. The SOC will be held at a sufficiently high level until the HT starts. This function decreases the flexibility of the EDCS, but increase product safety.

Hydraulic Symbols

Pipe connection

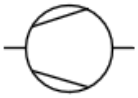

Compressor

Pump with constant mass flow

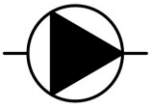

Pump with variable mass flow

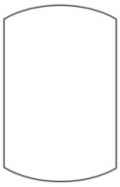

Thermal energy storage

Counter flow plate heat exchanger

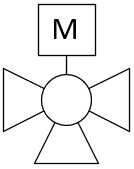

Three-way mixing valve with motor

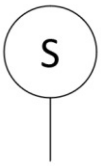

Rpm measurement

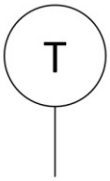

Temperature measurement

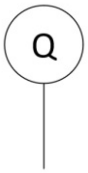

Heat flow meter

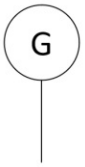

Valve position measurement

Bibliography

1. A.I. Propoi. in *Automn Remote Control 24:7* 912–920 (1963).
2. Abhat, A. Short term thermal energy storage. *Energy and Buildings* **3,** 49–76. ISSN: 0378-7788 (1981).
3. AIT. *Heat Pump Functional Mockup Unit (FMU)* 2020.
4. Anshoff, H. *et al.* in *Operations Research '72: Proceedings of the Sixth IFORS International Conference on Operational Research* (1972).
5. Arkun, Y. *et al.* Studies in the synthesis of control structures for chemical processes: Part IV. Design of steady-state optimizing control structures for chemical process units. *AIChE Journal* **26,** 975–991. ISSN: 0001-1541 (1980).
6. ASME. *Guide for verification and validation in computational solid mechanics: ASME V & V* New York, NY, 2006.
7. Balci, O. *Guidelines for successful simulation studies* in *1990 Winter Simulation Conference proceedings* (ed Balci, O.) (Assoc. for Computing Machinery, Baltimore/Md., 1990), 25–32. ISBN: 0-911801-72-3.
8. Balci, O. *Principles and techniques of simulation validation, verification, and testing* in *Proceedings, 1995 Winter Simulation Conference* (eds Alexopoulos, C. *et al.*) (Society for Computer Simulation International, San Diego, 1995), 147–154. ISBN: 0780330188. (1995).
9. Balci, O. Validation, verification, and testing techniques throughout the life cycle of a simulation study. *Annals of Operations Research* **53,** 121–173. ISSN: 1572-9338 (1994).
10. Balci, O. *et al.* A methodology for cost-risk analysis in the statistical validation of simulation models. *Communications of the ACM* **24,** 190–197. ISSN: 0001-0782 (1981).
11. Balci, O. *et al.* Formulated problem verification as an explicit requirement of model credibility. *SIMULATION* **45,** 76–86. ISSN: 0037-5497 (1985).
12. *Handbook of simulation: Principles, methodology, advances, applications, and practice* (ed Banks, J.) ISBN: 9780470172445 (Wiley, New York, Chichester, and Weinheim, 1998).
13. Beckmann, G. *et al. Thermal energy storage: Basics, design, applications to power generation and heat supply* ISBN: 9783211817643 (Springer, Wien, 1984).
14. Blottner, F. G. Accurate Navier-Stokes results for the hypersonic flow over a spherical nosetip. *Journal of Spacecraft and Rockets* **27,** 113–122. ISSN: 0022-4650 (1990).

15. Carson, J. S. *Verification and validation: a consultant's perspective* in *1989 Winter Simulation Conference proceedings* (eds MacNair, E. A. *et al.*) (Institute of Electrical and Electronics Engineers, New York, NY and s.l., 1989), 552–558. ISBN: 0911801588.

16. Coleman, T. F. *et al.* An Interior Trust Region Approach for Nonlinear Minimization Subject to Bounds. *SIAM Journal on Optimization* **6,** 418–445. ISSN: 1052-6234 (1996).

17. D. M. Prett *et al.* Optimization and constrained multivariable control of a catalytic cracking unit. *IEEE Transactions on Automatic Control* (1980).

18. Dassault Systèmes. *Dymola* 2020.

19. Davis, P. K. *Generalizing Concepts and Methods of Verification, Validation, and Accreditation (VV&A) for Military Simulations* (RAND Corporation, 1991).

20. Dincer, I. *et al. Thermal energy storage: Systems and applications* ISBN: 1119956625 (Wiley, Hoboken, N.J., 2013).

21. Dinçer, İ. *Heat transfer in food cooling applications* 1. ed. ISBN: 9781560325802 (Taylor & Francis, Washington, DC, 1997).

22. Eicker, U. *Solar technologies for buildings* ISBN: 9780471486374 (Wiley, Chichester, 2005).

23. Fishman, G. S. *et al.* The statistics of discrete-event simulation. *SIMULATION* **10,** 185–195. ISSN: 0037-5497 (1968).

24. Fuhrmann, F. *et al.* Prediction of pulsed heat loads in manufacturing plants. *IFAC-PapersOnLine* **53,** 10449–10454. ISSN: 24058963 (2020).

25. García, C. E. *et al.* Model predictive control: Theory and practice—A survey. *Automatica* **25,** 335–348. ISSN: 0005-1098 (1989).

26. Garg, H. P. *et al. Solar Thermal Energy Storage* ISBN: 9789400953017 (Springer Netherlands, Dordrecht, 1985).

27. Gass, S. I. *et al.* Concepts of model confidence. *Computers & Operations Research* **8,** 341–346. ISSN: 0305-0548 (1981).

28. Greig, I. D. Validation, statistical testing, and the decision to model. *SIMULATION* **33,** 55–60. ISSN: 0037-5497 (1979).

29. Gurobi Optimization, L. L. *Gurobi Optimizer* Software. Beaverton, Oregon, 2021. `https://www.gurobi.com/`.

30. ISO. *Konformitätsbewertung - Allgemeine Grundsätze und Anforderungen an Validierungs- und Verifizierungsstellen* 2019.

31. Keerthi, S. S. *et al.* Optimal infinite-horizon feedback laws for a general class of constrained discrete-time systems: Stability and moving-horizon approximations. *Journal of Optimization Theory and Applications* **57,** 265–293. ISSN: 0022-3239 (1988).

32. Kleindorfer, G. B. *et al.* Validation in Simulation: Various Positions in the Philosophy of Science. *Management Science* **44,** 1087–1099. ISSN: 00251909 (1998).

33. Landry, M. *et al.* In search of a valid view of model validation for operations research. *European Journal of Operational Research* **66,** 161–167. ISSN: 0377-2217 (1993).

34. MATLAB. *9.7.0.1190202 (R2019b)* (The MathWorks Inc., Natick, Massachusetts, 2019).

35. Mayne, D. Q. *et al.* Constrained model predictive control: Stability and optimality. *Automatica* **36,** 789–814. ISSN: 0005-1098 (2000).

36. McKane, A. T. *et al. Opportunities, Barriers and Actions for Industrial Demand Response in California* 2008.

37. MEADOWS, E. S. *et al.* Receding horizon control and discontinuous state feedback stabilization. *International Journal of Control* **62,** 1217–1229. ISSN: 0020-7179 (1995).

38. Modelica Association. *Modelica* 2020.

39. Oberkampf, W. *et al. Validation methodology in computational fluid dynamics* in *Fluids 2000 Conference and Exhibit* (American Institute of Aeronautics and Astronautics, Reston, Virigina, 2000).

40. Oberkampf, W. L. *et al.* Verification and validation benchmarks. *Nuclear Engineering and Design* **238,** 716–743. ISSN: 0029-5493 (2008).

41. Oberkampf, W. L. *et al. Verification and validation in scientific computing* Reprint. ISBN: 9780521113601 (Cambridge Univ. Press, Cambridge, 2012).

42. Oberkampf, W. L. *et al. Verification, validation, and predictive capability in computational engineering and physics* 2003.

43. Oreskes, N. *et al.* Verification, validation, and confirmation of numerical models in the Earth sciences. *Science (New York, N.Y.)* **263,** 641–646. ISSN: 0036-8075 (1994).

44. Palensky, P. *et al.* Demand Side Management: Demand Response, Intelligent Energy Systems, and Smart Loads. *IEEE Transactions on Industrial Informatics* **7,** 381–388. ISSN: 1941-0050 (2011).

45. Polak, E. *Optimization: Algorithms and Consistent Approximations* ISBN: 9781461206637 (Springer-Verlag, New York, 1997).

46. Qin, S. *et al.* A survey of industrial model predictive control technology. *Control Engineering Practice* **11,** 733–764. ISSN: 0967-0661 (2003).

47. Raković, S. V. in *Encyclopedia of Systems and Control* (eds Baillieul, J. *et al.*) 1–11 (Springer London and Imprint: Springer, London, 2020). ISBN: 978-1-4471-5102-9.

48. *Handbook of Model Predictive Control* (eds Raković, S. V. *et al.*) ISBN: 9783319774909 (Springer International Publishing, Cham, 2019).

49. Rao, C. V. *et al.* Application of Interior-Point Methods to Model Predictive Control. *Journal of Optimization Theory and Applications* **99,** 723–757. ISSN: 0022-3239 (1998).

50. Richalet, J. *et al.* Model predictive heuristic control. *Automatica* **14,** 413–428. ISSN: 0005-1098 (1978).

51. Roache, P. J. Verification of Codes and Calculations. *AIAA Journal* **36,** 696–702. ISSN: 0001-1452 (1998).

52. Robinson, S. *Simulation model verification and validation* in *1997 Winter Simulation Conference Proceedings* (eds Andradóttir, S. *et al.*) (IEEE, Piscataway, Nov. 1997), 53–59. ISBN: 078034278X.

53. S. Joe Qin *et al. An Overview Of Industrial Model Predictive Control Technology* (1997).

54. Sandell, N. *et al.* Survey of decentralized control methods for large scale systems. *IEEE Transactions on Automatic Control* **23,** 108–128. ISSN: 1558-2523 (1978).

55. Sargent, R. G. An Assessment Procedure and a Set of Criteria for Use in the Evaluation of 'Computerized Models and Computer-Based Modelling Tools'. *undefined* (1981).

56. Sargent, R. G. *Verification and validation of simulation models* in *1998 Winter Simulation Conference. Proceedings (Cat. No.98CH36274)* (1998), 121–130 vol.1.

57. Sargent, R. G. *et al. History of verification and validation of simulation models* in *WSC'17* (eds Chan, W. K. *et al.*) (IEEE, Piscataway, NJ, 2017), 292–307. ISBN: 978-1-5386-3428-8.

58. Scattolini, R. Architectures for distributed and hierarchical Model Predictive Control – A review. *Journal of Process Control* **19,** 723–731. ISSN: 0959-1524 (2009).

59. Schlesinger. Terminology for model credibility. *SIMULATION* **32,** 103–104. ISSN: 0037-5497 (1979).

60. Shannon, R. E. *Systems simulation: The art and science* ISBN: 0138818398 (Prentice-Hall, Englewood Cliffs, NJ, 1975).

61. Streckiene, G. *et al.* in *8th International Conference on Environmental Engineering, ICEE 2011* (2011).

62. VDI. *VDI-Wärmeatlas: Mit 320 Tabellen* 11., bearb. und erw. Aufl. ISBN: 978-3-642-19980-6 (Springer Vieweg, Berlin, 2013).

63. Wang, L. *Model Predictive Control System Design and Implementation Using MATLAB®* ISBN: 9781848823310 (Springer, London and Heidelberg, 2009).

64. Windholz, B. *EDCSproof* (ed AIT Austrian Institute of Technology GmbH) Wien, 2018-2021. `https://www.nefi.at/en/edcsproof/` (2021).

65. Wright, S. J. *Applying new optimization algorithms to more predictive control* 1996.

List of Figures

List of Tables